



TECHNISCHE  
UNIVERSITÄT  
WIEN

Vienna University of Technology

## DISSERTATION

# **Synthesis and Characterization of Coordination Compounds Using Novel Tetradentate Schiff Bases Aiming for Potential Fluorescence Applications**

ausgeführt zum Zwecke der Erlangung des akademischen Grades eines Doktors der  
technischen Wissenschaften unter der Leitung von

**Univ. Prof. Dr. Wolfgang Linert**

Institut für angewandte Synthesechemie 163,  
eingereicht an der Technischen Universität Wien

von

**Dipl.-Ing. Esther Theresa Knittl**

0825067

Panikengasse 43/13

1160 Wien

Wien, im Oktober 2017

---

Esther Knittl





TECHNISCHE  
UNIVERSITÄT  
WIEN  
Vienna University of Technology

Ich habe zur Kenntnis genommen, dass ich zur Drucklegung meiner Arbeit unter der Bezeichnung

## **Dissertation**

nur mit Bewilligung der Prüfungskommission berechtigt bin.

Ich erkläre weiters Eides statt, dass ich meine Dissertation nach den anerkannten Grundsätzen für wissenschaftliche Abhandlungen selbstständig ausgeführt habe und alle verwendeten Hilfsmittel, insbesondere die zugrunde gelegte Literatur, genannt habe.

Weiters erkläre ich, dass ich dieses Dissertationsthema bisher weder im In- noch Ausland (einer Beurteilerin/einem Beurteiler zur Begutachtung) in irgendeiner Form als Prüfungsarbeit vorgelegt habe und dass diese Arbeit mit der vom Begutachter beurteilten Arbeit übereinstimmt.

Wien, im Oktober 2017

---

Esther Knittl

## Acknowledgements / Danksagung

Zu allererst möchte ich mich bei **Prof. Dr. Wolfgang Linert** bedanken, der meine Arbeit hier an der TU Wien ermöglicht hat und meinem wissenschaftlichen Schaffen, auch bei der Auswahl meines Themas, sehr viel Freiraum eingeräumt hat, wodurch ich eine sehr selbstständige Arbeitsweise entwickeln durfte. Wenn es nötig war, hatte er jedoch immer ein offenes Ohr für mich und unterstützte mich außerordentlich!

I want to thank **Prof. Dr. Miki Hasegawa** for the extraordinary good cooperation between our groups and the possibility to perform ligand synthesis together with her students under her supervision.

Furthermore, I want to thank **Prof. Dr. Alexey Gusev**, who supported me during his yearly visits to our university with constructive discussions and advices concerning my science. Also, I want to thank him for performing the fluorescence measurements and elemental analysis on my compounds.

Für das Messen und Lösen der Kristallstrukturen meiner Einkristalle möchte ich mich bei **Berthold Stöger, Daniel Himmelbauer, Jan Pecak** und **Markus Rotter** außerordentlich bedanken.

Ich danke **Matthias Mastalir** und **Nikolaus Gorgas**, die mir bei der Aufnahme der NMR-Spektren eine sehr große Hilfe waren.

Außerdem möchte ich mich bei **Jan Pecak** für die Hilfe mit theoretischen Berechnungen meiner Verbindungen recht herzlich bedanken.

Ich möchte mich bei all meinen Kollegen bedanken! Marlene, Roland, Matthias, Julian, Clara, Stefan, Gerald, Wolfgang, Daniel, Jan, Markus, Nikolaus, Martin, Sara, Sarah, Sathy, Bernhard, Peter, Christian, Marco, Georg und Danny sind mir in den letzten Jahren sehr gute Freunde geworden. An dieser Stelle möchte ich mich auch bei meinen Bachelor-Studenten und Wahlpraktikanten bedanken, die etwas zu dieser Arbeit beigetragen haben.

Bei **Mathias Glatz** möchte ich mich ganz besonders bedanken, da er mir immer eine große Hilfe war und mir vor allem bei der Arbeit im Labor mit Rat und Tat zur Seite stand.

Bei den Mitgliedern meines Ultimate-Frisbee Teams **Lokomotive St. Oli** bedanke ich mich von ganzem Herzen, da sie mir in den letzten Jahren den nötigen Ausgleich gegeben haben und mich mit motivierenden Worten unterstützten. Bei **Diego Heatherman** möchte ich mich besonders für seine Hilfe mit der englischen Sprache bedanken.

Ich möchte mich bei meiner Chemieprofessorin **Mag. Elisabeth Dietrich** bedanken, die bereits während meiner Zeit im Gymnasium Kurzwiese in Eisenstadt mein Interesse an der Chemie geweckt hat.

Der größte Dank gebührt meiner Familie für die Ermöglichung meines Studiums. Meiner Mutter **Elisabeth** und meinem Vater **Joachim** danke ich, da sie mich bei meiner Arbeit immer motiviert und unterstützt haben, meiner **Oma** danke ich für den Antrieb, den sie mir während der Fertigstellung dieser Arbeit gab. Meinem Bruder **David** danke ich ganz besonders, da er mir **IMMER** eine große Hilfe ist.

## Kurzfassung

Die Forschung an Chemosensoren und Schaltern zur Detektion von Metallionen und Anionen erlangte in den letzten Jahren große Aufmerksamkeit, da die Konzentration unterschiedlichster Metallionen im menschlichen Organismus eine sehr große Rolle in einer Vielzahl biologischer Prozesse spielt. Aktive Zentren essentieller Enzyme enthalten oft Metallionen, deren Konzentrationsschwankungen dazu führen, dass diese Enzyme in ihrer Funktion beeinträchtigt werden, wodurch Krankheiten und Behinderungen ausgelöst werden können. Aus diesem Grund ist die Erforschung von Sensoren mit hoher Sensitivität und Selektivität von großer Bedeutung. Eine Technik, die auf der Messung von Fluoreszenz beruht, ist hierbei hoch interessant, da im Vergleich zu herkömmlichen Analysemethoden, sehr niedrige Konzentrationen erfasst werden können.

Zink-Ionen zählen zu den „stillen“ Metallionen, da sie weder eine Farbe haben, noch magnetisch oder redox-aktiv sind. Aus diesem Grund erkannte man erst relativ spät, wie wichtig es für den menschlichen Organismus ist und welche Rolle es darin spielt. Liganden-Systeme sind bereits bekannt, die grundsätzlich keine lumineszierenden Eigenschaften haben, jedoch entwickeln, sobald ein Übergangsmetall wie Zink koordiniert. Auf diese Weise kann eine sehr sensitive Methode zum Nachweis von Metallionen entwickelt werden.

Im Zuge dieser Arbeit wurden neue ONNO-Schiff Basen synthetisiert, die in ihrer Fähigkeit analysiert wurden, mit Zink, Cadmium und Vanadium Koordinationsverbindungen zu bilden. Die Struktur der Liganden selbst wurden möglichst so gestaltet, dass sie kaum bewegliche Teile enthält und über ein möglichst großes konjugiertes aromatisches System verfügt. Auf diese Weise können Intensitäten der Fluoreszenzeigenschaften der finalen Koordinationsverbindungen erzielt werden, wodurch ein Einsatz der Liganden im Bereich von sensitiven Chemosensoren ermöglicht wird. Die Strukturen der gebildeten Komplexe mit den untersuchten Metallionen sind relativ unterschiedlich: Zn-Komplexe, die mit diesen Liganden gebildet werden, weisen quadratisch planare Geometrien auf, während Cd-Verbindungen zweikernig sind und die Metallzentren sich in quadratisch pyramidalen Umgebungen befinden. Unter Verwendung eines Oxovanadium-Präkursors bilden sich quadratisch pyramidale Komplexe aus. Alle Koordinationsverbindungen wurden insbesondere auf ihre Fluoreszenzeigenschaften untersucht und erzielten einzigartige Ergebnisse.

## Abstract

The research on chemical sensors and switches for metal ions and anions has received great attention in recent years. The concentration of various metal ions in the human body plays a very important role in many biological processes, since they are often part of the active centres of enzymes. Their absence or overload can cause a wide range of diseases and disorders, which is why powerful sensors with high selectivity and sensitivity are of great importance. Techniques based on fluorescence are quite interesting in these terms, due to the fact that compared to usual analytical methods, very low concentrations can be recognized.

In general, zinc-ions are silent metal ions. They do not have a colour and are redox inactive and magnetically silent. This is one reason why its importance in the human organism was not realized, until analytical methods improved. To make them visible, ligand systems were developed, which do not exhibit fluorescence in their pure form, but become fluorescent, when transition metals like  $\text{Zn}^{2+}$  are included in their structures. In this way, powerful tools for a sensitive and selective detection of metal ions can be developed.

In the course of this thesis, new ONNO-Schiff bases were synthesized to be used as ligands, which were tested upon binding to zinc, cadmium and vanadium. By introducing rigid building blocks, which contain a huge aromatic system, into the ligand-structures, high fluorescence quantum yields could be achieved, which bear the possibility of a usage as highly sensitive chemo sensors. The structures of the synthesized coordination compounds were quite diverse: Zinc was found to form square planar complexes with this class of ligands, while cadmium developed two-nuclear complexes, with the metal centres in square pyramidal geometries. By using an oxo-vanadium metal precursor, square pyramidal complexes were formed, with the oxo-ligand remaining in the final coordination compound's structures. All coordination compounds were fully analysed, especially in terms of their fluorescence behaviour and revealed remarkable results.

Furthermore, a six dentate pyridyl-ligand was synthesized. This ligand plays a very important role in the coordination chemistry of lanthanides. In fact, this kind of complexes show, among other important characteristics, a very interesting luminescence behaviour, which bears the possibility of a usage in screens and other devices.

## Table of Contents

1	Introduction.....	1
2	Formula Schemes .....	3
2.1	Schiff-Base Ligands .....	3
2.2	Hexadentate N-Containing Ligand .....	4
2.3	Coordination Compounds .....	4
3	General Aspects.....	7
3.1	Luminescence .....	7
3.1.1	Historical Introduction.....	7
3.1.2	Importance of Luminescence .....	7
3.1.3	Types of Luminescence.....	9
3.1.4	Photochemical Pathways.....	10
3.2	Metals – a general Survey .....	12
3.2.1	Zinc.....	13
3.2.2	Cadmium.....	14
3.2.3	Vanadium.....	15
3.2.4	Rare Earth Metals .....	15
3.3	Ligand Architecture and Coordination Compounds .....	16
3.3.1	Schiff Bases .....	16
3.3.2	Pyridine-type Ligands .....	21
3.3.3	Ligands, including a Coumarin Building Block .....	25
4	Synthesis and Characterization of new Compounds .....	26
4.1	Synthesis of Ligands and Coordination Compounds.....	26
4.1.1	Bidentate Ligand.....	26
4.1.2	Tetradentate Ligands.....	27
4.1.3	Hexadentate Ligand.....	30



4.2	Characterization .....	31
4.2.1	Remarkable Features of Recorded NMR-Spectra .....	31
4.2.2	Results of IR-Measurements .....	35
4.2.3	UV/VIS.....	35
4.2.4	Fluorescence Analysis .....	42
4.2.5	X-Ray Analysis of Single Crystals.....	48
4.2.6	DFT-Calculations .....	54
5	Experimental .....	58
5.1	General remarks.....	58
5.2	Analytical Methods.....	58
5.2.1	NMR-spectroscopy .....	58
5.2.2	IR-spectroscopy .....	58
5.2.3	UV/VIS Spectroscopy .....	59
5.2.4	Luminescence Spectra .....	59
5.2.5	Elemental Analysis.....	60
5.2.6	X-Ray Structure Determination .....	60
5.2.7	DFT-Calculations .....	60
5.3	Synthesis of Organic Ligands.....	61
5.3.1	Synthesis of Benzoyl Acetonitrile .....	61
5.3.2	Synthesis of 1-Methyl-3-Phenyl-1H-Pyrazol-5-Amine.....	62
5.3.3	Synthesis of 1-Methyl-3-Phenyl-1H-Pyrazole-4,5-Diamine.....	63
5.3.4	Synthesis of 4.5-[Di(phenylimino)methyl]-1-Methyl-3-phenyl-1H-Pyrazole .....	64
5.3.5	Synthesis of Methyl Pivalate .....	65
5.3.6	Synthesis of 4,4-Dimethyl-3-Oxo-Pentanenitrile.....	65
5.3.7	Synthesis of 3-(1,1-Dimethylethyl)-1-Methyl-1H-Pyrazol-5-Amine .....	66

5.3.8	Synthesis of 3-(1,1-Dimethylethyl)-1-Methyl-1H-Pyrazole-4,5-Diamine .....	67
5.3.9	Synthesis of 3-(1,1-Dimethylethyl)-4,5-[Di(phenylimino)methyl]-1-Methyl-1H-Pyrazole .....	68
5.3.10	Synthesis of 1,2-Bis[[2-Hydroxyphenyl]Methylene]Amino]Benzene.....	69
5.3.11	Synthesis of 3-Acetyl-4-Hydroxychromen-2-One .....	70
5.3.12	Synthesis of [1,2-Phenylbis(Iminoethylidyne)]Bis[2H-1-Benzopyran-2,4(3H)-Dione] .....	71
5.3.13	Synthesis of (3E,3'E)-3,3'-[1,2-Ethanediybis (Iminoethylidyne)] Bis [2H-1-Benzopyran-2,4(3H)-Dione] .....	72
5.3.14	Synthesis of [1,2-Cyclohexylbis(Iminoethylidyne)]Bis[2H-1-Benzopyran-2,4(3H)-Dione] .....	73
5.3.15	Synthesis of 2-Methyl-1,10-Phenanthroline .....	74
5.3.16	Synthesis of 1,10-Phenanthroline-2-Carbaldehyde .....	75
5.3.17	Synthesis of N,N'-(Ethane-1,2-Diyl)-Bis(1,10-Phenanthroline-2-Yl)Methanimin .....	76
5.4	Synthesis of coordination Compounds .....	76
5.4.1	Coordination Compounds of Zn .....	77
5.4.2	Coordination Compounds of Cd .....	81
5.4.3	Coordination Compounds of V .....	86
6	Conclusion and Outlook .....	91
7	Appendix.....	92
7.1	UV/VIS spectra - detailed results .....	92
7.2	X-ray – detailed results.....	99
7.2.1	Ia pyridine .....	99
7.2.2	Ia DMSO .....	101
7.2.3	IIa DMSO .....	103
7.2.4	8b DMSO.....	104

---

7.2.5	Ic.....	105
7.2.6	I .....	106
7.2.7	II .....	107
7.2.8	III .....	109
8	Abbreviations .....	111
9	List of Figures.....	113
10	List of Formulas .....	120
11	List of Tables.....	121
12	List of References .....	123



# 1 Introduction

Luminescent material plays a very important role in our daily life, in screens, as safety features of certain documents, and light-emitting diodes. It can hence no longer be set aside in the scientific world, as many analytical methods and reaction processes are based on this phenomenon. Even in nature, it isn't an unknown event, when we think about fluorescent rocks or fireflies.

In terms of analysis, the usage of chemo sensors, molecular switches and their applications in selective logic gate systems is gaining great attention. This will especially be the case, if it can be used in single molecule-systems. [1-3] Single analyte chemo sensors based on fluorescence signalling, which can be applied on the detection of transition metals, are very powerful tools in terms of analytical chemistry. In many biological systems, certain metal ions are essential for the activity of enzymes as part of their active centres. Since their concentration in the material is very low, their detection by conventional analytical methods is quite difficult. [4, 5]

The average concentration of zinc ions in the human body is 2 g per 70 kg body weight. It is, after iron, the second most common 3d-transition metal in the human organism. [6] This metal is part of many indispensable enzymes in our organism, and its detection is of vital importance, due to the fact that its absence can lead to a variety of disorders and diseases. [7] Therefore, powerful systems should be discovered for their analysis and detection.

One well-known system uses ONNO Schiff bases as tetradentate ligands for the detection of  $\text{Zn}^{2+}$ - and  $\text{Al}^{3+}$ -ions. The ligand itself is not luminescent, but becomes fluorescent after binding to certain metal ions, which enables their detection at very low concentrations. [8] By a modification of this ligands, the usage of rigid building blocks with big aromatic residues, fluorescence intensities can be increased, which leads to a more sensitive system for the detection of the respective analytes.

In the course of this thesis, new ligand systems were developed, and coordination compounds of zinc, cadmium, vanadium and europium were synthesized and analysed, in particular with regards to their fluorescence behaviour, which indicates the possibility of their applicability in luminescent materials and as chemo sensors.

## General Remarks

### Description of Compounds in the Text

Organic compounds, which were mentioned before in the chemical literature are designated with Arabic numerals. In this work synthesized compounds, which were not mentioned in the chemical literature before, are introduced with Roman numerals.

Coordination compounds are named with the number of their ligand and a letter (a = Zn, b = Cd, c = V, d = Eu).

### References to the Literature

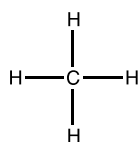
Within the text, references are marked with Arabic numerals in angular brackets.

### Nomenclature

The nomenclature of compounds, which have not yet been mentioned in the chemical literature, uses the IUPAC-based rules of Chemical Abstracts. Already known chemicals and reagents are partly designated by their trivial names.

In the experimental part, the empirical formula and the molar mass in [g/mol] are written below the structures.

Example:



chemical structure

CH<sub>4</sub>

sum formula

16.04

molar mass [g/mol]

## 2 Formula Schemes

### 2.1 Schiff-Base Ligands

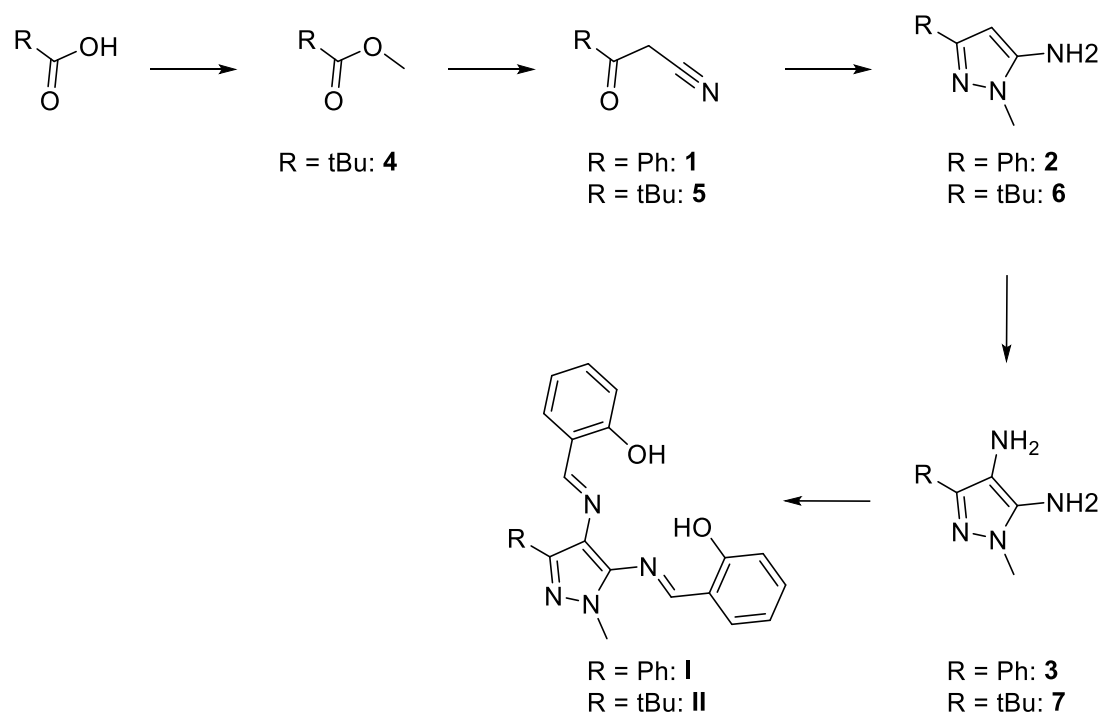


Figure 1: Synthesis of the Schiff-base Ligands I and II

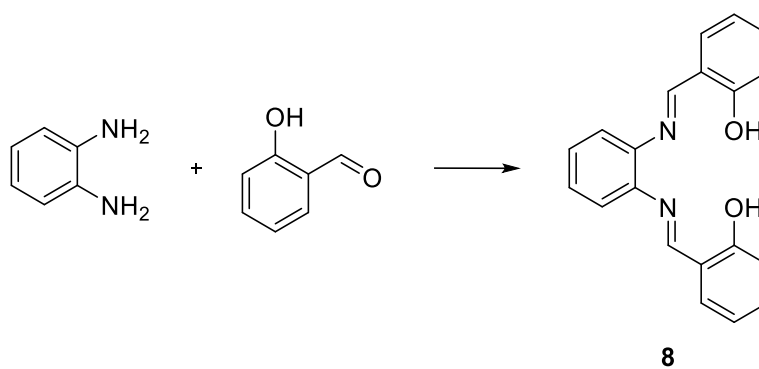


Figure 2: Synthesis of the simple Schiff-base Ligand 8

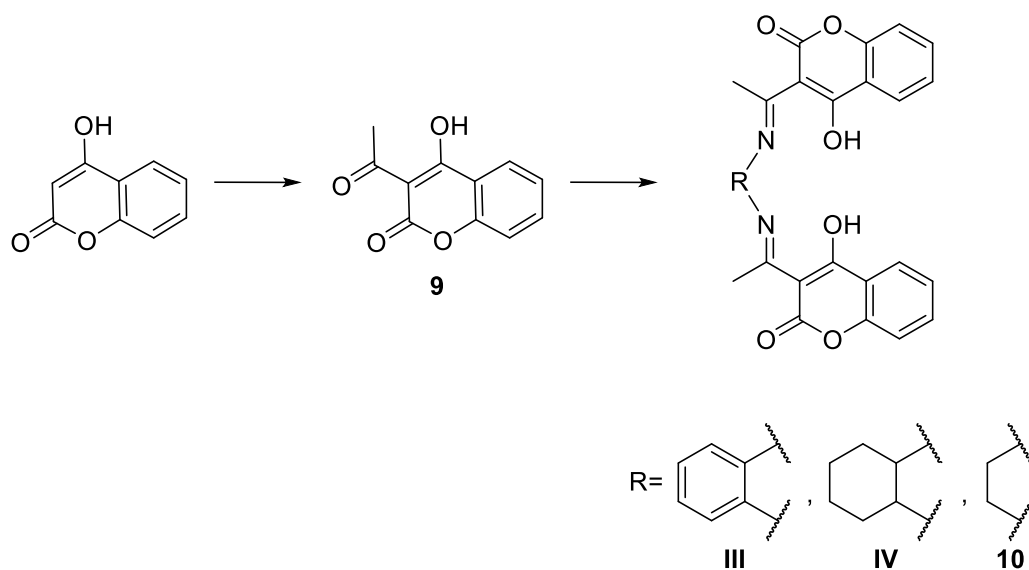


Figure 3: Synthesis of the Schiff-base Ligands III, IV and 10

## 2.2 Hexadentate N-Containing Ligand

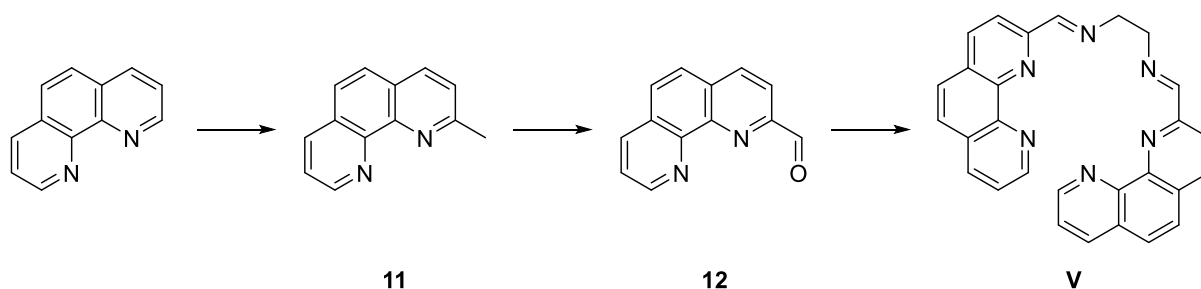


Figure 4: Hexadentate N-containing Ligand

## 2.3 Coordination Compounds

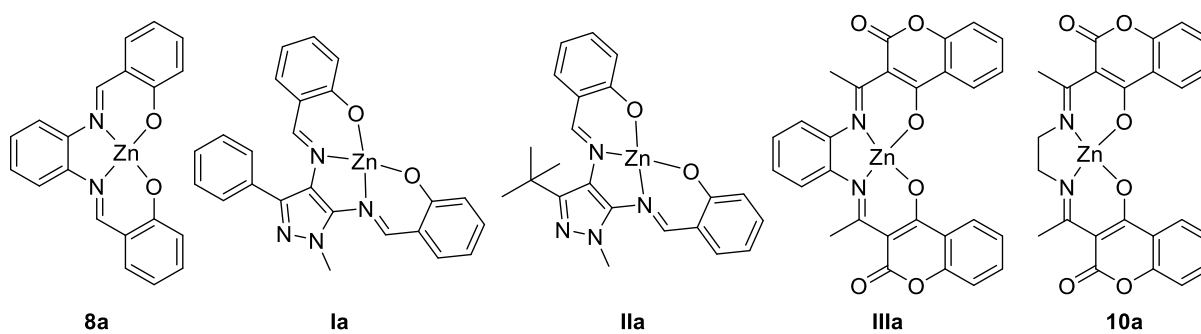
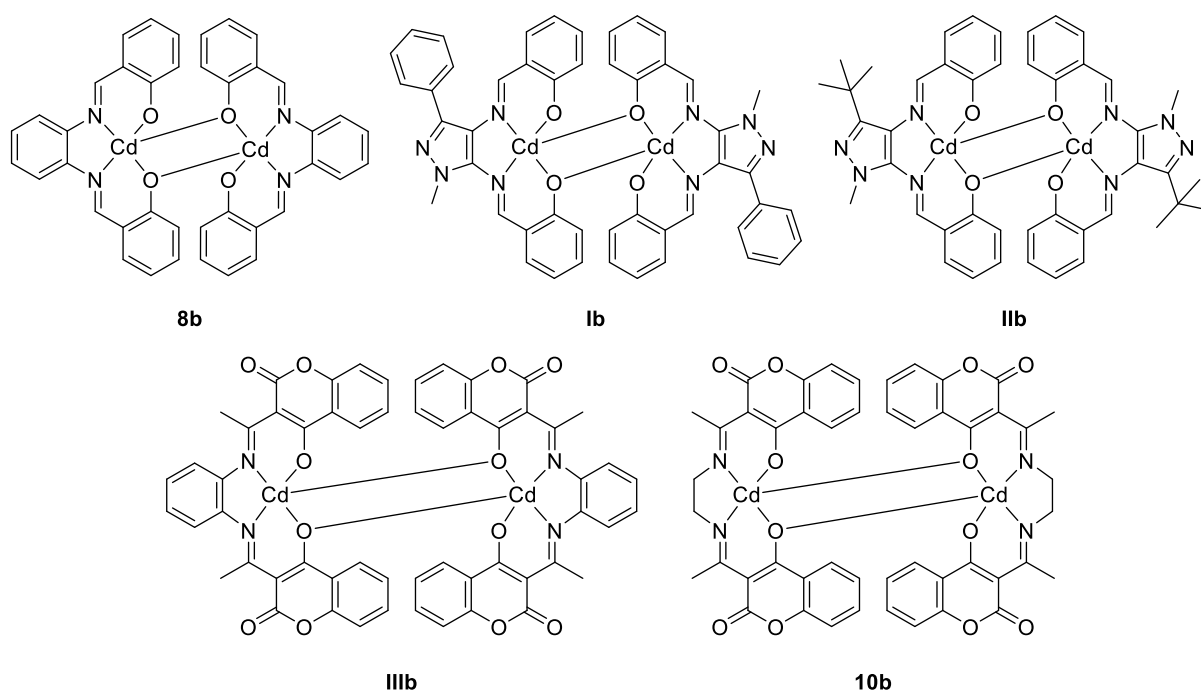
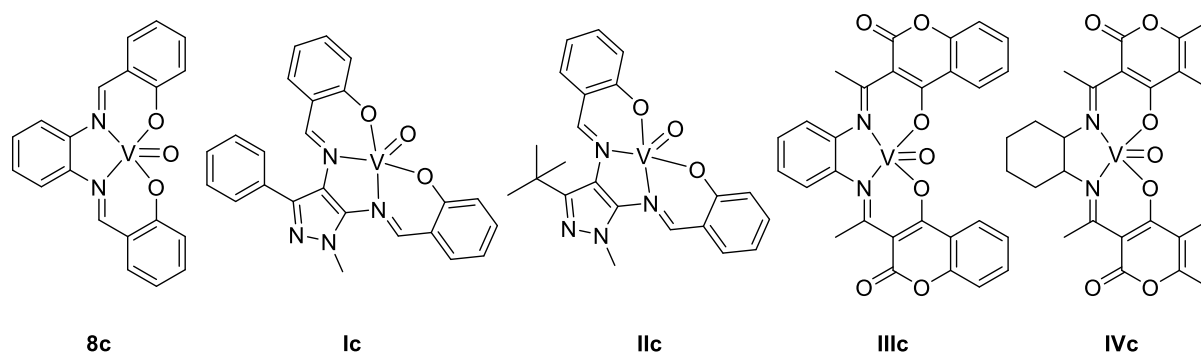
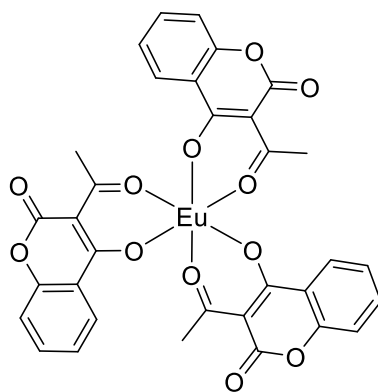


Figure 5: Coordination Compounds of Zn



**Figure 6: Coordination Compounds of Cd****Figure 7: Coordination Compounds of V**

**9d****Figure 8: Coordination Compound of Eu**

## 3 General Aspects

### 3.1 Luminescence

#### 3.1.1 Historical Introduction

People have been aware of the phenomenon of “luminescence” (lat.: lumen = light) for a very long time. In the era of Greek antiquity, the properties of luminescent material were already well-known. Theophrastus, a student of Aristotle, reported on stones, which were heated up in the sun and would glow afterwards in the dark [9].

#### 3.1.2 Importance of Luminescence

We meet luminescence in our daily life without our active recognition. When we turn on the light, the television or even just the screen of our computer at work, luminescence is present. Many documents like bank notes and passports contain luminescent material, to distinguish the original from a fake, which can be seen in the following Figure 9 and Figure 10.



Figure 9: Under UV-light the 20 euro note exhibits luminescence of Eu-oxides [10]



**Figure 10: The Austrian passport exhibits luminescence of Ln-compounds under UV-light [10]**

Even in nature, luminescence is a well-known phenomenon, if we think about fireflies, which have fluorescent minerals. Luminescence techniques even play a very important role concerning analytical techniques.

Luminescence describes the emission of electromagnetic radiation in the UV/VIS- and IR-region as a result of the input of energy, which does not end up in the heating of the material. It is ascribed to a transition from an excited state to the ground state. Light, which is emitted by luminescent material, is mostly located in the visible region of the spectrum and appears as cold glowing [11-13]. In Figure 11 the electromagnetic spectrum can be seen. The visible region of light is a quite small part, compared to the whole spectrum. [14]

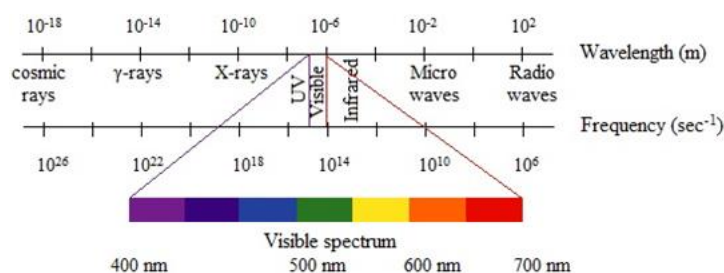


**Figure 11: the electromagnetic spectrum [14]**

### 3.1.3 Types of Luminescence

Different substances and materials can be excited by different forms of energy, whereby they are able to again release parts of this energy in the form of light. In this way, different types of luminescence can be differentiated by the way of their excitation:

- **Photoluminescence:**

Photoluminescence is the most well-known type. Here energy is transferred by means of the photons of light (often UV-light).

- **Chemiluminescence:**

Energy is here released as a result of a chemical reaction, for example the oxidation of phosphorus or the effect of chemical radicals. [15]

- **Bioluminescence:**

Here the source for the transfer of energy is a biological and thus associated with a chemical reason.

- **Radioluminescence:**

The material is excited by X-ray or nuclear particles (for example  $\alpha$ - and  $\beta$ -particles or  $\gamma$ -radiation).

- **Electroluminescence:**

In the case of electroluminescence, the effect of an electric field on the substance leads to an uptake of energy and thus, to its excitation.

- **Ionoluminescence:**

Ionoluminescence occurs by the activity of ions, which are at a high energy level and able to transfer energy.

- **Thermoluminescence:**

In compounds which release thermoluminescence, an activator is present, which can spend enough energy to lift the molecules of a certain substance to an excited energy level. In this case, it cannot be equated with thermic radiation, since this phenomenon happens at far lower temperature than glowing occurs.

All these types of luminescence lead to the same action – the release of energy in form of light after the excitation process. They only differ in the way of the uptake of energy to be lifted to the upper energy level. [9]

### 3.1.4 Photochemical Pathways

In fact, the excitation in a photochemical way is very different from a thermal one. A thermal excitation at 500 °C, for example, is not possible, if 400 °C were not reached before. In a photochemical way, everything is much more precise. Every molecule can be excited with a prior calculated energy [16]:

$$E = \frac{h \cdot c}{\lambda}$$

**Formula 1: Relation between energy and wavelength [16]**

This can be summarized in the words of Porterfield: *“It is thus possible to have a hot molecule without ever having had a warm molecule”*. [17]

In the following, various operations, which can be related to luminescence, are discussed in detail. Therefore, the Jablonski-diagram is illustrated in Figure 12. [18]

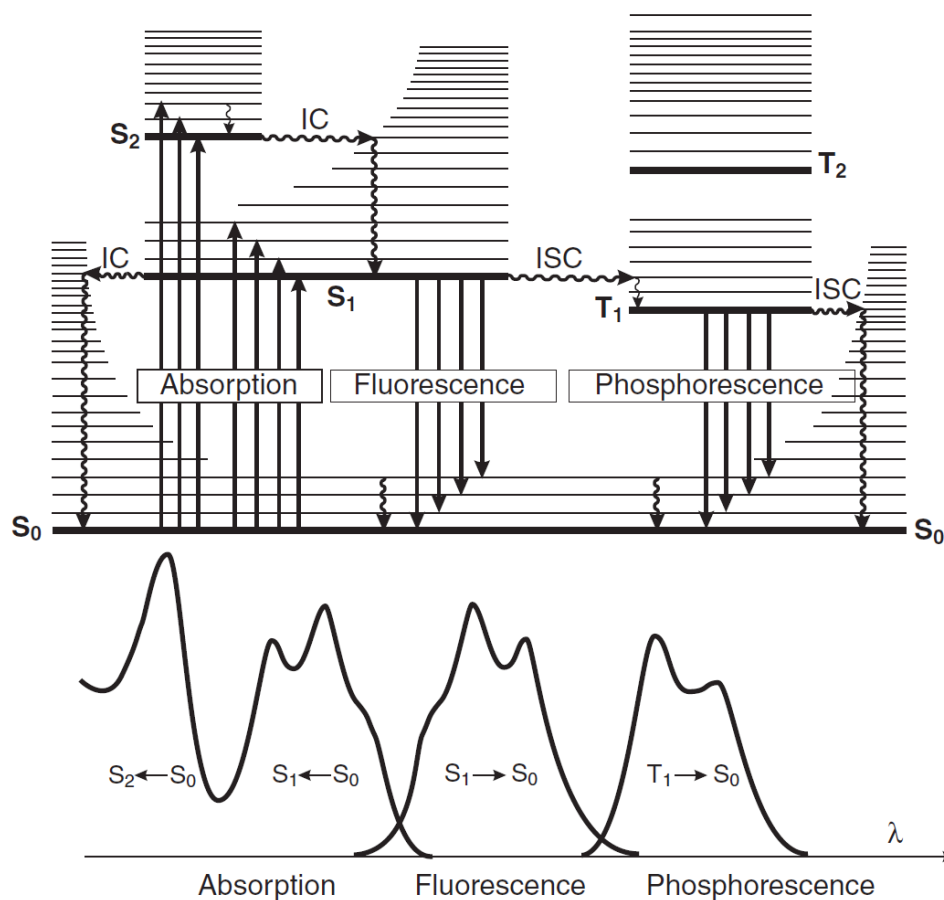


**Figure 12: Perrin-Jablonski diagram [18]**

**Absorption:** ( $10^{-15}$  s)

Absorption (lat.: absorptio = drink, beverage, swallowing) is the uptake of energy and thus the transition from the ground state ( $S_0$ ) to an excited level ( $S_1$  or  $S_2$ ) or a vibrational level of one of them, which usually happens very fast compared to the other processes. [18] In general, the absorption happens to start from the vibrational level of  $S_0$  with the lowest energy, since most molecules are located in this level at RT according to Boltzmann law. [19]

**Vibrational relaxation:** ( $10^{-12}$ - $10^{-10}$  s)

In general, vibrational levels are always associated with an electronic state, regardless of whether it is a singlet or triplet state. In the case of a vibrational relaxation, the energy is released non-radiational after the excitation, for example in the form of heat, which can be collisions with solvent molecules. [20]

**Internal conversion:** IC ( $10^{-11}$ - $10^{-9}$  s)

An internal conversion is a transition which proceeds without an irradiation of light between two electronic levels with the same spin multiplicity (for example  $S_2$  to  $S_1$ ). If this happens in solution, a vibrational relaxation will happen next until the lowest level of the final electronic state is reached. [18]

**Fluorescence:** ( $10^{-10}$ - $10^{-7}$  s)

Fluorescence is the relaxation from the  $S_1$ -singulet state to  $S_0$ . Despite some exceptions, the emission of fluorescence occurs from the  $S_1$ -level and therefore does not depend on the wavelength of the excitation. [18] Stokes rule says that the wavelength of the fluorescence-emission is always higher than its absorption wavelength. This is due to an energy loss, which can be related to vibrational relaxation processes. [21]

**Intersystem crossing:** ISC ( $10^{-10}$ - $10^{-8}$  s)

An intersystem crossing is a transition process from a singlet-state to a triplet-state, for example from  $S_1$  to  $T_1$ . It happens without any release of radiation between two isoelectronic vibrational levels. This process is always followed by other actions like vibrational relaxation or phosphorescence. In general, the transition between two levels of different multiplicity is forbidden, but it can be made possible, if spin-orbit coupling is big enough. Also, if heavy atoms (Pb, Pt, Br) are included in the luminescent material, spin-orbit coupling increases and thus, ISC can be favoured. [18]

**Phosphorescence:** ( $10^{-6}$ - $10$  s)

Phosphorescence is the transition from the  $T_1$ -triplet state to the ground state  $S_0$ . In fact, there is always a competition between phosphorescence and nonradiative relaxation, since this transition is actually a spin forbidden one. Because this process is very slow, many collisions of the material in the excited state with for example solvent molecules can happen, thus favouring an energy loss without irradiation of light. Only at very low temperatures and in solid media is phosphorescence favoured to occur, since under these conditions the lifetime of the triplet state can last longer. [22]

### 3.2 Metals – a general Survey

In this thesis, new coordination compounds of zinc, cadmium and vanadium were synthesized. In Figure 13 the periodic table of the elements is given, where the position of the before-mentioned metals can be seen.

Vanadium and zinc are first row transition metals. Cadmium is positioned just under zinc, which explains their chemical relation.

The occurrence of zinc and cadmium in the Earth's crust is 76 ppm and 0.16 ppm, respectively. These metals are amongst the group of the chalcophiles (from χαλκός (chalkos, greek) = ore, metal, in particular copper). During the solidifying phase of the Earth's crust, these metals precipitated in a reductive atmosphere as sulphides, that is why this form is also the most important occurrence of these metals. In the course of the effects of weathering, zinc and



cadmium were washed out of the rocks, after which carbonates, silicates and phosphates were formed. The coordination chemistry of these metals has not yet been extensively studied, compared to the other transition metals, but though there has been quite significant research on these as well. [6, 23, 24]

The periodic table displays elements from Hydrogen (1) to Oganesson (118). It includes the Lanthanide Series (57-71) and Actinide Series (89-103) at the bottom. Each element cell contains its atomic number, symbol, and name. Some cells also include the atomic weight.

Figure 13: periodic table of the elements [25]

Compared to zinc and cadmium, vanadium is with 136 ppm quite abundant in the Earth's crust, which is actually the 19<sup>th</sup> highest among all elements. Although this metal is quite widespread, its concentration in its natural mineral deposits is often low. In general, it occurs in the form of oxygen containing ore, although many important natural deposits include polysulfide (VS<sub>4</sub>) as a vanadium-source. [6]

The rare earth metals include scandium, yttrium and the lanthanides. These metals have very similar characteristics, which makes purification processes difficult and expensive. Mineral deposits with the highest economic importance include the minerals monazite, which contains La-, Th- and Ln-phosphates, and bastnaesite, which is a family of carbonate-fluoride minerals. [6]

### 3.2.1 Zinc

Zinc is a d<sup>10</sup>-transition metal, which occurs only in one oxidation state, namely zinc(II). [6]

### 3.2.1.1 Zinc and its Biochemical Importance

With a concentration of 2 g per 70 kg body weight, zinc is the second most common 3d-metal in the human organism after iron. It is extremely noticeable that, from a biological point of view, zinc is a very important metal, on which many forms of life are dependent, since it is included in many enzymes and thus, controls their activity. Cadmium, on the other hand, does not have any biological function, moreover, it is one of the elements with the highest toxicity. [6]

With its completed d-orbital, zinc(II) is diamagnetic and almost always colourless in coordination compounds. As a result, the detection of zinc-containing proteins was not possible, until analytical methods improved. So far, more than 300 enzymes are known. Amongst these are many essential ones, which catalyse the synthesis (synthetase, polymerase, ligase or transferase) and degradation (hydrolase) of proteins, nucleic acids, lipid-molecules and other bioorganic compounds. [26] A deficiency of zinc can lead to anorexia, blunting of taste, tendency to inflammation and impairment of the immune system, which are symptoms similar to AIDS. [7]

There are many ways in which metals can be involved in biochemical pathways and systems. In general, metals like zinc, which do not change their oxidation states easily, may function as structural elements in enzymes, such as superoxide dismutase and zinc fingers, or as triggers for the activity of proteins. In these functions, zinc(II) can have coordination numbers of 4 or 5 in tetrahedral or square pyramidal geometries, respectively. [27, 28]

### 3.2.2 Cadmium

Cadmium is, just as zinc, a  $d^{10}$ -transition metal, which almost exclusively occurs in the oxidation state +2. [6]

Due to its high toxicity, the exposure of human beings to cadmium can cause serious health problems. Many diseases and dysfunctions are related to a contact with this toxic element. Even certain forms of cancer can have their origin in a cadmium contamination of the humans environment and food. [29]

Since cadmium can cause a variety of problems, analytical methods have to be found to detect it, especially in very low concentrations.

### 3.2.3 Vanadium

Since vanadium has 5 valence electrons, its maximum oxidation state is +5. It can exist in its  $d^0$ ,  $d^1$ ,  $d^2$  and  $d^3$ -configurations and thus, various oxidation states. In this thesis, the focus was on V-coordination compounds in their  $d^1$ -configuration, where complexes with the metal in its oxidation state +4 were synthesized. Under these circumstances, vanadium-complexes have coordination numbers of 5, at which almost exclusively square pyramidal geometries are formed. [6, 30] As starting material for the here synthesized V-complexes,  $\text{VO}(\text{acac})_2$  was used. In the final coordination compounds, the oxygen remained, while the acetylacetonate-moieties were replaced by a tetradentate ligand. This was accompanied by a colour-change from turquoise to green.

### 3.2.4 Rare Earth Metals

The lanthanides are the first metals where the 4f-orbitals are filled with electrons. All of them occur in the oxidation state of +3. Since the ionic radii (Figure 14) of the  $\text{Ln}^{3+}$ s are quite similar to  $\text{Sc}^{3+}$  and  $\text{Y}^{3+}$ , there is quite a relationship between these metals and they are thus combined into a group – the rare earth metals. [30]

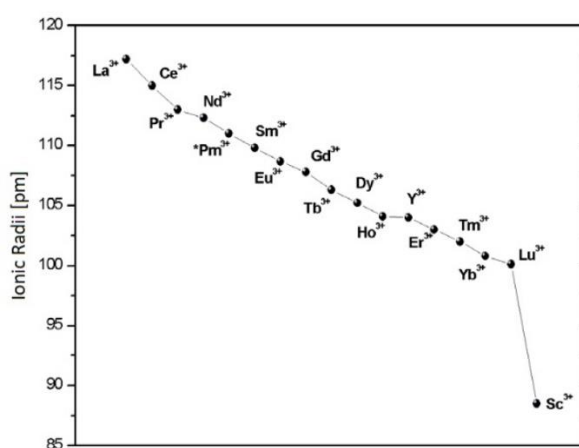


Figure 14: Ionic radii of the lanthanides [30]

One of the most important aperiodic characteristics of the rare earth metals is the lanthanide contraction, which is the decrease of the  $\text{Ln}^{3+}$ -ionic radius with increasing atomic number. In fact, this happens due to the rising charge of the atomic nucleus, which therefore exerts a

growing force of attraction on the atomic shell. The fourteen elements after lanthanum feature the electronic configuration  $6s^2 5d^1 4f^n$  with  $n = 1-14$ . [30]

In general, the rare earth metals are very electropositive and reactive metals. Their coordination chemistry is quite different, compared to that of the d-transition metals. The coordination numbers are always quite high, and the complexes are noticeably labile, which is why mostly multidentate ligands are used in this research area. Only when the ligands are extremely bulky a coordination number of six and below can be achieved. Since d-electrons are not available for a  $\pi$ -back-bonding and the f-orbitals are quite indifferent, carbonyl complexes are extremely labile and thus could only be obtained at low temperatures and Ar-atmosphere. [6]

### 3.3 Ligand Architecture and Coordination Compounds

#### 3.3.1 Schiff Bases

The structure of Schiff bases, used as ligands in coordination chemistry can differ a lot. In general, they include N- and O-donor atoms, but there are even known ligands including just N-atoms or N- and S-donor atoms for coordination reactions. As a result, this kind of ligands can be mono-, bi-, or even tetra-functional. Their denticity can be very diverse, many ligands even have six or more donor-atoms, by which even polymeric coordination compounds can be formed.[31-37] In the following, tetradentate (N,N,O,O)-ligands are going to be discussed, since this group of ligands is one of the key issues, about which this thesis is about.

One of the most well-known tetradentate Schiff base ligands is  $sal_2en$  (Figure 15). This ligand is a bifunctional (N,N,O,O)-ligand. In fact,  $\pi$ -acceptor properties can be exhibited by the imine nitrogen, having an influence on its coordination chemistry. These kind of tetradentate ligands are in general synthesized by a nucleophilic addition, where a hemiaminal is formed. The imine itself, is finally built by a dehydration-reaction. In general, a coordination to a metal occurs via the two oxygen-atoms of the hydroxyl-groups after their deprotonations and the two nitrogen-atoms of the imine-groups. [38]

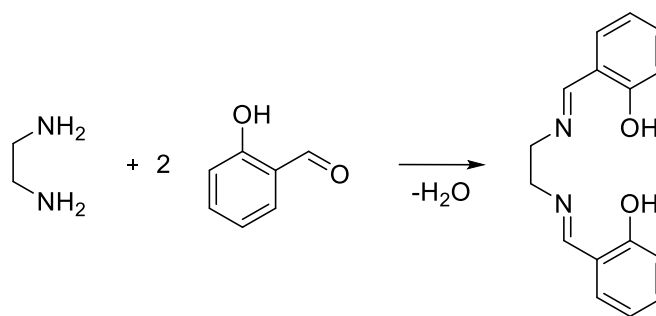


**Figure 15: Synthesis of Bis(salicylaldehyde)ethylenediamine (sal<sub>2</sub>en)**

The structural features of this system can be changed easily and thus, a big variety of ligands can be synthesized by just exchanging simple building blocks, namely the used diamines and aldehydes. The diamine for example can be aliphatic, aromatic, or even chiral, bearing the possibility of introducing new characteristics to the final complexes. Thus, the structural features of the used aldehydes contribute a lot to the properties of the final compounds. Also, the used aldehydes can be aliphatic or aromatic, if two different aldehydes are used, even asymmetrical ligand systems can be formed.

#### **3.3.1.1 Usage as Switches**

Molecular switches are – simply said – molecules, which can be switched between two stable or meta-stable states in a reversible fashion by means of an outside stimulus, just as the ON- or OFF-button of a bulb. One of the oldest molecular switches are pH-indicator systems, which are compounds that change their colour after a protonation or deprotonation and thus, give information about the pH of the system. [4, 39]

Another interesting example from the field of biochemistry is the protein rhodopsin (Figure 16 left). It is a transmembrane protein, which is part of the human's eye, where it is essential in the rod cells for the photonic vision. Humans, who lack this protein, are night-blind. In fact, rhodopsin includes the aldehyde retinal (Figure 16 right), which is the molecular switch in this system. When light reaches the human's eye, it is absorbed by this molecule, which immediately undergoes an isomerization reaction, leading to a conformational change of rhodopsin and consequently to a visual photo transduction. [40]

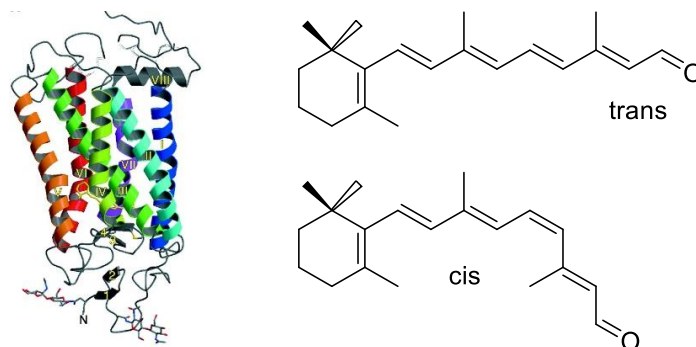


**Figure 16: LEFT: Rhodopsin [40], RIGHT: Retinal in its cis- and trans-conformation**

In the world of today, a tendency evolved to make every kind of technology smaller and thus more convenient. A similar characteristic can be observed in the scientific world, where chemists try to create a technology, which depends on just one single molecule. During the last years, a variety of new molecular systems was created, which reminds on technology in the macroscopic world. Systems, which act like machines [41], motors [42], gears [43], batteries, where coordination compounds of V with salophen-ligands come into play [44], and plugs[45] were developed already. Even more extraordinary systems were found, where single molecules act as logic gates, based on fluorescent signals [1-3].

Another practical and interesting application of fluorescent switches is the usage as single-analyte chemo sensors. Small molecules, such as simple cations (for example transition metals) or anions can be detected by means of a chemo sensor – a synthetic system. This kind of systems are developed for the selective binding of an analyte to a sensor, which includes a chromophore in its structure. The optical signal of the chemo sensor itself should be modified in a sufficient fashion after the analyte is included into its structure. [4, 5]

A well-known chemo sensor for cadmium is azacryptand. This is a ligand system, which does not show any fluorescence behaviour. Just, when cadmium-ions are included into its structure, high fluorescence can be measured. The quantum yield of this ligand in combination with cadmium is many times higher, compared to other metals, which accounts for its selectivity (Figure 17). In fact, there is another interesting feature of this system. A reversible ON/OFF situation can be caused, when anions ( $\text{Cl}^-$ ,  $\text{N}_3^-$ ,  $\text{SCN}^-$ ), which are able to form a coordinative bond with cadmium, are present. In this case, the metal is released again from azacryptand,

which results again in a loss of the fluorescence of this system. In this way, also anions can be detected. [46, 47]

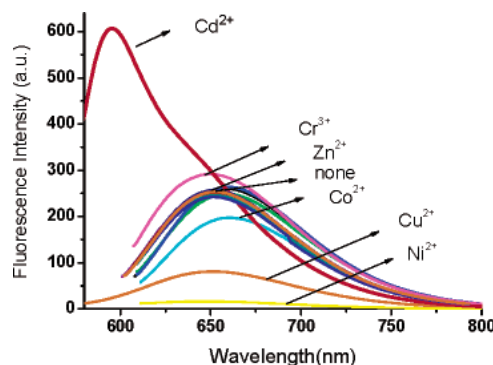


Figure 17: Fluorescence behaviour of the azacryptand system with different metal ions - selectivity [47]

### 3.3.1.2 Requirements

In fact, there are certain requirements, which should be fulfilled, to receive efficient signalling. One of the key-features of this kind of systems is that molecules, which are little- or non-fluorescent (OFF-mode), can easily and reversibly be converted into highly fluorescent molecules (ON-mode). If the enhancement of the fluorescence abilities of the molecule in the ON-mode is extremely high, there is even the possibility to detect in single molecule domains. Another important property is the formation of a rigid and planar systems, which bears the possibility to hold the active parts of the molecule in a fixed pre-oriented conformation and thus gain higher quantum yields of the fluorescent active mode of the molecule and reduce its possibility to be quenched without any irradiation of light. It was found that systems, which include a pyrazoline-derivative (Figure 18), achieve higher quantum yields, due to this facts. [48, 49]

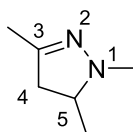


Figure 18: pyrazoline-derivative [48]

Moreover, transition metals are, regarding their properties, very powerful tools concerning their usage as molecular switches. Most transition metals can easily change between a variety of oxidation states. Just a simple redox reaction can result in a change of the transition metal's properties and thus its fluorescence behaviour. Just by an uptake or a release of one electron, the metal's characteristics can change drastically. It may have different magnetism properties, can differ in its electron-transfer tendencies, or even have different affinities in binding to a certain ligand. [39] In some cases, transition metals are not likely to change their oxidation states. It is then possible to adjust other parameters of the system to receive the desired action, by a change of the pH-value for example. If a ligand exists in both, a protonated and non-protonated form, according to the pH of the solution, the translocation of a metal may be possible more easily. [50]

### 3.3.1.3 Logic Gate Systems

Binuclear  $\text{Zn}^{2+}/\text{Ln}^{3+}$ -coordination compounds with the N,N'-bis(3-ethoxy-2-hydroxybenzyl)-substituted cyclohexane-1,2-diamine Schiff base were synthesized by Gloe and co-workers. It was found by applying X-ray single crystal analysis that zinc coordinates to the deprotonated ligand by its central  $\text{N}_2\text{O}_2$ -donor atoms and to one oxygen of an acetate-ion, which forms the bridge to  $\text{Ln}^{3+}$ . In this way,  $\text{Zn}^{2+}$  is surrounded by a distorted trigonal bipyramidal environment. [51] A logic gate system is known with a salen-ligand, which acts as a chemo sensor in the presence of  $\text{Zn}^{2+}$ - and  $\text{Al}^{3+}$ -ions (Figure 19). When Zn coordinates to the ligand in a tetradentate fashion, an AND logic-gate is formed, which is observed by an enhancement of the fluorescence at 450 nm. When  $\text{Al}^{3+}$  is present in the system too, high fluorescence can be observed at 500 nm, which leads to the formation of a second AND logic gate. The result is a three inputs AND logic gate system. [8]

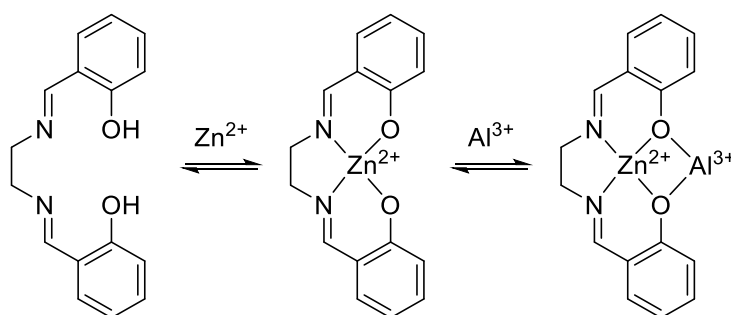


Figure 19: Logic gate system based on salen-ligand



It was further proved that even the pH-value had a major influence on this system. At very low pH, the fluorescence was very low, which led the system to be set to the OFF-mode. With increasing pH, the deprotonation of the salen-ligand is favoured and thus also fluorescence increases, which results the system to be switched to the ON-mode again. Since fluorescence is quenched with increasing temperature, higher fluorescence activity could be observed at lower temperatures. [8, 49, 52]

In order, to be useful as selective chemo sensor, the ability of the ligand to show the same fluorescence behaviour in the presence of other metals must be proved. It is possible to see in Figure 20 (left) that the fluorescence of the salen-system is many times higher in the presence of Zn-ions compared to other metal-ions. In a similar way it can be observed that the couple Zn-Al results in a much higher fluorescence compared to other metal couples (Figure 20 right). [8]

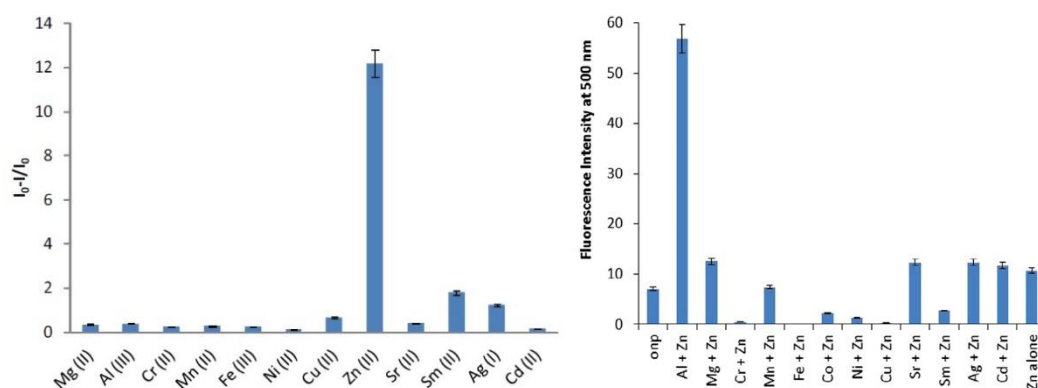


Figure 20: Selectivity of the salen-system in the presence of Zn<sup>2+</sup>-ions (LEFT) and Zn<sup>2+</sup>- and Al<sup>3+</sup>-ions (RIGHT) [8]

### 3.3.2 Pyridine-type Ligands

In fact, pyridine-type ligands show a much stronger ability to form coordination compounds compared to amine type ligands.

This is due to their capability of forming strong interactions between their  $\pi$ -conjugated system with the metal's orbitals. In Figure 21, a general survey of well-studied pyridine-type

ligands is given. This kind of ligands include two or more N-atoms in their structures, by which a coordinative bond to a metal can be formed. [53]

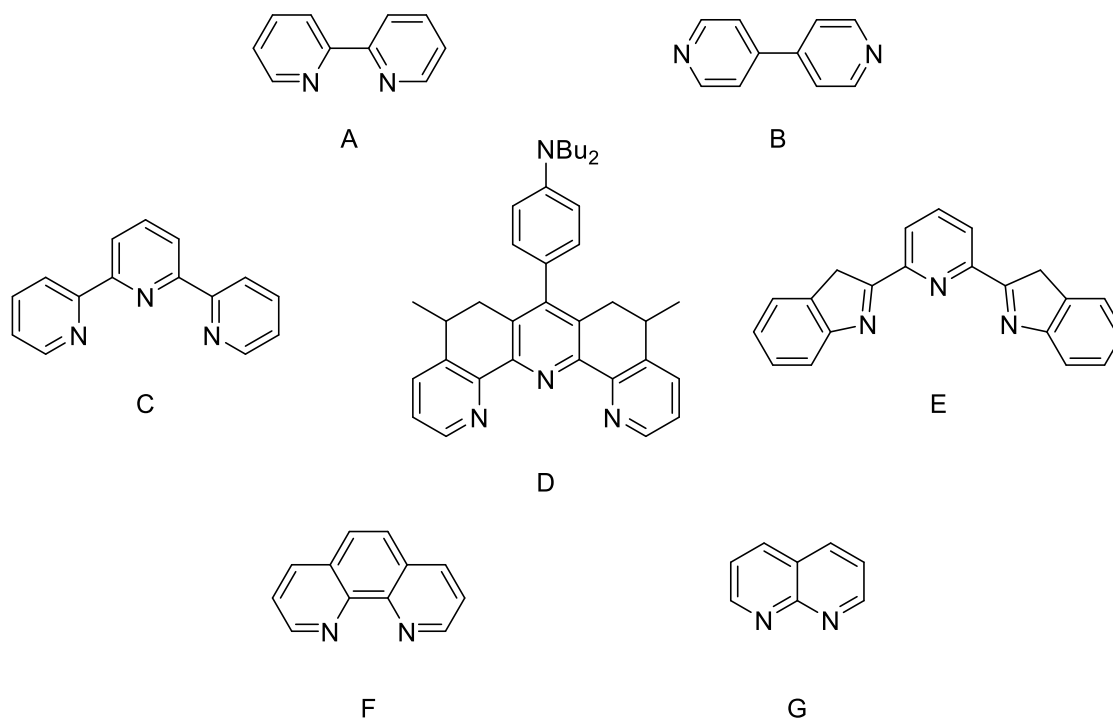


Figure 21: Pyridine-type ligands [53]

### 3.3.2.1 Usage in Luminescent Material

Luminescence is always a huge topic when it comes to coordination compounds of lanthanides. In general, this class of coordination compounds exhibit a very interesting luminescence behaviour, which is based on transitions of the metal's f-orbitals. Since these transitions are forbidden, the exhibited luminescence is quite weak. Higher quantum yields can be achieved by the usage of organic compounds with a huge conjugated  $\pi$ -system, which bears the possibility to act as a so-called photo antenna (Figure 22) by donating the via UV-light absorbed energy to the metal centre. The metal ion is held by the ligand in a quite fixed position by high coordination numbers (sometimes even 8 or 9), which reduces the probability of the metal in the excited state to be quenched in form of a non-radiative relaxation and thus enhances the intensity of the luminescence. [48, 53, 54]

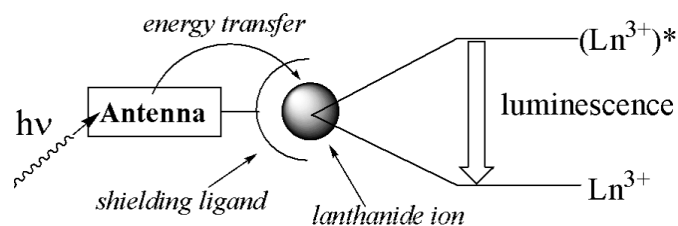


Figure 22: Energy-transfer in coordination compounds of pyridyl-like ligands [54]

In Figure 23 a simple energy diagram is portrayed, which gives an idea about how the energy can be transferred between the organic ligand system and the lanthanide metal centre in coordination compounds. After the absorption of UV-light of the ligand (photo antenna), the energy is transferred via an ISC beyond a triplet state or directly over an IC directly to the metal ion, to form the excited state. In the following, luminescence can be observed with a sufficient quantum yield by a relaxation of the metal to its ground state. [54]

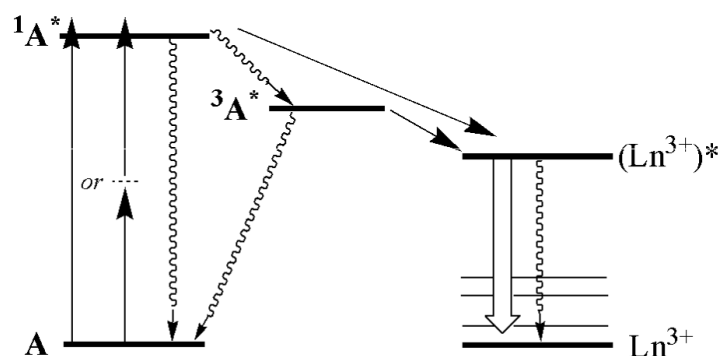
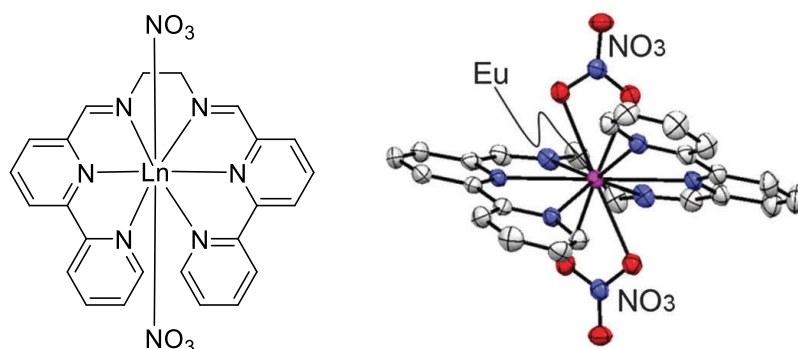


Figure 23: Transitions of luminescent lanthanide complexes in the energy diagram [54]

Due to a big variety of applications of highly luminescent lanthanide complexes, which is their usage in OLEDs [55-62], in systems for solar cells [63, 64] and as chemo sensors [65-68], they attracted many researcher's attention in the last years.

Ln-complexes with the metals Nd, Eu, Gd, Tb and Ho were prepared with a hexadentate pyridine-type ligand (Figure 24, left). The ligand consists of two bipyridine moieties, which are linked via an ethylenediamine-unit. The crystal structure of the Eu-complex of this ligand (Figure 24, right) reveals that the ligand forms a helical structure around the metal centre. Each bipyridine-part is positioned in one certain plane, whereby an angle is included between

these planes. Depending on the metal, this angle can differ between  $28.04^\circ$  and  $32.84^\circ$ . It was found that this kind of ligands are good energy donors to enhance the luminescence properties of lanthanides and thus, gain high quantum yields. [69]



**Figure 24: Structure of Ln-complexes with a hexadentate ligand (LEFT) and crystal structure of Eu-coordination compound (RIGHT) [69]**

The prior discussed coordination compounds can easily be transformed into MOFs (metal-organic framework) or PCPs (porous coordination polymers) by the addition of benzene-1,4-dicarboxylate, or similar dicarboxylic acids to the Ln-complex (Figure 25). [70] Due to the structure of this class of polymers, which is easily tuneable, they are of great interest because of their potential applicability as functional materials with extremely interesting fluorescence behaviours. [71-76]

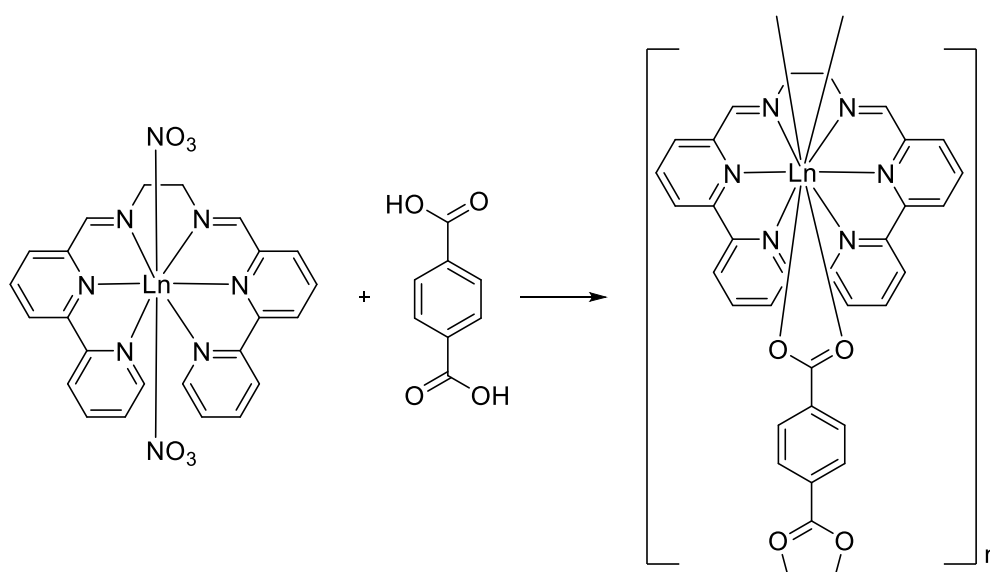


**Figure 25: Molecular structure of a polymeric lanthanide-coordination compound [70]**

### 3.3.3 Ligands, including a Coumarin Building Block

In fact, coumarins (Figure 26) can have special photochemical properties, which were found to show a fluorescence in the blue or green region of light. These compounds, in general, exhibit large stokes shifts and high quantum yields, concerning their fluorescence behaviour. [77] This facts lead to their easy applicability as laser dyes, fluorescent colours and sensitizers in phototherapy. [78, 79]

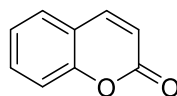


Figure 26: Coumarin building block

Coumarins, which are equipped with certain functional groups, are capable of being used in coordination chemistry as ligands and thus, metal complexes in various binding modes can be synthesized, which are used as therapeutically agents. With aldehyde-functionalities in the coumarin building block, it is possible to form ligands in form of Schiff base derivatives by simple condensation reactions with diamines, and thus, bearing the possibility of forming complexes of higher coordination numbers and stabilities. [80-82] Many of these compounds even show interesting biological and optical activities. [83] Coordination compounds of coumarin-derived ligands with various transition metals and lanthanides as for example zinc and europium were synthesized and analysed already. [84]

## 4 Synthesis and Characterization of new Compounds

### 4.1 Synthesis of Ligands and Coordination Compounds

In the course of this thesis, the synthesis and characterization of new di- tetra- and hexadentate ligands was carried out and coordination compounds thereof were formed for being utilized in fluorescent material, chemo sensors and switches.

#### 4.1.1 Bidentate Ligand

A bidentate ligand, carrying a coumarin building block in its structure, was synthesized by a acetylation reaction of 4-hydroxy-coumarin according to [85] with a yield of 79 %.

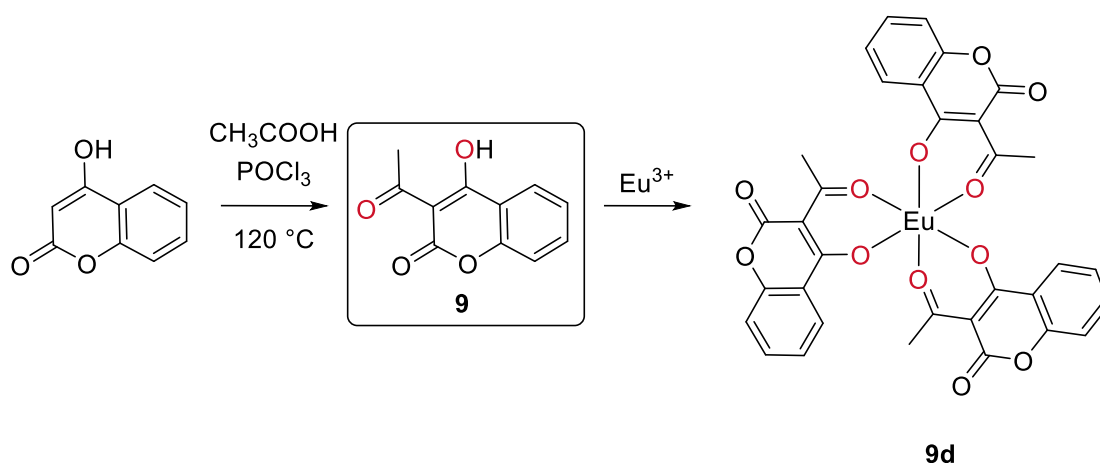


Figure 27: Synthetic pathway of 9 and its Eu-complex 9d

The synthesis was carried out, using acetic acid as an acetylation agent (Figure 27). In this way, a carboxyl-functionality was introduced into its structure. The two oxygen-atoms, marked red in Figure 27, are responsible for the formation of coordination compounds. By addition of Eu<sup>3+</sup>, a complexation occurs, whereby three ligand-molecules bind to the metal centre, thus, forming an octahedral coordination compound. In fact, this complex was found to exhibit characteristic red luminescence upon excitation with UV light.

### 4.1.2 Tetradentate Ligands

Using the bidentate ligand **9**, new tetradentate ligands could be synthesized by condensation reactions of the carboxyl-group marked blue in Figure 28 with 1,2-phenylenediamine, 1,2-cyclohexane and ethylenediamine, forming the ligands **III**, **IV** and **10**, respectively. [86] The results are ONNO-ligands, bearing two imine-groups and two hydroxyl-groups in their structures for binding to a transition metal. These two functional groups are capable of undergoing keto enol tautomerism, which results in the hydroxyl-group's proton being attributed to the imine-nitrogen and the formation of a ketone. It is worth to mention that this fact does not influence the behaviour of this ligands towards transition metals, since these protons were removed by a base prior the coordination reactions were carried out.

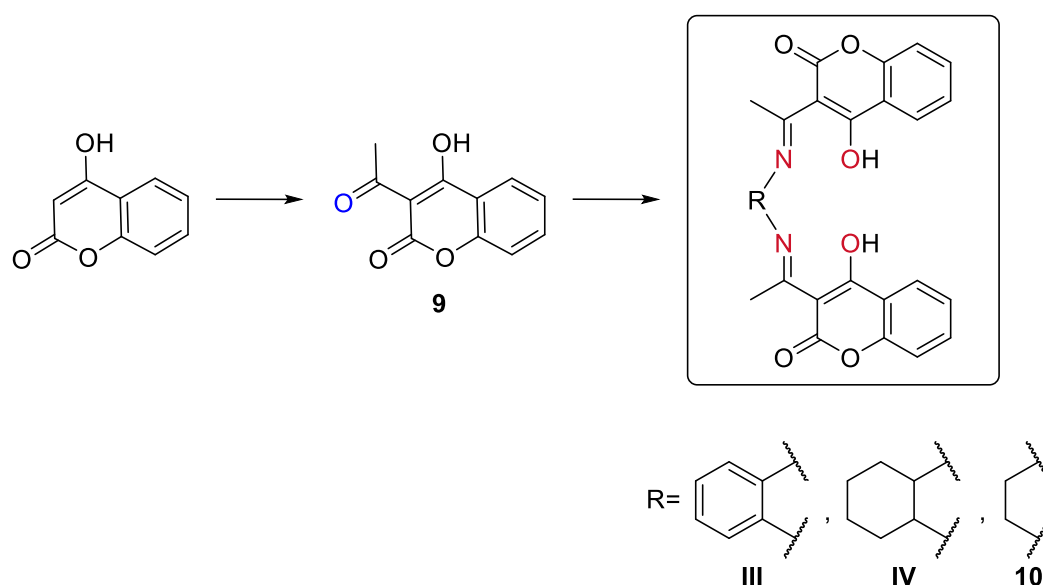


Figure 28: Approach of the synthesis of tetradentate Schiff bases, based on **9**

A second group of tetradentate Schiff bases was synthesized in 5 steps in course of this work, the approach is given in Figure 29. In a first step, an esterification was carried out in methanol under reflux conditions with the addition of sulfuric acid, whereby methyl-esters were formed. [87] Furthermore, the respective nitriles were formed by condensation reactions with acetonitrile, which was prior deprotonated with NaH in DMSO. [88] By a further reaction with methylhydrazine in MeOH, 5-membered rings (1H-pyrazol), which have one amine-group, could be synthesized. [89] In the next step, a second amine-group was introduced into the

structures of the ligand's precursors by first forming a nitro group by the addition of  $\text{NaNO}_2$ , which could then be reduced by the addition of  $\text{SnCl}_2 \cdot 2 \text{H}_2\text{O}$  in diluted  $\text{HCl}$ . In this way, diamines could be formed, which are not symmetrically. [90] The final ligands **I** and **II** could finally be received by simple condensation reactions of salicylaldehyde with both amine-groups of the prior synthesized diamines with overall yields of 12.4 % and 13.2 %, respectively, over all five steps. [86]

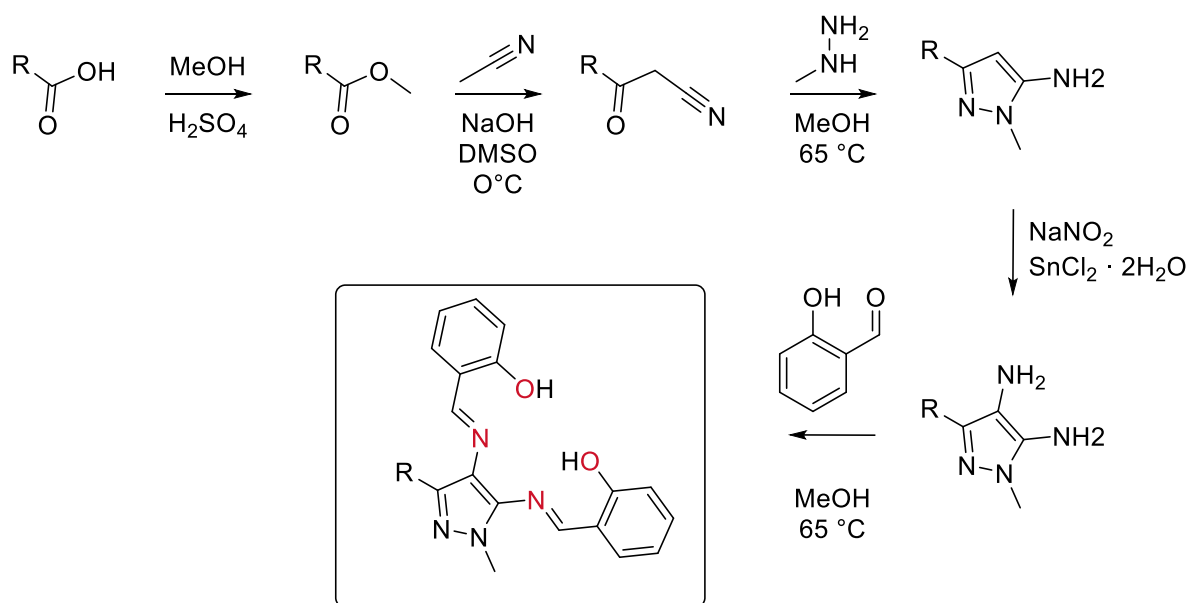


Figure 29: Approach of the synthesis of a tetradentate Schiff bases **I** ( $\text{R} = \text{Ph}$ ) and **II** ( $\text{R} = \text{tBu}$ )

It is worth to mention, that these ligands carry a pyrazol-building blocks in their structures. With the rigidity of this moiety, a better fluorescence behaviour can be achieved, whereby a non-radiative relaxation of the highly fluorescent excited states of the coordination compounds can be prevented, by holding the transition metal in a certain position and hinder it from moving. [48]

For the synthesis of the coordination compounds, in general, the ligands need to be deprotonated to be able to act as tetradentate ligand. To facilitate this deprotonation reaction, a base was added to the ligand's solution prior the addition of the transition metal, which improved the yield manifold. Also, the used metal precursor had a great impact on the formation of the coordination compounds. Thus, trials were carried out with ligand **8** and zinc,



to check, which conditions lead to the best results. In Table 1 the conditions are summarized with the achieved yields.

**Table 1: Tested conditions for the synthesis of 8a**

<i>metal precursor</i>	<i>base</i>	<i>yield (%)</i>
$Zn(AcO)_2 \cdot 2 H_2O$	-	< 5 %
	Et <sub>3</sub> N	< 5 %
	tBuOK	< 5 %
	MeLi	< 5 %
$ZnCl_2$	-	7 %
	Et <sub>3</sub> N	71 %
	tBuOK	65 %
	MeLi	63 %
$Zn(NO_3)_2 \cdot 6 H_2O$	-	6 %
	Et <sub>3</sub> N	<b>72 %</b>
	tBuOK	70 %
	MeLi	67 %

#### 4.1.2.1 Used Metal Precursors

As metal precursors in general zinc nitrate, -chloride and -acetate were tested. It is worth to mention that for  $Zn(AcO)_2 \cdot 2 H_2O$  under any conditions less than 5 % yield were achieved. This might be due to a quite strong bond between the acetate-oxygen and zinc. Quite good results were obtained by the usage of  $ZnCl_2$  and  $Zn(NO_3)_2 \cdot 6 H_2O$ , where yields between 60 % and 72 % were reached, whereupon with the nitrate slightly greater yields were gained.

#### 4.1.2.2 Effect of the Base

For the performed trials, no yield higher than 7 % could be achieved without addition of a base.

As a result, Et<sub>3</sub>N, tBuOK and MeLi were tested, to obtain greater yields. The best performance for the tested system was obtained by the usage of Et<sub>3</sub>N, which resulted in yields of 71 % and 72 % for zinc chloride and -nitrate, respectively, which were the best results. For these two metal precursors in combination with tBuOK and MeLi also quite good results could be received, with yields between 60 % and 70 %.

#### 4.1.2.3 Structure and Geometry of the Synthesized Coordination Compounds

Coordination compounds of the herein synthesized tetradentate ligands have quite different structures concerning the used metals (Figure 30). Zinc complexes form square planar geometries, while cadmium results in binuclear complexes, where cadmium-ions end up in square pyramidal environments with one hydroxyl-oxygen of each ligand bridging between the two metal centres. Since vanadium carries a oxo-ligand, it forms square-pyramidal complexes with the tetradentate Schiff bases.

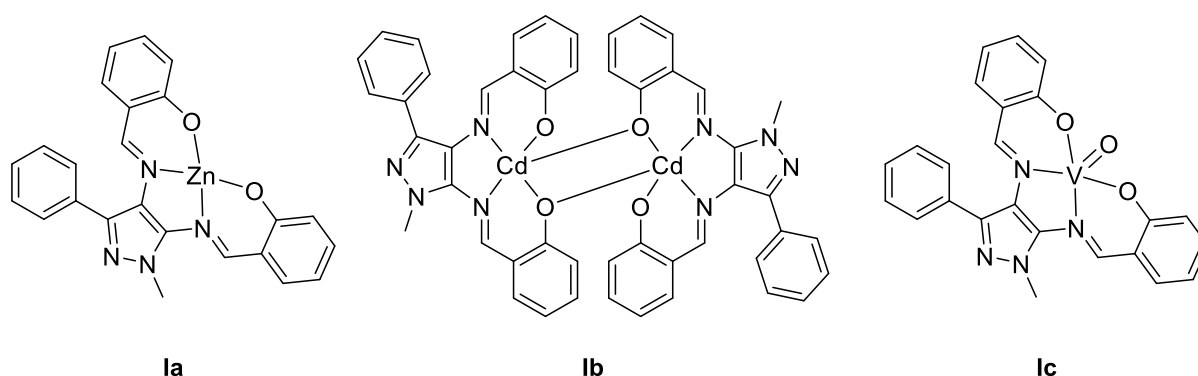


**Figure 30: Coordination compounds of tetradentate Schiff base I as an example**

The in Figure 30 demonstrated structures of the coordination compounds are proved by X-ray analysis of single crystals.

#### 4.1.3 Hexadentate Ligand

The hexadentate ligand **V** was synthesized in three steps, the detailed approach is given in Figure 31. In a first step, a methyl group was introduced into the structure of 1,10-phenanthroline by the addition of MeLi. [91] Furthermore, an oxidation of this methyl-group was done by refluxing **11** with SeO<sub>2</sub> in dioxane. In this step, it was essential to check the progress of the reaction by TLC. If the experiment was not stopped at the right moment, the oxidation would keep going to form the carboxylic acid, which is not preferable. [92] The final ligand **V** could be achieved by a condensation of **12** and ethylenediamine with an overall yield of 41.7 % over all three steps. [93]

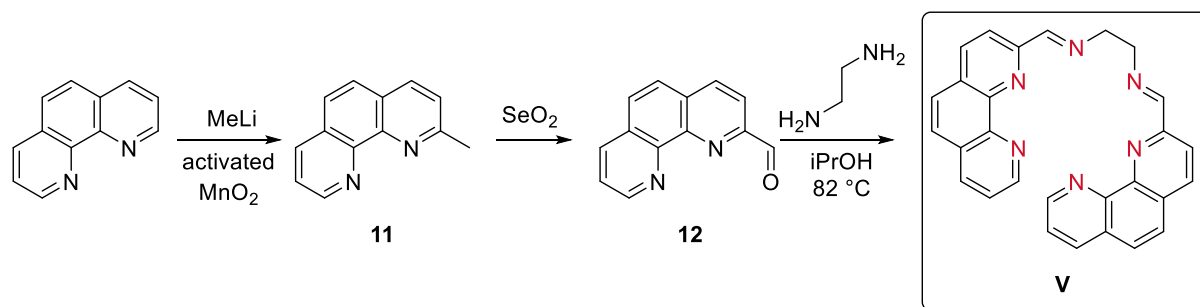


Figure 31: Approach of the synthesis of the hexadentate ligand **V**

This ligand is very useful for the synthesis of complexes of rare earth metals, forming coordination compounds with very interesting fluorescence behaviour. A coordination occurs via all six nitrogen atoms in the ligand's structure, thus building coordination compounds with high coordination numbers.

When the newly synthesized ligand **V** is compared with the one in Figure 24, where ethylenediamine bridges to bipyridine moieties, one can see that the structure of **V**, where the bipyridines are replaced by phenanthrolines, is much more rigid. This rigidity has a positive influence on the fluorescence behaviour of its lanthanide coordination compounds. Moreover, the  $\pi$ -aromatic system is expanded in the new ligand, thus bearing the possibility of achieving higher fluorescence quantum yields through a better uptake of the energy of the absorbed light.

## 4.2 Characterization

### 4.2.1 Remarkable Features of Recorded NMR-Spectra

$^1\text{H}$  and  $^{13}\text{C}$  NMR-spectra were recorded of all organic compounds and intermediates, Zn- and Cd-complexes. An overview of remarkable features of the recorded NMR-spectra is given in this section. For coordination compounds of Zn and Cd, it was even possible to demonstrate that a coordination of the metals to the respective ligands occurred by  $^1\text{H}$  NMR-experiments. This assumption was further proved by the determination of the complexes' structures by X-ray crystallography of single crystals (Results are given in the respective section.).

In following Figure 32 two spectra of ligand **I** are compared. The first spectrum was recorded in  $\text{CDCl}_3$  (in red) and the other spectrum after the addition of  $\text{D}_2\text{O}$  to the solution (in turquoise). There is no shift observable in both spectra for any signal. It is conspicuous that two broad signals in the region between 12 and 13 ppm are absent after the addition of  $\text{D}_2\text{O}$ . These signals are ascribed to the OH-hydrogens of the ligand, which are acidic ones. Due to their acidity, these peaks appear broader compared to the other signals. When  $\text{D}_2\text{O}$  is added to the solution before the measurement of the second NMR, an exchange occurs between hydrogen and deuterium and thus, the signals are not visible anymore in the NMR and disappear.

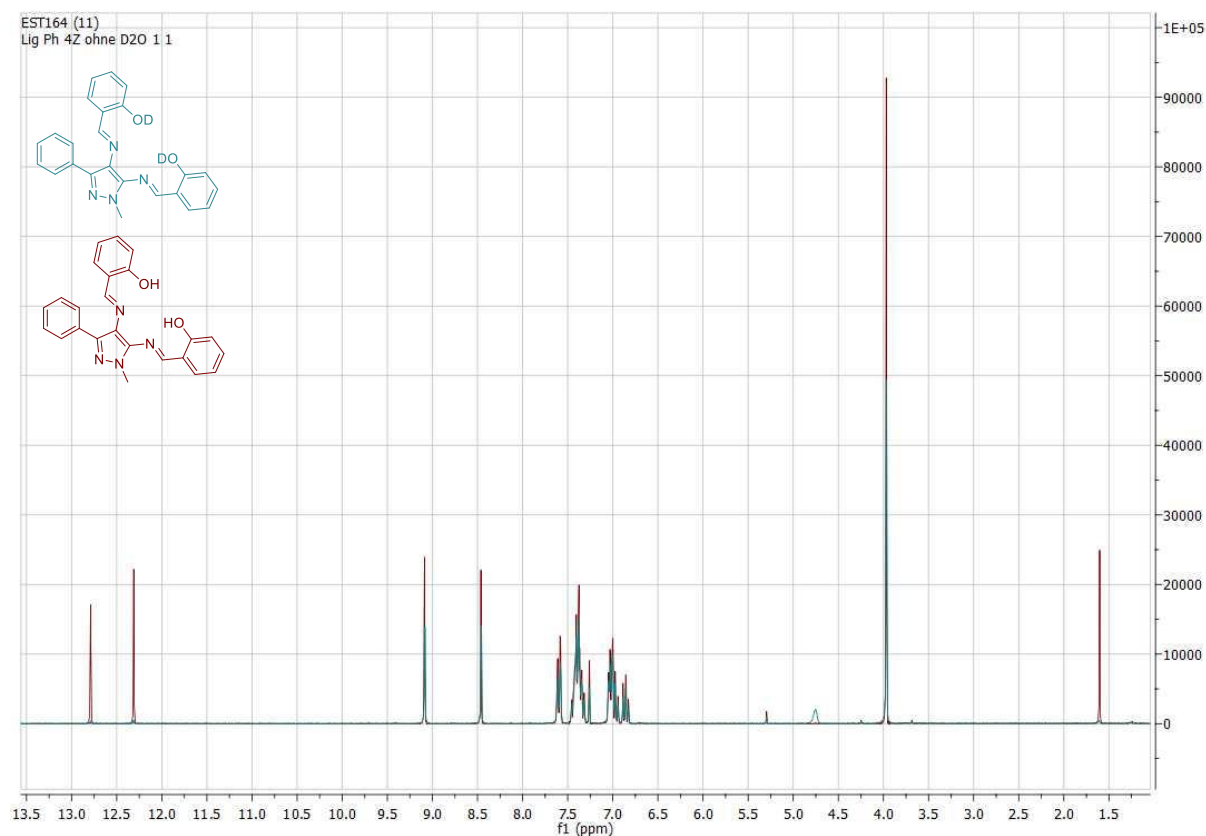


**Figure 32: Comparison of the  $^1\text{H}$  NMR-spectra of **I** in  $\text{CDCl}_3$  (red) and after addition of  $\text{D}_2\text{O}$  (turquoise)**

In Figure 33 below, the proton NMR-spectrum of the Zinc-complex **Ia** is compared with the spectrum of its free ligand **I**. Both spectra were measured in DMSO. At 3.33 ppm, a water-peak can be seen in both spectra, which has its origin in the hygroscopicity of the deuterated solvent itself. IR-measurements were carried out, to guarantee the dryness of the samples.

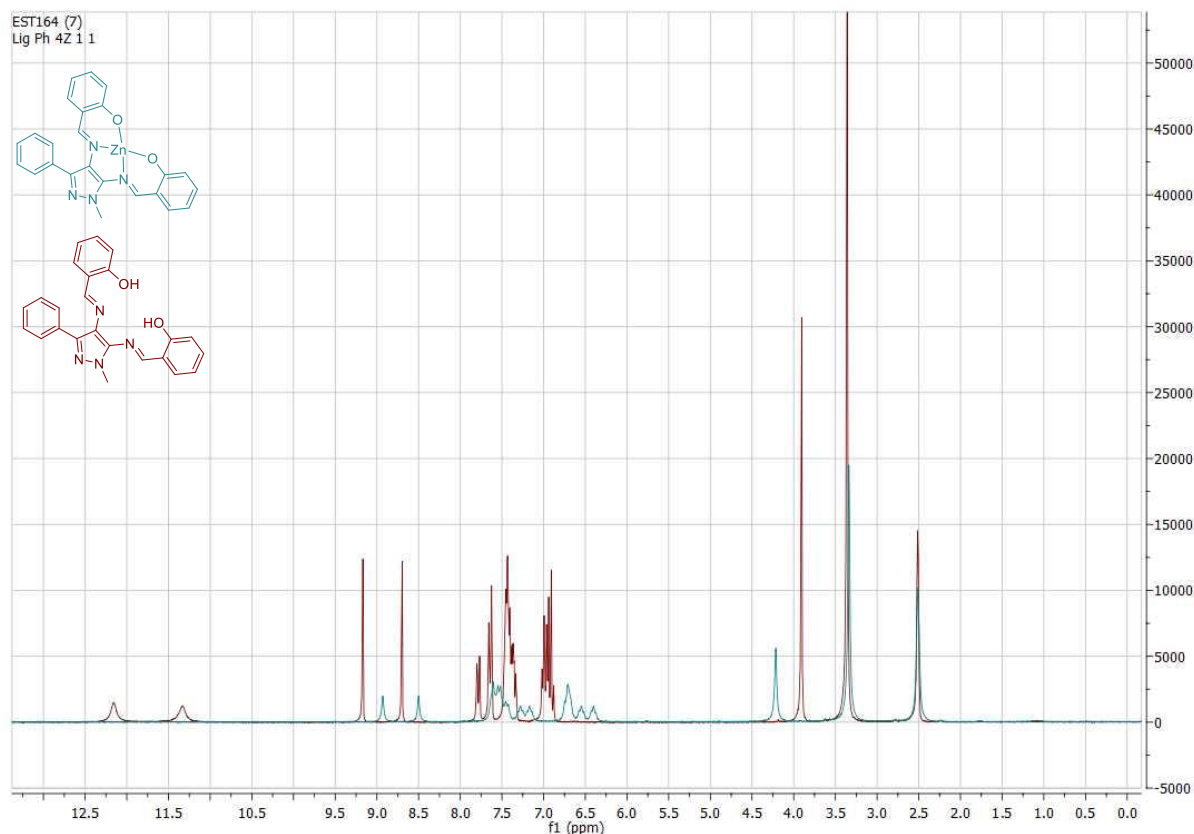


Figure 33: Comparison of the  $^1\text{H}$  NMR-spectra of I (red) and Ia (blue) in DMSO

It is clear that nearly all signals underlie a significant shift, when the spectra are compared. All peaks in the aromatic region are shifted to the right, while it can be perceived easily that signals in the aliphatic region are shifted to the left. Due to the metal's influence, all peaks in the complexes' spectrum are broader, when it is compared with the one of the free ligand, where nearly all signals are quite sharp. In the range between 11.0 and 12.5 ppm, the spectrum of the ligand displays two signals, which are quite broad due to the acidic character of these protons. In fact, they are attributed to the hydroxyl-groups, which are included in the ligand's structure. When the coordination reaction is carried out, the addition of a base removes these protons, whereby a doubly negatively charged ligand is generated. By its coordination to  $\text{Zn}^{2+}$ , a neutral complex Ia is formed, which does not include this signal in its  $^1\text{H}$  NMR spectrum.

Similar shifts of the signals can also be observed by the comparison of the  $^{13}\text{C}$  NMR-spectra of the complexes and the corresponding ligands.

The above discussed spectroscopic characteristics of complex **1a** and its ligand **I** are similar for all coordination compounds of Zinc and Cadmium and their respective ligands.

Other interesting spectroscopic features are revealed by the comparison of the spectra of two complexes – **1a** and **1b**. These coordination compounds include the same ligand **I**, but vary in their metal centre, which is Zinc and Cadmium, respectively (Figure 34).

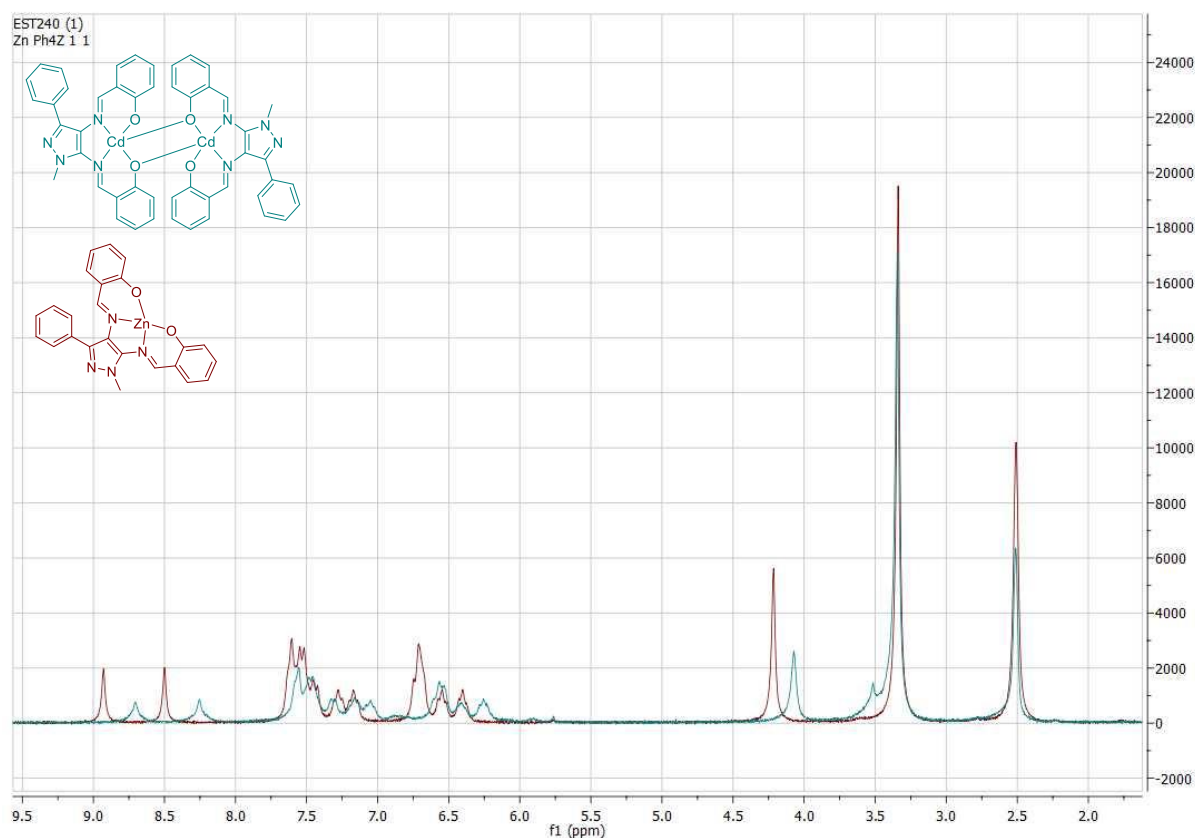


Figure 34: Comparison of the <sup>1</sup>H NMR spectra of **1a** (red) and **1b** (blue) in DMSO

Because Cd is positioned in the periodic table just under Zn, these two metals act very similar, when it comes to their coordination features. The bigger size of Cd leads to a diffuser shape of its orbitals, which can be observed in their proton NMR spectra. Each peak in the spectrum of Cd is broader, compared to the ones in the spectrum of Zn. On top of that, a remarkable shift of each signal to the right can be noticed just by a quick glance at the plot.

Analogical spectroscopic behaviour is noticed for all Zn- and Cd- complexes. Also, <sup>13</sup>C-NMR experiments reveal similar shifts of the signals.

## 4.2.2 Results of IR-Measurements

IR-measurements were recorded of all final ligands and their coordination compounds. It is worth to mention that especially the C-O- and C=N-bonds of the ligands underlie a quite big shift in the spectra after their coordination to a metal.

In Table 2 the IR-bands of the C=N-, C-O-, M-O-, M-N- and V-O-bonds are summarised. [94]

**Table 2: Comparison of the IR-bands of the C=N-, C-O-, M-O-, M-N- and V-O-bonds in cm<sup>-1</sup>**

	$\nu(\text{C}=\text{N})$		$\nu(\text{C}-\text{O})$	$\nu(\text{M}-\text{O})$	$\nu(\text{M}-\text{N})$	$\nu(\text{V}-\text{O})$
<i>I</i>	1599	1571	1405	-	-	-
<i>Ia</i>	1602	1526	1395	556	490	-
<i>Ib</i>	1595	1532	1397	554	495	-
<i>Ic</i>	1598	1533	1390	567	501	982
<i>II</i>	1600	1570	1380	-	-	-
<i>IIa</i>	1602	1548	1365	550	478	-
<i>IIb</i>	1601	1538	1362	554	465	-
<i>IIc</i>	1603	1560	1361	561	484	995
<i>III</i>	1605	1574	1420	-	-	-
<i>IIIa</i>	1604	1561	1389	532	496	-
<i>IIIb</i>	1601	1568	1387	530	497	-
<i>IIIc</i>	1602	1563	1388	534	498	932
<i>8</i>	1560		1275	-	-	-
<i>8a</i>	1528		1244	532	490	-
<i>8b</i>	1538		1249	525	476	-
<i>8c</i>	1534		1257	540	484	983
<i>10</i>	1606	1569	1245	-	-	-
<i>10a</i>	1594	1561	1232	570	496	-
<i>10b</i>	1597	1563	1231	568	495	-
<i>IV</i>	1687	1571	1272	-	-	-
<i>IVc</i>	1696	1567	1268	549	486	931

## 4.2.3 UV/VIS

UV/VIS spectra were recorded for each complex and the corresponding ligand to investigate their luminescence behaviour and find out, which wavelength is absorbed best by the synthesized organic and inorganic compounds. In this way, it is possible to find out, which structural features can have an influence on the absorption of light and in the following change their fluorescence behaviour.

For the ligands **I**, **II** and **8** and their coordination compounds of Zn, Cd and V, UV/VIS-measurements were carried out in DMSO at four different concentrations in the range of 250-

800 nm. For each maximum, the molar attenuation coefficient  $\varepsilon$  was calculated according to the following formula:

$$A(\lambda) = \log \frac{I}{I_0} = \varepsilon(\lambda) c d$$

Formula 2: Lambert-Beer law [9]

The approach of this calculations is shown exemplarily for the Cd-complex **Ib**, for all other compounds related to ligands **I**, **II** and **8** all calculations were carried out in the same way. For **Ib**, UV/VIS spectra were recorded of DMSO-solutions with the concentrations 3.7E-05 mol/l, 2.96E-5, 2.22E-05 and 1.48E-05. The resulting spectra are plotted in Figure 35 (left). Values of  $\varepsilon$  were then determined at each maximum for all concentrations. The average values of  $\varepsilon$  could then be calculated for each maximum. In this way, more accurate values could be obtained. Also, regression lines, derived from this data, were formed for each maximum (Figure 35 right). Because the coefficients of determination were 0.99-1 for each line, the quality of the regressions can be indicated as very good.

To have an overview of the results of the compounds related to the ligands **I**, **II** and **8**, all maxima and the average values of  $\varepsilon$  are summarized in Table 3-Table 5 and are discussed subsequently. In section 7.1, the data and all spectra for each analysed complex are given in detail.

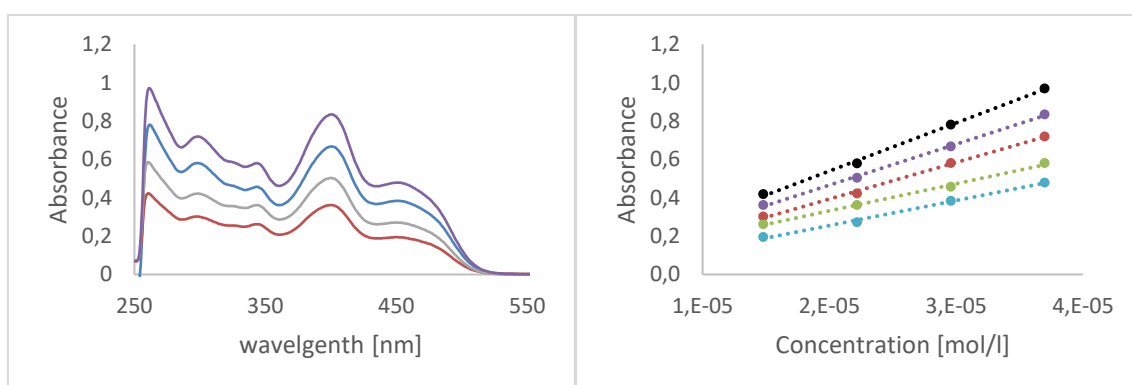


Figure 35: LEFT: UV/VIS-spectra of **Ib**, recorded with different concentrations (3.70E-05 / violet, 2.96E-05 / blue, 2.22E-05 / grey, 1.48E-05 / red); RIGHT: linear regression of the maxima at 262 nm (black), 298 nm (red), 344 nm (green), 400 nm (violet) and 450 nm (turquoise)



For ligand **III** and its coordination compounds of Zn and Cd, measurements were carried out in acetone, since the stability of the complexes was not sufficient in DMSO. Measurements of Zn- and Cd-complexes of **10** were done in DMSO. Results related to coordination compounds of ligands **III** and **10** are summarized in Table 6

In the following, special features of the spectra are discussed in detail:

There can be done general assignments for the transitions, observed in the UV/VIS spectra. The transitions around 260-270 nm can be ascribed to the  $\pi-\pi^*$ -transitions of the aromatic units in the ligand's structure, while the bands around 330-345 nm can be attributed to the  $n-\pi^*$ -transition of the electrons in the non-bonding orbitals of the  $-\text{CH}=\text{N}$ -moieties of the respective Schiff bases. [95] Also, the bands around 220-230 nm can be ascribed to the  $\pi-\pi^*$ -transitions of the aromatic system and the azomethine groups. Brought bands with a low intensity appear around 400-410 nm. These transitions are forbidden and can be related to  $n-\pi^*$ -transition of the imine moieties. [96] Since  $d^{10}$ -ions do not have any d-d-transitions, there are none of them in these spectra. It is interesting to mention that absorption bands, which appear in the spectrum of the ligands **I** and **II**, are shifted about 10 nm to lower wavelengths in the spectra of the corresponding complexes.

In Table 3 the maxima of the electronic spectra with the molar attenuation coefficients  $\varepsilon$  of ligand **I** and its coordination compounds are summarized.

**Table 3: Maxima of the UV/VIS spectra of ligand **I** and its coordination compounds of Zn (**Ia**), Cd (**Ib**) and V (**Ic**)**

	$\lambda_{\text{max}}$ [nm]	$\varepsilon(\lambda)$ [m <sup>2</sup> /mol]
<b>I</b>	272	2.63E+06
	334	1.93E+06
<b>Ia</b>	261	2.54E+06
	299	2.47E+06
	326	2.25E+06
	343	2.32E+06
	400	2.80E+06
	451	1.69E+06
<b>Ib</b>	262	2.67E+06
	298	1.96E+06
	344	1.63E+06
	400	2.31E+06
	450	1.28E+06

$\lambda_c$	260	3.39E+05
	329	2.48E+05
	348	2.51E+05
	406	2.41E+05

In Figure 36 the spectra of the Zn-complex **1a** (black) and its ligand **1** (red) are plotted. Both measurements were carried out at the same concentration ( $3 \times 10^{-5}$  mol/l). In fact, the inorganic Zn-compound starts to absorb light already in the region of 515 nm, while its ligand does not until 450 nm. In the spectrum of the ligand, two maxima are present, while the one of the complex indicates five. Another interesting singularity of this plot is that at 299 nm, the Zn-complex exhibits a maximum, while its ligand has a minimum.

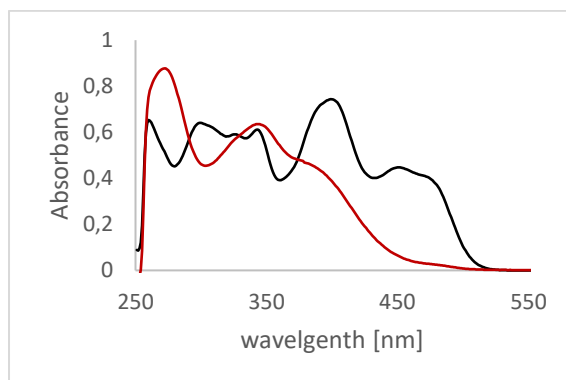


**Figure 36: Plotted UV/VIS spectra of the Zn-complex **1a** (black) and its ligand **1** (red), measured of DMSO-solutions with same concentrations ( $3 \times 10^{-5}$  mol/l)**

It is also of great interest to compare the spectra of complexes **1a** and **1b**, which include the same ligand, but different metals – Zn (black) and Cd (blue), respectively (Figure 37). Their spectra are quite similar, with a very slight difference. Even their maxima are nearly at same wavelengths. Also, the intensities of the absorbed light is almost the same. This issue is not very astonishing since Cd lies just under Zn in the periodic

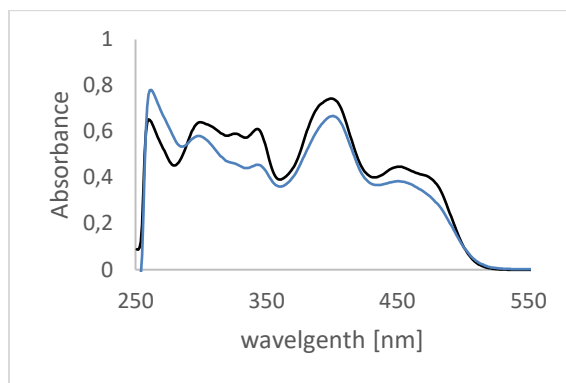


**Figure 37: Plotted UV/VIS spectra of Ia (black) and Ib (blue) measured of DMSO-solutions with same concentrations (3E-5 mol/l)**

In Table 4, the maxima of the electronic spectra with the molar attenuation coefficients  $\varepsilon$  of ligand II and its coordination compounds are summarized.

**Table 4: Maxima of the UV/VIS spectra of ligand II and its coordination compounds of Zn (IIa), Cd (IIb) and V (IIc)**

	$\lambda_{max}$ [nm]	$\varepsilon (\lambda)$ [m <sup>2</sup> /mol]
II	271	2.82E+06
	341	2.32E+06
IIa	260	1.25E+06
	295	1.24E+06
	342	1.23E+06
	393	1.38E+06
	451	9.10E+05
IIb	261	1.41E+06
	346	1.01E+06
	386	1.15E+06
IIc	266	7.86E+05
	306	7.98E+05

In Figure 38, the UV/VIS-spectra of the two Zn-complexes **Ia** (black) and **IIa** (green) are plotted. In this case, just the ligands are different, the concentrations, at which the spectra were recorded, are the same (3E-5 mol/l). The first feature, which arises from these spectra is that both compounds interact quite similar with the light – the maxima are almost at the same wavelengths. It is just quite remarkable that the intensity of the absorbed light differs a lot. The complex, which includes ligand **II**, absorbs far less light – almost half of it – compared to

the coordination compound with **I**. This can be explained by the structure of ligand **I**, which is consisting of a much bigger aromatic system compared to ligand **II**, and thus affects the uptake of the light.

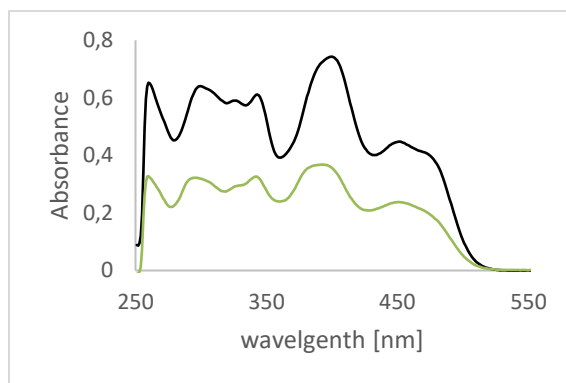


Figure 38: Plotted UV/VIS spectra of Ia (black) and IIa (green) measured of DMSO-solutions with same concentrations (3E-5 mol/l)

In Table 5, the maxima of the electronic spectra with the molar attenuation coefficients  $\varepsilon$  of ligand **8** and its coordination compounds are summarized.

Table 5: Maxima of the UV/VIS spectra of ligand **8** and its coordination compounds of Zn (**8a**), Cd (**8b**) and V (**8c**)

	$\lambda_{max}$ [nm]	$\varepsilon(\lambda)$ [m <sup>2</sup> /mol]
<b>8</b>	334	1,52E+06
	272	1,98E+06
<b>8a</b>	402	2,25E+06
	297	2,51E+06
	260	1,93E+06
<b>8b</b>	400	2,50E+06
	294	2,74E+06
	260	2,89E+06
<b>8c</b>	406	1,73E+06
	312	2,09E+06
	261	2,36E+06

In the following Figure 39, the spectra of two Zn-complexes, namely **Ia** and **8a**, are plotted. Both spectra were recorded of DMSO-solutions with same concentration (3E-5 mol/l). In fact,

the spectrum of **8a** includes just three maxima compared to **1a**. The maxima in these spectra occur due to charge transfer interactions from ligand to metal.

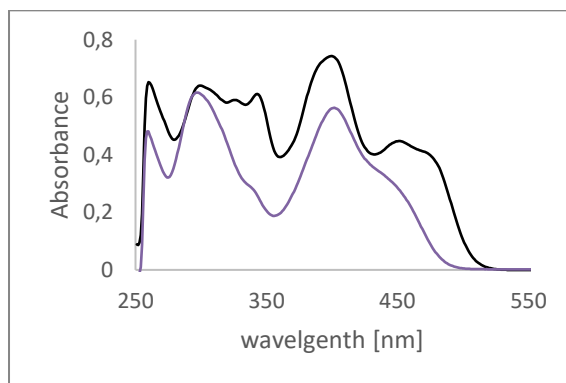


Figure 39: Plotted UV/VIS spectra of **1a** (black) and **8a** (violet) measured of DMSO-solutions with same concentrations ( $3\text{E-}5$  mol/l)

In Table 6, the maxima of the electronic spectra with the molar attenuation coefficients  $\epsilon$  of ligands **III** and **10** and their coordination compounds are summarized.

Table 6: Maxima of the UV/VIS spectra of the ligands **III** and **10** and their coordination compounds of Zn and Cd

	$\lambda_{\text{max}}$ [nm]	$\epsilon(\lambda)$ [m <sup>2</sup> /mol]
<b>III</b>	441	2.08E+04
<b>IIIa</b>	337	2.45E+06
<b>IIIb</b>	340	1.20E+06
<b>10</b>	337	1.89E+06
<b>10a</b>	325	6.54E+05
<b>10b</b>	322	2.02E+06

Due to the fact, that the stability of the coordination compounds of ligand **III** is not sufficient in DMSO, these complexes were analysed in an acetone solution. The spectra were recorded with concentrations of  $3.1\text{E-}05$ ,  $2.5\text{E-}05$  and  $3.9\text{E-}05$  mol/l for the compounds **III**, **IIIa** and **IIIb**, respectively. The spectra are plotted in Figure 40.

In this plot one can see, that the spectra of this group of compounds just include one maximum. Compared to the spectra discussed previously, this is quite less. The ligand absorbs light of a higher wavelength, in contrast to its coordination compounds, which absorb light of a slightly higher energy.

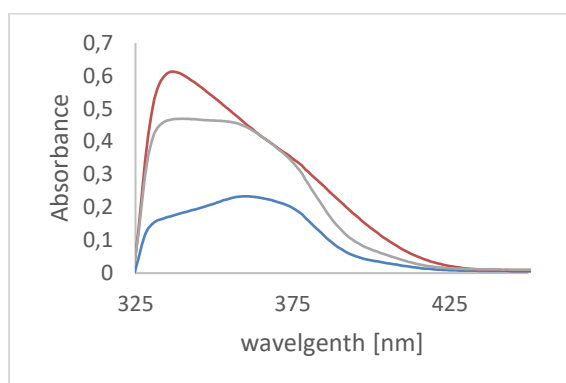


Figure 40: Plotted UV/VIS spectra of III (red), IIIa (grey) and IIIb (blue) measured of acetone-solutions with the concentrations 3.1E-05, 2.5E-05 and 3.9E-05 mol/l, respectively

#### 4.2.4 Fluorescence Analysis

Fluorescence analysis was carried out of coordination compounds to gain information concerning their luminescence behaviour and estimate their applicability for the usage in fluorescent material and as chemo sensors.

##### 4.2.4.1 Fluorescence Analysis of Solid Samples

Coordination compounds **Ia** and **IIa** exhibit moderate luminescence in the solid state upon excitation of light in the visible region of light. The quantum yield for luminescence of complex **Ia** is with 4.95 % higher than for complex **IIa** with 1.62 %, which may be due to the presence of a further phenyl ring in the structure of **Ia**, promoting greater luminescence efficiency. In the spectra of **IIa**, the emission spectrum exhibits a maximum at  $\lambda = 561$  nm, while the excitation was carried out at  $\lambda = 420$  nm. When these values are compared to the ones of complex **Ia** (Figure 41), it can be seen that the wavelengths are shifted to higher energies. In fact, the maximum of the emission for **IIa** is shifted to the red region of the light in comparison to complex **Ia**, which may be due to various electronic effects of the different substituents of their ligands. It is noteworthy that the most effective emission occurs with excitation of light

in the visible range, which is especially important for applications of luminescence in biological systems.

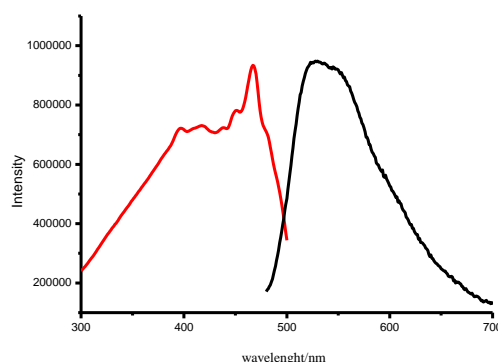


**Figure 41: Emission (black, 528 nm) and excitation (red, 475 nm) spectra for the solid sample Ia. (Quantum yield = 4.95 %)**

#### 4.2.4.2 Fluorescence Analysis in Solution

Emission spectra of DMSO-solutions with a concentration of  $10^{-5}$  mol/l were recorded at 298 K, upon ultraviolet and visible excitation. Excitation wavelengths were determined from excitation spectra, monitored at the maximum of the emission. The spectra can be seen in Figure 42-Figure 46, the received data is summarized in Table 7.

Most zinc- and cadmium-complexes demonstrate fluorescence in the yellow-orange region. Only **10a** and **10b** demonstrate emissions in the blue region, probably due to a smaller  $\pi$ -aromatic system and thus a reduced delocalization effect.

**Table 7: Summarized data of the fluorescence measurements of all zinc and cadmium complexes in DMSO-solutions with a concentration of  $10^{-5}$  mol/l at 298 K, upon ultraviolet and visible excitation**

Comp.	$\lambda_{max}$ (nm)	$I$	$Q$ (%)	$\tau$ (ns)	Comp.	$\lambda_{max}$ (nm)	$I$	$Q$ (%)	$\tau$ (ns)
8a	521	$6.8 \cdot 10^6$	2.1	4.3	8b	525	$4.4 \cdot 10^6$	1.5	4.6
Ia	560	$5.4 \cdot 10^6$	1.8	2.9	Ib	561	$3.4 \cdot 10^6$	1.1	3.0
IIa	556	$8.6 \cdot 10^5$	0.3	2.2	IIb	612	$4.5 \cdot 10^6$	1.7	4.2
10a	408	$7.5 \cdot 10^6$	2.2	3.1	10b	475	$11.5 \cdot 10^6$	2.4	2.8
IIIa	600	$3.4 \cdot 10^5$	0.5	2.7	IIIb	600	$1.6 \cdot 10^6$	0.9	2.9

For the pairs of similar complexes **IIla-IIIb**, **Ia-Ib** and **8a-8b** the exchange of the metal from zinc to cadmium did not result in a shifting of the emission, only the emission intensity changed, which indicates the emission site in the relevant molecules. In the complex couples **Ila-IIb** and **10a-10b**, a red-shift of the fluorescence can be observed when the metal is exchanged from zinc to cadmium.

It is of interest, to compare the luminescence parameters of complexes with similar structural features. The comparison of the complexes, carrying a pyrazole-moiety in their structures, reveals that the exchange of a substituent from a phenyl- to a t-butyl-group, leads to a bathochromic shift of the luminescence maximum, but only for cadmium-complexes. For the zinc-analogues, the luminescence bands are not displaced, when the substituents change. This may be due to the difference in the type of molecular orbitals between which an electronic transition occurs in course of the emission.

The comparison of complexes **IIla-IIIb** and **8a-8b** exhibits a bathochromic shift, when the salicylic aldehyde in ligand **8** is replaced by a coumarin-derivative in ligand **III**. This shift is obviously associated with a significant delocalization of the electron density in the complexes.

Despite the overall strong emission, the quantum efficiencies of the complexes are quite low (0.3-2.4 %), which indicates a great loss of excitation energy by non-radiative relaxation. Lifetime of all complexes are in the nanosecond region, which typical for fast-fluorescence.

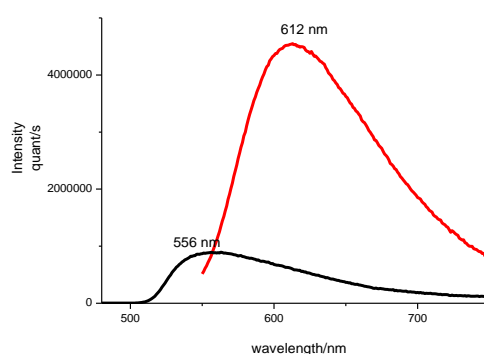


Figure 42: Emission spectra for  $10^{-5}$  M DMSO-solutions of **IIa** (black) and **IIb** (red)



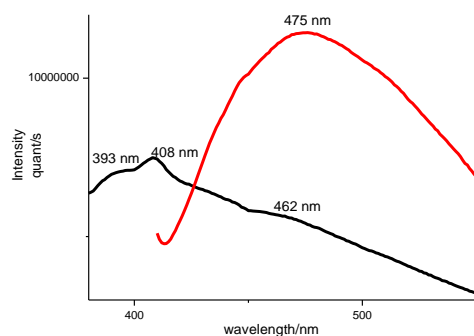


Figure 43: Emission spectra for 10<sup>-5</sup> M DMSO-solutions of 10a (black) and 10b (red)

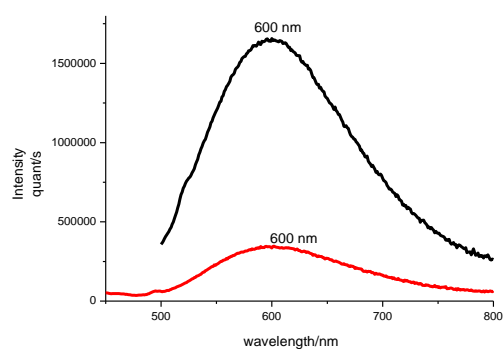


Figure 44: Emission spectra for 10<sup>-5</sup> M DMSO-solutions of IIIb (black) and IIIa (red)

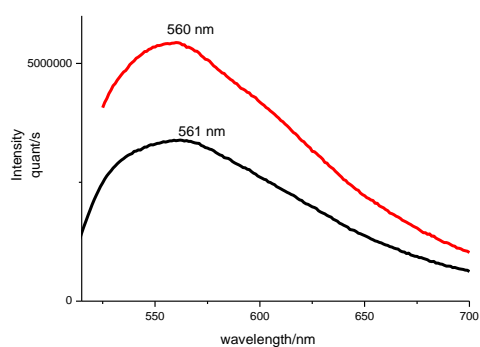
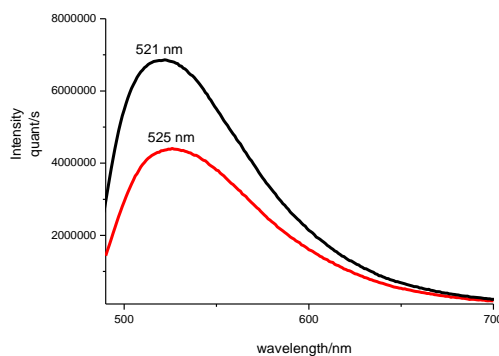
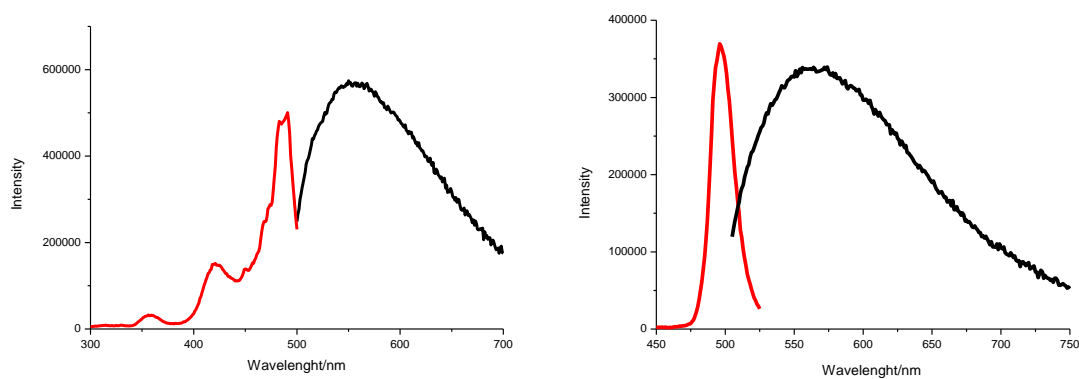


Figure 45: Emission spectra for 10<sup>-5</sup> M DMSO-solutions of Ib (black) and Ia (red)



**Figure 46:** Emission spectra for  $10^{-5}$  M DMSO-solutions of **8a** (black) and **8b** (red)

Complexes exhibit solvatochromic properties that manifest themselves in the shift of the emission maximum by changing the solvent from a low polar THF to polar MeOH. Like the solid samples of **Ia** and **IIa**, solutions show luminescence in the yellow-orange region, while luminescence of **IIIa** is shifted to the blue region of the light. The spectra are given in (Figure 47-Figure 49)



**Figure 47:** LEFT: Emission ( $\lambda = 550$  nm) and excitation ( $\lambda = 490$  nm) spectra for a MeOH solution of **Ia**;  
RIGHT: Emission ( $\lambda = 563$  nm) and excitation ( $\lambda = 496$  nm) spectra for a THF solution of **Ia**.

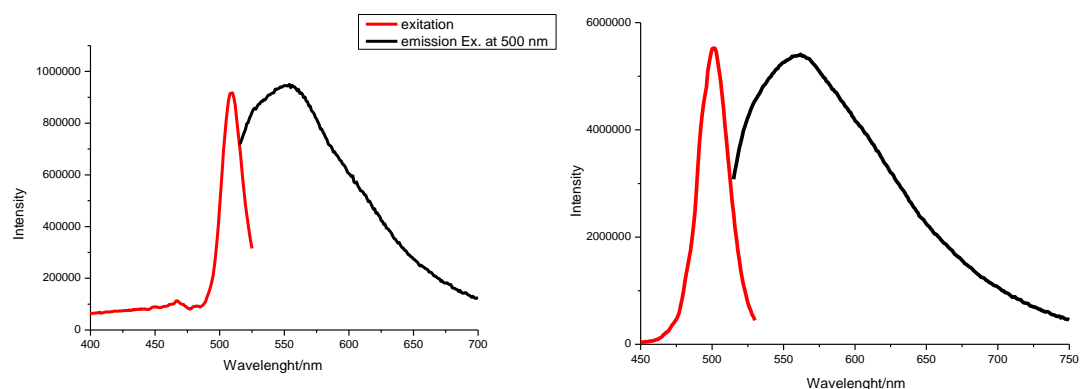


**Figure 48:** LEFT: Emission ( $\lambda = 550$  nm) and excitation ( $\lambda = 490$  nm) spectra for a MeOH solution of IIa; RIGHT: Emission ( $\lambda = 560$  nm) and excitation ( $\lambda = 500$  nm) spectra for a THF solution of IIa.

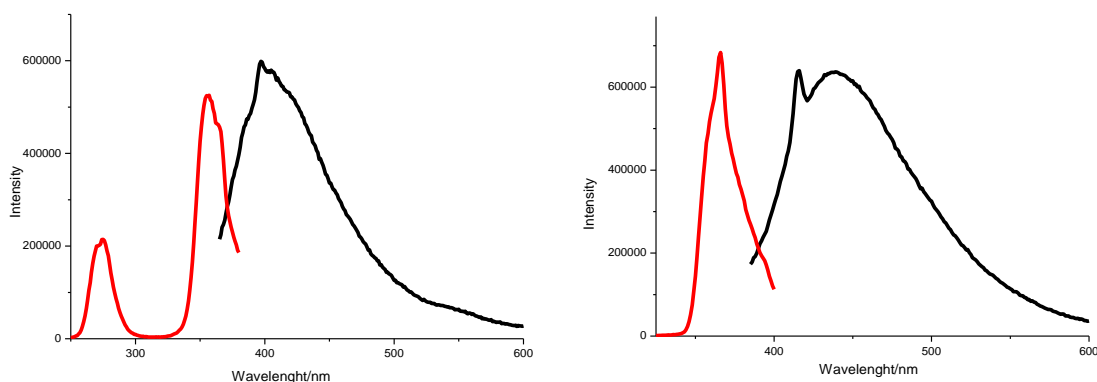


**Figure 49:** LEFT: Emission ( $\lambda = 396$  nm) and excitation ( $\lambda = 350$  nm) spectra for a MeOH solution of IIIa; RIGHT: Emission ( $\lambda = 413$  and  $440$  nm) and excitation ( $\lambda = 365$  nm) spectra for a THF solution of IIIa.

Also, the luminescence of europium in the presence of ligand **9** was studied. The highest luminescence-intensity was achieved with a ratio of europium : ligand of 1:3 at a pH of 7.5. Upon excitation with UV-light, the europium complex **9d** emits characteristic red luminescence with a line-like spectrum in the range of 575-730 nm, which can be attributed to the metal's  $^5D_0 \rightarrow ^7F_J$ -transition ( $J = 0-4$ ) (Figure 50). The emission spectra of this compound are independent from the excitation wavelength. The excitation spectrum corresponds to the ligand's absorption transitions, thus, confirming the energy transfer from the ligand to the europium-metal centre. At 463 nm and 528 nm in the absorption-spectrum, transitions with low intensity can be observed, which can be assigned to the transitions  $^5D_3 \rightarrow ^7F_4$  and  $^5D_1 \rightarrow ^7F_2$ , respectively, determined from Dieke's diagram. The intensity of the luminescence is comparable with stronger sensitizing ligands (diketones and azoles).

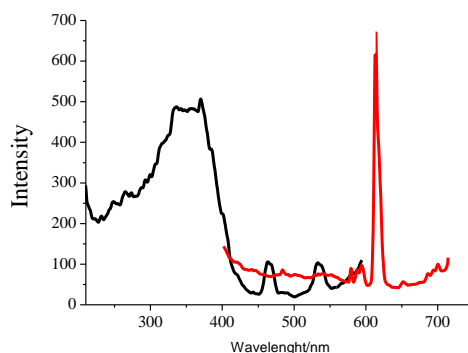


Figure 50: Emission ( $\lambda = 614$  nm) and excitation ( $\lambda = 371$  nm) spectra for complex 9d

#### 4.2.5 X-Ray Analysis of Single Crystals

Analysis of single crystals was carried out to clarify the bonding behaviour of the ligands to the respective metals.

It was possible to obtain suitable single crystals for X-ray analysis of **1a** by a slow evaporation of the solvents pyridine and DMSO, forming **1a** pyridine and **1a** DMSO, respectively. In the course of the analysis, it was found out that the solvent-molecules coordinate to zinc, forming coordination compounds with square pyramidal geometries in triclinic and monoclinic crystal systems for pyridine and DMSO, respectively. The molecular formulae are given in Figure 51 with information of selected bond lengths and angles in the figure caption.

It was found by Escudero-Adán and coworkers that there is a strong but also dynamic interaction between zinc and various N-heterocycles. This bears the possibility of an applicability of this system to be used as recognition sites for more functional molecules, which are important in biochemical systems, such as purines or imidazoles. This feature, in combination with an efficient fluorescent behaviour of the coordination compounds, enables the usage as specific sensor material. [97] The bond length of the Zn-(salphen)-complex, linked to a N-heterocycle is reported by Escudero-Adán and co-workers to be 2.065 Å, which is shorter than the bond length between zinc and its pyridyl-ligand of compound **1a**, which was found, to be 2.114 Å.

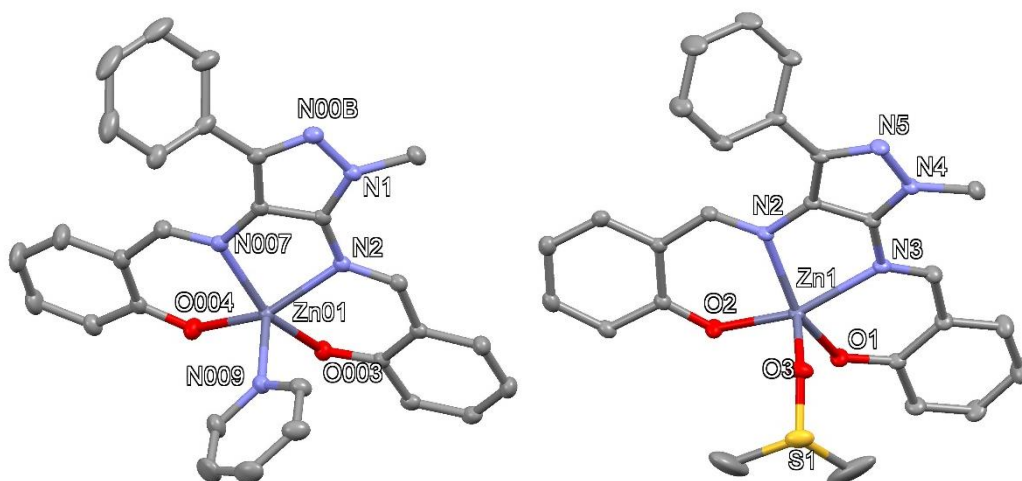


**Figure 51: LEFT:** Molecular structure of Ia Pyridine (H-atoms are omitted for clarity). Selected bond-lengths (in Å) and bond angles (in deg): Zn01-O003 1.973, Zn01-N2 2.126, Zn01-N007 2.124, Zn01-O004 1.963, Zn01-N009 2.114, O003-Zn01-O004 95.11, O004-Zn01-N007 89.28, N007-Zn01-N2 80.29, N2-Zn01-O003 87.15; **RIGHT:** Molecular structure of Ia DMSO (H-atoms are omitted for clarity). Selected bond-lengths (in Å) and bond angles (in deg): Zn1-O1 1.968, Zn1-N3 2.159, Zn1-N2 2.108, Zn1-O2 1.965, Zn1-O3 2.061, O1-Zn1-N3 86.86, N3-Z1-N2 79.38, N2-Zn1-O2 90.00, O2-Zn1-O1 95.59

A suitable single crystal for X-ray analysis of **Ila** could be obtained upon slow evaporation of a saturated solution of the complex in DMSO. It was found that for **Ila**, similar to complex **Ia** DMSO, also one solvent molecule coordinates to the metal centre. Thus, a square pyramidal geometry can be found for this complex in a monoclinic crystal system. The molecular formula is given in Figure 52 with information of selected bond lengths and angles in the figure caption.

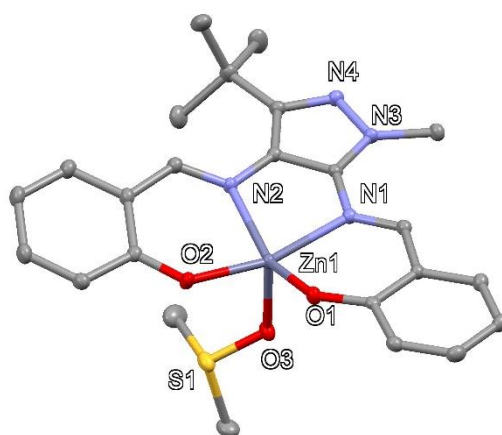


**Figure 52:** Molecular structure of IIa DMSO (H-atoms are omitted for clarity). Selected bond-lengths (in Å) and bond angles (in deg): Zn1-O1 1.970, Zn1-N1 2.118, Zn1-N2 2.132, Zn1-O2 1.979, Zn1-O3 2.082, O1-Zn1-N1 88.98, N1-Zn1-N2 80.14, N2-Zn1-O2 89.34, O2-Zn1-O1 94.90

For complex **8b** a suitable single crystal could be obtained upon slow evaporation of a saturated solution of the coordination compound in DMSO. It is interesting to mention that the tetradentate Schiff base ligand **8** formed binuclear complexes with cadmium, while this is not the case for the analogue zinc-compound **8a**. Similar to zinc, DMSO also coordinates to the metal centre via its oxygen atom in the cadmium-coordination compound and stays in the structure of the solid complex. In **8b** DMSO, cadmium is surrounded in an octahedral way by its ligands. One oxygen of each Schiff base (O003) is forming a bridge between the cadmium-atoms, no direct bond between the metals is present. **8b** DMSO forms a monoclinic crystal system. The molecular formula is given in Figure 53 with information of selected bond lengths and angles in the figure caption.

In Figure 53, the bond lengths between the hetero-atoms, which bind directly to the centres are summarized.

Table 8: Summarized bond lengths of the central metal of compounds **Ia**, **IIa** and **8b** in Å

Compound	DMSO-O/oxo-O	Schiff base-N		Schiff base-O	
<i>Ia</i> DMSO	2.061	2.159	2.108	1.965	1.968
<i>IIa</i> DMSO	2.082	2.132	2.118	1.970	1.979
<i>8b</i> DMSO	2.391	2.310	2.272	2.171	2.278
<i>Ic</i>	1.590	2.103	2.088	1.919	1.921

The bond lengths within the complexes **Ia** DMSO and **IIa** DMSO are quite similar and differ just about 0,02 Å. It is remarkable, that the bond length between the metal centres and the DMSO-O is quite long, compared to the other metal-oxygen distances, which shows that these bonds may be quite loosely. Cadmium exhibits much larger bond lengths compared to the zinc compounds, which can be attributed to the bigger size of the metal itself. The oxovanadium-complex **Ic** features the shortest bond lengths of the herein compared complexes, with the bond of vanadium to its oxo-ligand being only 1.590 Å.

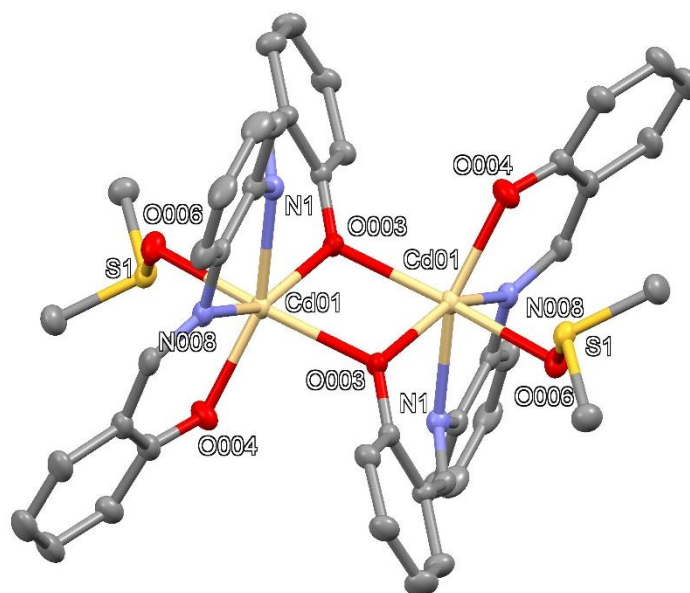


**Figure 53:** Molecular structure of **8b** DMSO (H-atoms are omitted for clarity). Selected bond-lengths (in Å) and bond angles (in deg): Cd01-O003 2.278, Cd01-N1 2.310, Cd01-N008 2.272, Cd01-O004 2.171, Cd01-O006 2.391, O003-Cd01-N1 78.78, N1-Cd01-N008 72.64, N008-Cd01-O004 86.17, O004-Cd01-O003 122.71

A suitable single crystal for X-ray analysis of **1c** could be grown by slow diffusion of abs. n-pentane into a saturated solution of the complex in abs. THF. In this case, no solvent molecules are coordinated to the metal centre in the solid state. The coordination compound crystallizes in a square pyramidal geometry with a monoclinic crystal system. The molecular formula is given in Figure 54 with information of selected bond lengths and angles in the figure caption. The distance between vanadium and its oxo-ligand is with 1.590 Å quite short, which displays a very strong interaction and affinity of the metal centre to oxygen. When this bond length is compared to the one of the starting material VO(acac)<sub>2</sub>, which was found to be 1.586 Å [98], it can be seen that there is quite a huge structural similarity between these two compounds.

Gloe and co-workers, and Constable and co-workers reported on copper-coordination compounds with tetradentate ONNO-Schiff bases. The determination of the crystal structures of these compounds revealed that the coordination occurs, like the here presented complexes, via the ligand's central N<sub>2</sub>O<sub>2</sub>-donor atoms. In addition, in the solid state even helical structures are formed. [99, 100]

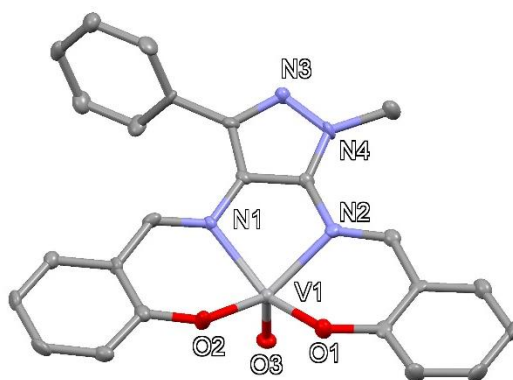


**Figure 54: Molecular structure of 1c (H-atoms are omitted for clarity). Selected bond-lengths (in Å) and bond angles (in deg): V1-O1 1.919, V1-N2 2.103, V1-N2 2.088, V1-O2 1.912, V1-O3 1.590, O1-V1-N2 86.94, N2-V1-N1 80.33, N1-V1-O2 86.83, O2-V1-O1 87.67**

For ligand **I**, a suitable single crystal for X-ray analysis could be obtained upon slow diffusion of abs. n-pentane into a saturated solution of the ligand in abs. THF. The molecular formula is given in Figure 55 with information of selected bond lengths and angles in the figure caption. The ligand crystallizes in a triclinic crystal system.

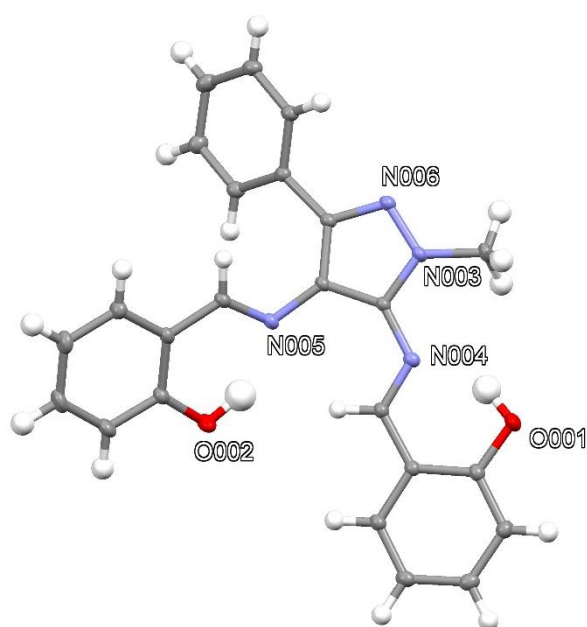


**Figure 55: Molecular structure of 1. Selected bond-lengths (in Å) and bond angles (in deg): O001-N004 2.623, N004-N005 3.211, N005-O002 2.680, O001-C00H 1.357, O002-C00A 1.356, N005-C00C 1.294, N005-C009 1.408, N004-C00E 1.299, N004-C00D 1.383, C00E-N004-C00D 122.14, C00C-N005-C009 118.64**



A suitable single crystal for X-ray analysis of **II** could be grown by slow evaporation of a saturated solution of the ligand in abs. THF. The molecular formula is given in Figure 56 with information of selected bond lengths and angles in the figure caption. Compound **II** crystallizes in an orthorhombic crystal system.

It is interesting to mention that the crystal structures of the two ligands **I** and **II** are very similar, apart from the phenyl-group in compound **I**, which is exchanged by a tert-butyl group in the structure of ligand **II**. Furthermore, the OH-groups, which were found to be involved in the formation of coordination compounds after their deprotonation, are not present in the conformation, in which they occur in all coordination compounds, since one hydroxyl-group is positioned at the far side and thus, points out of the final coordination plane. As a result, these ligands must undergo a conformational change prior a coordination reaction can occur.

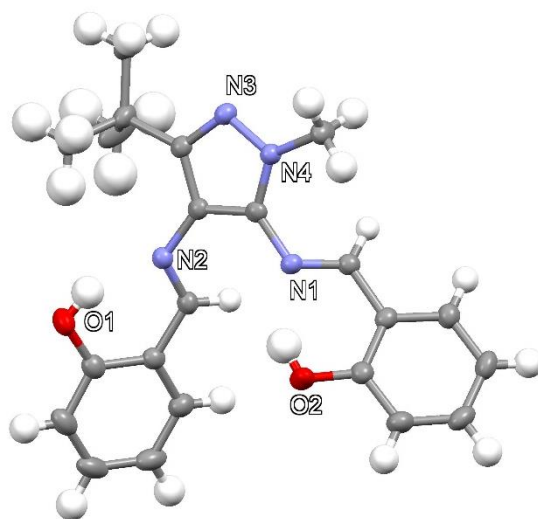


**Figure 56:** Molecular structure of **II**. Selected bond-lengths (in Å) and bond angles (in deg): O1-C13 1.345, O2-C10 1.350, N1-C8 1.287, N1-C7 1.393, N2-C5 1.280, N2-C6 1.404, O1-N2 2.589, N1-N2 3.066, N1-O2 2.642, C7-N2-C8 121.30, C5-N2-C6 120.32

For ligand **III**, a suitable single crystal for X-ray analysis could be obtained upon slow evaporation of a saturated solution of the ligand in abs. THF. The molecular formula is given in Figure 57 with information of selected bond lengths and angles in the figure caption. It was found that ligand **III** crystallizes in a monoclinic crystal system. In the solid state, ligand **III** behaves quite different to its analogues **I** and **II**. It is interesting to mention, that all atoms,

which are crucial for the occurrence of the coordination to a metal, are already oriented in the way it is needed, so no conformational change is required prior a coordination. A reason for this is the presence of the coumarin-moiety's hetero-atoms, which underlie a huge repulsion and thus, occur in the conformation with the maximum distance to each other. Since this kind of compounds can underlie keto-enol tautomerism, ligand **III** is present in its keto-form in the solid state, while compounds **I** and **II** are in an enol-tautomeric form.

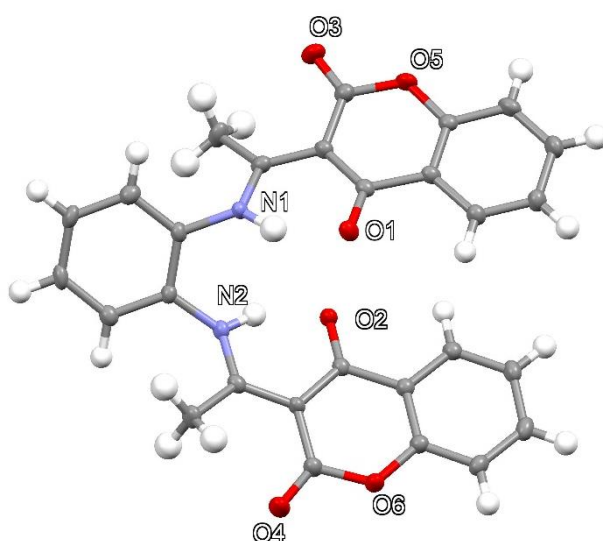


Figure 57: Molecular structure of **III**. Selected bond-lengths (in Å) and bond angles (in deg): O1-C10 1.243, O2-C21 1.244, N1-C1 1.420, N1-C7 1.326, N2-C2 1.423, N2-C18 1.329, O1-N1 2.562, N1-N2 2.722, N2-O2 2.544, C1-N1-C7 125.07, C2-N2-C18 128.83

#### 4.2.6 DFT-Calculations

DFT-calculations were carried out of selected complexes **Ia**, **8b** and **Ic** to determine their metric parameters. A comparison of calculated and experimentally determined parameters was done, the compared values can be seen in Table 9-Table 11.

For the complexes **Ia** and **Ic**, the calculated and determined values are quite similar, thus, confirming that the used method for the calculations is suitable.

**Table 9: Comparison of calculated and experimentally determined metrical parameters of complex **1a** (closed shell ( $S = 0$ ))**

<i>Parameter Å / °</i>	<i>Exp</i>	<i>Calc</i>
<i>Zn1-O3</i>	2.061	2.126
<i>Zn1-N2</i>	2.108	2.111
<i>Zn1-N3</i>	2.159	2.175
<i>Zn1-O1</i>	1.968	1.997
<i>Zn1-O2</i>	1.965	1.996
<i>O1-Zn1-O2</i>	95.59	94.161
<i>N2-Zn1-O1</i>	153.87	159.27
<i>N2-Zn1-O3</i>	98.75	97.03

In the following Figure 58, the calculated HOMO- and LUMO-orbitals of complex **1a** are displayed. Since zinc is a  $d^{10}$ -transition metal, in the UV/VIS-spectra of all Zn-complexes, just ligand to ligand charge-transfer bands could be observed. This fact is further confirmed by the calculated HOMO- and LUMO-orbitals.

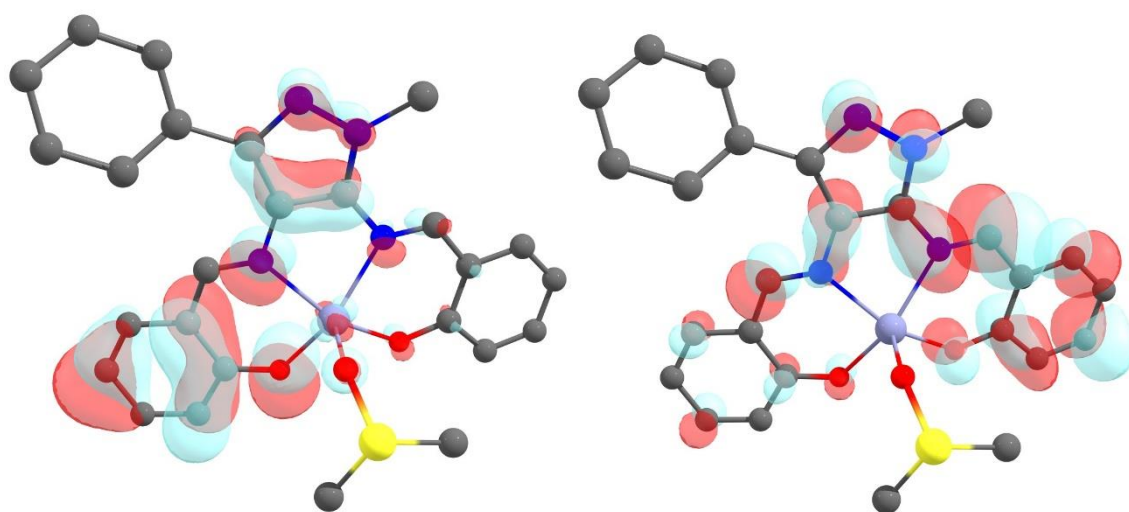
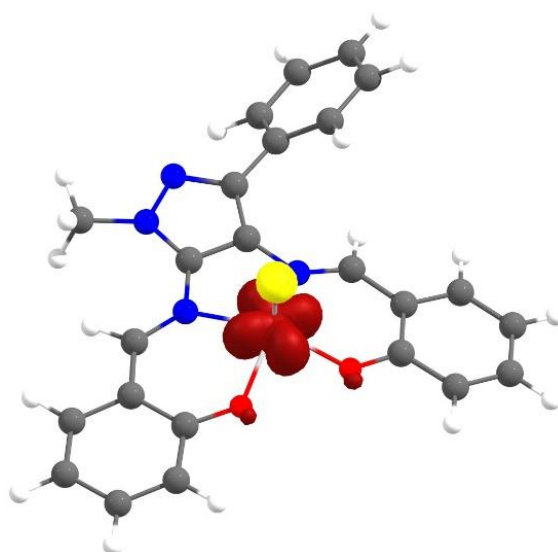
**Figure 58: LEFT: HOMO of **1a**, RIGHT: LUMO of **1a****

Table 10: Comparison of calculated and experimentally determined metrical parameters of complex **1c**

<i>Parameter Å / °</i>	<i>Exp</i>	<i>Calc</i>
<i>V1-O3</i>	1.590	1.593
<i>V1-N1</i>	2.088	2.095
<i>V1-N2</i>	2.103	2.120
<i>V1-O1</i>	1.919	1.944
<i>V1-O2</i>	1.912	1.930
<i>O1-V1-O2</i>	87.67	86.37
<i>N2-V1-O1</i>	86.94	86.06
<i>N2-V1-O3</i>	103.95	104.47

In Figure 59, a spin density plot of complex **1c** can be seen. It shows the place of the unpaired electron of this compound, which was found to be just between the bonds of the vanadium-centre to the hetero-atoms of the ligand, together with the surrounding of the oxygen-atoms in this compound.

Figure 59: Spin density plot of **1c**, iso-surface value 0.02

The calculated and the experimental values of compound **8b** are not as similar, as they are for **1a** and **1c**. Since the structure of **8b** is more complex compared to **1a** and **1c** – **8b** is a binuclear complex – the comparison of the values underlies a bigger deviation.

**Table 11: Comparison of calculated and experimentally determined metrical parameters of complex 8b  
(closed shell (S = 0))**

<b><i>Parameter Å / °</i></b>	<b><i>Exp</i></b>	<b><i>Calc</i></b>
<i>Cd01-O3</i>	2.245	2.304
<i>Cd01-N1</i>	2.310	2.348
<i>Cd01-N008</i>	2.272	2.333
<i>Cd01-O004</i>	2.171	2.230
<i>Cd01-Cd01'</i>	3.523	3.691
<i>Cd01-O006</i>	2.391	2.411
<i>Cd01-O003-Cd01</i>	102.32	105.66
<i>N008-Cd01-O004</i>	86.17	82.98

## 5 Experimental

### 5.1 General remarks

All reagents, which were purchased from commercial suppliers, were used without prior purification.

All solvents were distilled before use. Absolute solvents were purified using the PURESOLV-system from it-innovative-technology-inc.

To perform experiments under an inert atmosphere of Ar, Schlenk techniques or a MBraun inert-gas glovebox was used.

The commercially available lithiation reagent MeLi was used without additional quantitative analysis, using the declared value.

TLC was performed by using TLC aluminum foil (Merck. Silica gel 60 F<sub>254</sub>).

### 5.2 Analytical Methods

#### 5.2.1 NMR-spectroscopy

NMR spectra were recorded on Bruker AVANCE-200, AVANCE-250 and AVANCE-400-spectrometers. Data for <sup>1</sup>H-NMR is reported as follows: chemical shift in parts per million from TMS with the residual solvent signal as an internal reference [101], multiplicity (s = singlet, d = doublet, t = triplet and m = multiplet), coupling constant in Hz and integration. <sup>13</sup>C NMR spectra are reported in ppm from TMS as internal standard, using the central peak of the solvent as reference [102].

Deuterated solvents were purchased from Aldrich. To CDCl<sub>3</sub> basic Al<sub>2</sub>O<sub>3</sub> was added and filtered prior all NMR-experiments.

#### 5.2.2 IR-spectroscopy

IR-spectra were recorded using a Perkin Elmer UATR Two spectrometer in the ATR mode. Spectra were recorded of solid samples at RT.

### 5.2.3 UV/VIS Spectroscopy

UV-VIS spectra were recorded on a Perkin Elmer Lambda 900 (UV/VIS/NIR spectrometer). The spectra were measured from 250 to 800 nm at room temperature, using quartz glass cuvettes with a diameter of 1 cm. To record the spectra, solutions were prepared in DMSO or acetone.

### 5.2.4 Luminescence Spectra

The registration of the excitation and luminescence spectra was carried out on a FluoroMax-3 Spectro fluorimeter, for solutions of THF and MeOH and for solid samples. All measurements were done at RT. Quantum yields were determined on the same instrument by an absolute method with a Quanta- $\phi$  integrating sphere.

Luminescence spectra of DMSO solutions were recorded on a FluoroMax-4 spectrofluorometer. Quantum yields were determined at 298 K by the optical dilution method of Demas and Crosby against quinine sulphate as a standard ( $\Phi_r = 0.546$ ) [103]. Absolute values were calculated using the standard reference sample, which has a fixed and known value of fluorescence quantum yield, according to the following equation:

$$Q = Q_r \frac{I OD_r n^2}{I_r OD n_r^2}$$

**Formula 3: Determination of the quantum yields**

In Formula 3,  $Q$  is the quantum yield,  $I$  the measured integrated emission intensity,  $n$  the refractive index, and  $OD$  is the optical density. The subscript  $r$  refers to the reference fluorophore with a known quantum yield. In order to minimize reabsorption effects, absorbances in the 10-mm fluorescence cuvette were kept below 0.05 at the excitation wavelength.

Lifetime studies were performed on a Panorama spectrofluorometer, using a photon-counting system with a pulse lamp as the excitation source. The emission decays were analysed by exponential functions. The decay curve is well fitted into a double exponential function:

$$I(t) = A e^{(-t/\tau)}$$

**Formula 4: Lifetime-studies**

In Formula 4,  $I$  is the luminescence intensity, and  $\tau$  is the lifetime for the exponential component.

### 5.2.5 Elemental Analysis

Elemental analyses of C, H, and N was performed on a Perkin–Elmer 240 C analyser.

### 5.2.6 X-Ray Structure Determination

The X-ray diffraction data was collected at  $T = 100$  K in a dry stream of nitrogen with a Bruker Kappa APEX II diffractometer system with graphite-monochromated Mo- $K_{\alpha}$  radiation ( $\lambda = 0.71073$  Å) and fine-sliced  $\phi$  and  $\omega$  scans. The data was reduced to intensity values with SAINT. An absorption correction was applied with the multiscan approach implemented in SADABS or TWINABS [104]. The structures were solved by direct methods implemented in SHELXS [105], or charge flipping implemented in SUPERFLIP [106]. Non-hydrogen atoms were refined anisotropically. The H atoms connected to C atoms were placed in calculated positions and thereafter refined as riding on the parent atom. Molecular graphics were generated with the program MERCURY [107]. The crystal data and experimental details are given in Table 24-Table 31

### 5.2.7 DFT-Calculations

All calculations were performed using density functional theory (DFT) as implemented in the Gaussian 09 [108] on the Vienna Scientific Cluster (VSC3). Geometry optimization was carried out with Gaussian 09 using the BP86 approach to DFT without any symmetry constraints. The relativistic Stuttgart-Dresden ECP was used to describe the metal centres (Zn, V, Cd) and the 6-31G(d,p) basis set for the remaining ligands (C, N, H, O, S). Frequency calculations were performed to confirm the nature of the stationary points yielding no imaginary frequencies.



## 5.3 Synthesis of Organic Ligands

### 5.3.1 Synthesis of Benzoyl Acetonitrile

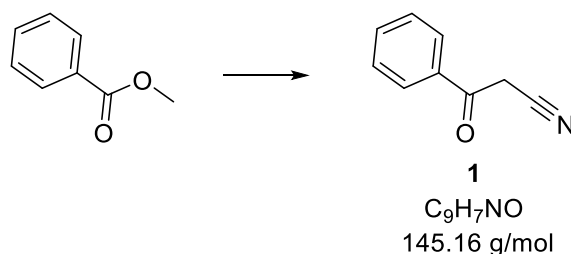


Figure 60: Synthesis of benzoyl acetonitrile

Synthesis according to: [88]

NaH (55-60 % dispersion in minera oil) (14.42 g, 330.1 mmol) was washed twice with absolute THF before use under an Ar-atmosphere. 10 ml dry DMSO and dry acetonitrile (18.09 ml, 343.2 mmol) were mixed and cooled to 0°C. At this temperature washed NaH was added slowly in little portions to the solution under inert conditions. After 30 min methyl benzoate (28 ml, 220.1 mmol) was added to the suspension. The reaction mixture could warm up to RT. After 22 h the reaction was completed according to TLC ( $R_f = 0.5$ , PE:EE = 5:2), the mixture was cooled again to 0 °C and hydrolysed with dest. H<sub>2</sub>O. The clear and yellowish solution was then acidified with conc. HCl until pH = 1, whereby the solid product was formed. It was then filtered off, washed several times with dest. H<sub>2</sub>O until pH = 7 and then three times with Et<sub>2</sub>O. The product was finally dried under reduced pressure.

21.84 g (68 %) white solid

<sup>1</sup>H NMR (CDCl<sub>3</sub>, 200 MHz, 20 °C)  $\delta$  = 7.95 (d, J = 7.3, 2H, PhH), 7.71 (t, J = 7.4, 1H, PhH), 7.57 (t, J = 7.4, 2H, PhH), 4.76 (s, 2H, CH<sub>2</sub>)

<sup>13</sup>C NMR (DMSO, 200 MHz, 20 °C)  $\delta$  = 189.71 (s), 134.62 (s), 134.30 (s), 128.91 (s), 128.41 (s), 115.90 (s), 30.03 (s)

### 5.3.2 Synthesis of 1-Methyl-3-Phenyl-1H-Pyrazol-5-Amine

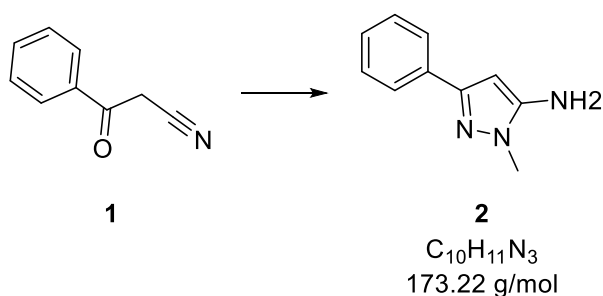


Figure 61: Synthesis of 1-methyl-3-phenyl-1H-pyrazol-5-amine

Synthesis according to: [89]

**1** (44.47 g, 306.0 mmol) was dissolved in 1000 ml abs. MeOH. Methylhydrazine (48 ml, 919.2 mmol) was added to the solution under an Ar-atmosphere and refluxed for 19 h. After that time, the reaction was completed according to TLC ( $R_f = 0.63$ , PE:EE = 1:1), so the solvent was removed and the residue was resolved in 300 ml EE. The solution was then extracted once with brine and once with H<sub>2</sub>O. The combined organic layers were dried with Na<sub>2</sub>SO<sub>4</sub> and the solution was reduced to 20 ml, whereby white crystals were formed. The solid was filtered off under Ar-atmosphere, washed three times with PE:EE = 1:1 and finally dried under reduced pressure.

30.63 g (58 %) white crystalline solid

<sup>1</sup>H NMR (DMSO, 200 MHz, 20 °C)  $\delta$  = 7.66 (d,  $J = 7.5$  Hz, 2H, PhH), 7.33 (t,  $J = 7.4$  Hz, 2H, PhH), 7.21 (t,  $J = 6.9$  Hz, 1H, PhH), 5.70 (s, 1H, CH), 5.27 (s, 2H, NH<sub>2</sub>), 3.58 (s, 3H, CH<sub>3</sub>)

<sup>13</sup>C NMR (DMSO, 200 MHz, 20 °C)  $\delta$  = 148.11 (s), 147.77 (s), 134.34 (s), 128.36 (s), 126.79 (s), 124.60 (s), 85.24 (s), 34.28 (s)

### 5.3.3 Synthesis of 1-Methyl-3-Phenyl-1H-Pyrazole-4,5-Diamine

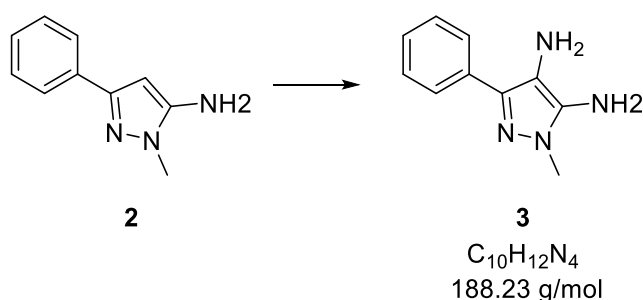


Figure 62: Synthesis of 1-methyl-3-phenyl-1H-pyrazole-4,5-diamine

Synthesis according to: [90]

In this step, water was degassed with Ar-gas before use. Under inert conditions, **2** (1g, 5.77 mmol) was dissolved in 75 ml 0.8 M HCl and cooled to 0 °C. NaNO<sub>2</sub> (398.1 mg, 5.77 mmol) was dissolved in 4 ml dest. H<sub>2</sub>O and added to the reaction mixture, whereby the solution turned red immediately. After 30 min SnCl<sub>2</sub> · 2H<sub>2</sub>O (5.2105 g, 23.09 mmol) was dissolved in 30 ml conc. HCl and added to the solution. The reaction mixture could warm up to RT. After 3 h the reaction mixture turned yellow and the experiment was completed according to TLC (*R<sub>f</sub>* = 0.26, 100 % EE). Therefore, NaOH was added until pH = 7 at 0 °C. Voluminous yellow solid was formed, which was filtered off. The clear and colourless filtrate was extracted 3 times with EE. The combined organic layers were dried with Na<sub>2</sub>SO<sub>4</sub> and the solution was reduced to 5 ml. At -30 °C crystals were formed, which were filtered off, washed 3 times with PE:EE = 1:1 and dried under reduced pressure.

483.9 mg (45 %) white solid

<sup>1</sup>H NMR (DMSO, 200 MHz, 20 °C) δ = 7.84 (d, *J* = 7.1 Hz, 2H, PhH), 7.32 (t, *J* = 7.4 Hz, 2H, PhH), 7.17 (t, *J* = 7.2 Hz, 1H, PhH), 4.64 (s, 2H, NH<sub>2</sub>), 3.53 (s, 3H, CH<sub>3</sub>), 3.27 (s, 2H, NH<sub>2</sub>)

### 5.3.4 Synthesis of 4.5-[Di(phenylimino)methyl]-1-Methyl-3-phenyl-1H-Pyrazole

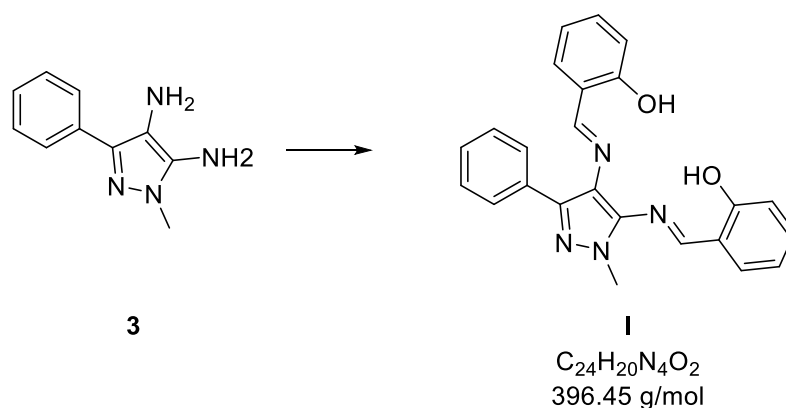


Figure 63: Synthesis of 4.5-[di(phenylimino)methyl]-1-methyl-3-phenyl-1H-pyrazole

Synthesis according to: [86]

**3** (4.43 g, 23.59 mmol) was dissolved in 220 ml abs. MeOH under inert conditions. Salicylaldehyde (7.7 ml, 70.76 mmol) was added to the solution. The reaction mixture was refluxed for 22 h, after which time the reaction was completed according to TLC ( $R_f$  = 0.16, 100 % EE). The reaction mixture was then cooled to -30 °C, whereby yellow crystals were formed, which were filtered off and washed several times with Et<sub>2</sub>O. The product was finally dried under reduced pressure.

6.54 g (70 %) yellow crystalline solid

<sup>1</sup>H NMR (DMSO, 400 MHz, 20 °C)  $\delta$  = 12.15 (s, 1H, OH), 11.32 (s, 1H, OH), 9.16 (s, 1H), 8.69 (s, 1H), 7.77 (dd,  $J$  = 8.1, 1.5 Hz, 1H, PhH), 7.67 – 7.59 (m, 2H, PhH), 7.43 (ddd,  $J$  = 7.6, 6.8, 3.0 Hz, 4H, PhH), 7.39 – 7.32 (m, 2H, PhH), 6.98 (t,  $J$  = 7.3 Hz, 2H, PhH), 6.90 (td,  $J$  = 8.6, 1.5 Hz, 2H, PhH), 3.89 (s, 3H, CH<sub>3</sub>)

<sup>13</sup>C NMR (DMSO, 400 MHz, 20 °C)  $\delta$  = 163.60 (s), 163.02 (s), 159.54 (s), 159.45 (s), 141.04 (s), 139.79 (s), 134.13 (s), 132.92 (s), 132.65 (s), 130.89 (s), 130.19 (s), 128.72 (s), 127.78 (s), 127.21 (s), 120.53 (s), 119.97 (s), 119.93 (s), 119.64 (s), 119.35 (s), 116.75 (s), 116.55 (s), 35.94 (s)

IR (ATR, cm<sup>-1</sup>): 1599 ( $\nu_{C=N}$ ), 1571 ( $\nu_{C=N}$ ), 1405 ( $\nu_{C-O}$ )

UV/VIS (nm ( $\epsilon_{\lambda}$ [m<sup>2</sup>/mol]): 277 (2.63E+06), 334 (1.93E+06)

### 5.3.5 Synthesis of Methyl Pivalate

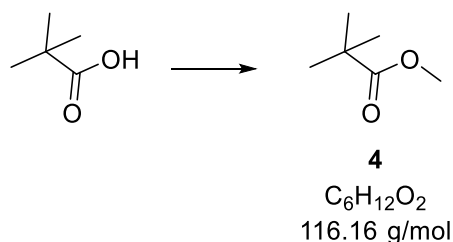


Figure 64: Synthesis of methyl pivalate

Synthesis according to: [87]

Pivalic acid (50 g, 489.6 mmol) was dissolved in 500 ml MeOH. 3 ml H<sub>2</sub>SO<sub>4</sub> were added to the solution, which was then refluxed for 10 h. After the reaction mixture was cooled to RT, 500 ml sat. NaHCO<sub>3</sub> solution were added. The solution was extracted 3 times with DCM. The combined organic layers were dried with Na<sub>2</sub>SO<sub>4</sub> and the solvent was removed. The product was purified by distillation (bp = 101 °C).

38.11 g (67 %) oily colourless liquid

<sup>1</sup>H NMR (DMSO, 200 MHz, 20 °C)  $\delta$  = (s, 3H, CH<sub>3</sub>), 1.14 (s, 9H, tBu)

<sup>13</sup>C NMR (DMSO, 200 MHz, 20 °C)  $\delta$  = 177.82 (s), 51.53 (s), 38.09 (s), 26.86 (s)

### 5.3.6 Synthesis of 4,4-Dimethyl-3-Oxo-Pentanenitrile

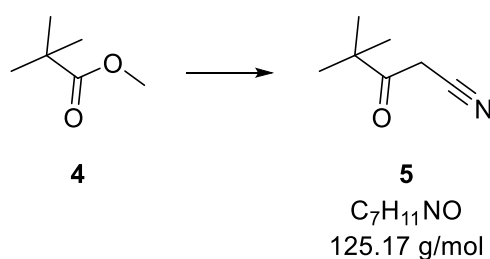


Figure 65: Synthesis of 4,4-dimethyl-3-oxo-pentanenitrile

Synthesis according to: [88]

The synthesis was carried out according to **1**, using **4** (33 g, 284.1 mmol), acetonitrile (30 ml, 568.2 mmol) and NaH (55-60 % dispersion in mineral oil) (18.59, 426.2 mmol).

After the reaction mixture was acidified with conc. HCl, the product didn't precipitate, as it was the case for **1**. Therefore, the solution was extracted 3 times with Et<sub>2</sub>O. The combined organic layers were dried with Na<sub>2</sub>SO<sub>4</sub> and the solvent was removed until dryness. The residue was an oily colourless liquid, a crystallization could be initiated by scratching with a glass stick on the flask's surface.

22.00 g (60 %) white crystalline solid

<sup>1</sup>H NMR (DMSO, 200 MHz, 20 °C)  $\delta$  = 4.24 (s, 2H, CH<sub>2</sub>), 1.09 (s, 9H, tBu)

<sup>13</sup>C NMR (DMSO, 200 MHz, 20 °C)  $\delta$  = 205.17 (s), 116.03 (s), 43.75 (s), 28.25 (s), 25.61 (s)

### 5.3.7 Synthesis of 3-(1,1-Dimethylethyl)-1-Methyl-1H-Pyrazol-5-Amine

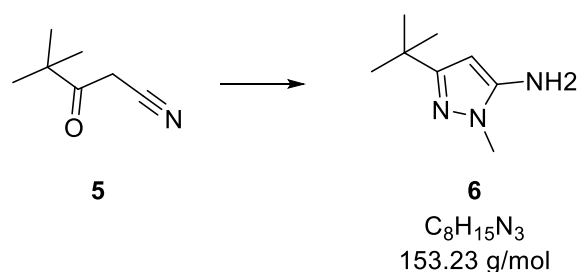


Figure 66: Synthesis of 3-(1,1-dimethylethyl)-1-methyl-1H-pyrazol-5-amine

Synthesis according to: [89]

The synthesis was carried out according to **2**, using **5** (23 g, 183.8 mmol) and methylhydrazine (29 ml, 551.3 mmol).

24.27 g (86 %) crystalline white solid

<sup>1</sup>H NMR (CDCl<sub>3</sub>, 200 MHz, 20 °C)  $\delta$  = 5.12 (s, 1H, CH), 4.95 (s, 2H, NH<sub>2</sub>), 3.43 (s, 3H, CH<sub>3</sub>), 1.14 (s, 9H, tBu)

$^{13}\text{C}$  NMR (DMSO, 200 MHz, 20 °C)  $\delta$  = 158.29 (s), 146.77 (s), 84.62 (s), 33.75 (s), 31.60 (s), 30.43 (s)

### 5.3.8 Synthesis of 3-(1,1-Dimethylethyl)-1-Methyl-1H-Pyrazole-4,5-Diamine

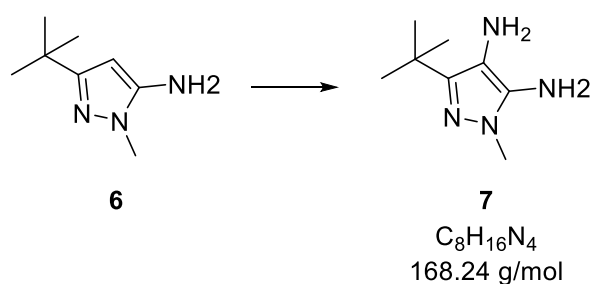


Figure 67: Synthesis of 3-(1,1-dimethylethyl)-1-methyl-1H-pyrazole-4,5-diamine

Synthesis according to: [90]

The synthesis was carried out according to **3**, using **6** (1 g, 6.526 mmol),  $\text{NaNO}_2$  (448.4 mg, 6.526 mmol) and  $\text{SnCl}_2 \cdot 2\text{H}_2\text{O}$  (5.8892 g, 26.10 mmol).

646.7 mg (59 %)

$^1\text{H}$  NMR (DMSO, 200 MHz, 20 °C)  $\delta$  = 4.38 (s, 2H,  $\text{NH}_2$ ), 3.39 (s, 3H,  $\text{CH}_3$ ), 2.77 (s, 2H,  $\text{NH}_2$ ), 1.22 (s, 9H, tBu)

$^{13}\text{C}$  NMR (DMSO, 200 MHz, 20 °C)  $\delta$  = 148.83 (s), 138.04 (s), 108.24 (s), 34.17 (s), 32.16 (s), 29.14 (s)

### 5.3.9 Synthesis of 3-(1.1-Dimethylethyl)-4.5-[Di(phenylimino)methyl]-1-Methyl-1H-Pyrazole

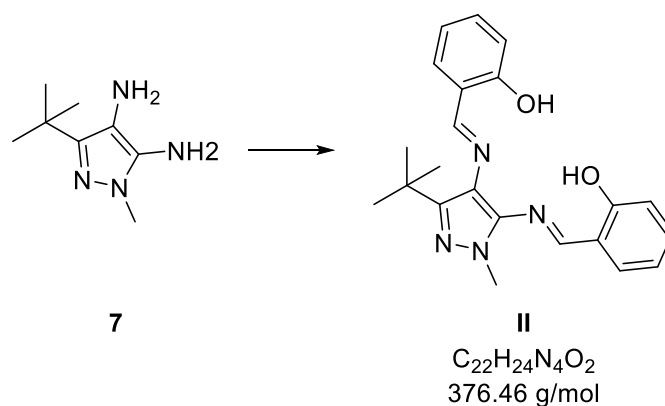


Figure 68: Synthesis of 3-(1.1-dimethylethyl)-4.5-[di(phenylimino)methyl]-1-methyl-1H-Pyrazole

Synthesis according to: [86]

The synthesis was carried out according to I, using **7** (3 g, 17.83 mmol) and salicylaldehyde (5.8 ml, 53.50 mmol).

4.32 g (65 %)

$^1\text{H}$  NMR (DMSO, 400 MHz, 20 °C)  $\delta$  = 12.79 (s, 1H, OH), 11.44 (s, 1H, OH), 8.96 (s, 1H, CH), 8.72 (s, 1H, CH), 7.72 (dd,  $J$  = 8.1, 1.5 Hz, 1H, PhH), 7.48 – 7.24 (m, 3H, PhH), 7.08 – 6.77 (m, 4H, PhH), 3.75 (s, 3H,  $\text{CH}_3$ ), 1.34 (s, 9H, tBu)

$^{13}\text{C}$  NMR (DMSO, 400 MHz, 20 °C)  $\delta$  = 164.04 (s), 162.99 (s), 159.68 (s), 159.58 (s), 151.34 (s), 138.22 (s), 134.07 (s), 132.71 (s), 131.43 (s), 130.54 (s), 120.24 (s), 119.76 (s), 119.70 (s), 119.56 (s), 119.26 (s), 116.74 (s), 116.47 (s), 36.06 (s), 32.80 (s), 29.42 (s)

IR (ATR,  $\text{cm}^{-1}$ ): 1600 ( $\nu_{\text{C=N}}$ ), 1570 ( $\nu_{\text{C=N}}$ ), 1380 ( $\nu_{\text{C-O}}$ )

UV/VIS (nm ( $\epsilon_{\lambda}[\text{m}^2/\text{mol}]$ ): 271 (2.82E+06), 341 (2.32E+06)



### 5.3.10 Synthesis of 1,2-Bis[[2-Hydroxyphenyl]Methylene]Amino]Benzene

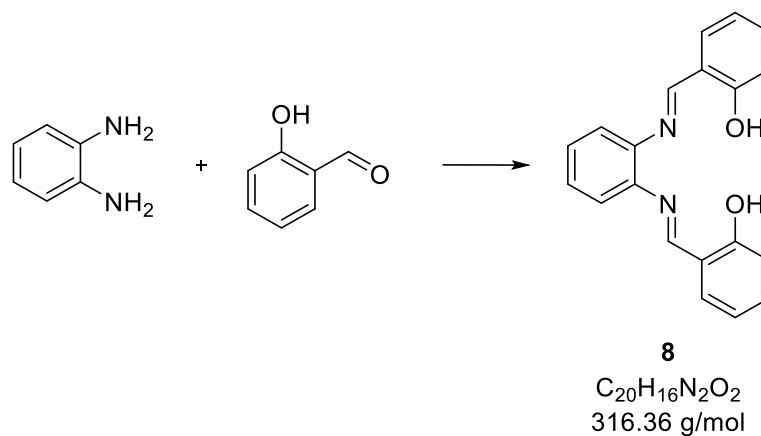


Figure 69: Synthesis of 1,2-Bis[[2-hydroxyphenyl]methylene]amino]benzene

Synthesis according to: [93]

1,2-Phenylenediamine (5 g, 46.24 mmol) was dissolved in 160 ml iPrOH. After salicylaldehyde (11.6 ml, 110.97 mmol) was added to the solution, it was refluxed for 30 min, whereby it turned orange. After the reaction mixture was cooled to -30 °C, orange crystals were formed, which were filtered off, washed three times with Et<sub>2</sub>O and dried under reduced pressure.

9.24 g (63 %) orange crystalline solid

<sup>1</sup>H NMR (DMSO, 250 MHz, 20 °C) δ = 12.94 (s, 2H, OH), 8.94 (s, 2H, CH), 7.67 (d, J = 8.0 Hz, 2H, PhH), 7.44 (q, J = 9.3 Hz, 6H, PhH), 6.98 (t, J = 7.2 Hz, 4H, PhH)

<sup>13</sup>C NMR (DMSO, 250 MHz, 20 °C) δ = 164.04 (s), 160.37 (s), 142.26 (s), 133.43 (s), 132.44 (s), 127.80 (s), 119.75 (s), 119.48 (s), 119.07 (s), 116.66 (s)

IR (ATR, cm<sup>-1</sup>): 1560 (ν<sub>C=N</sub>), 1275 (ν<sub>C-O</sub>)

UV/VIS (nm (ε<sub>λ</sub>[m<sup>2</sup>/mol])): 272 (1.98E+06), 334 (1.52E+06)

### 5.3.11 Synthesis of 3-Acetyl-4-Hydroxychromen-2-One

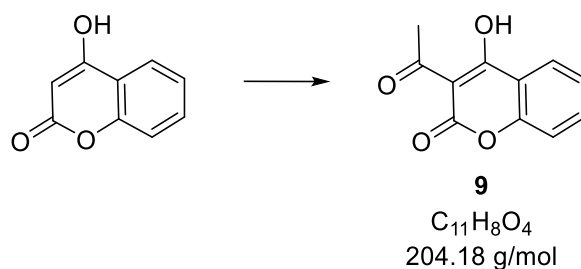


Figure 70: Synthesis of 3-acetyl-4-hydroxychromen-2-one:

Synthesis according to: [85]

4-Hydroxycoumarin (28.02 g, 172.8 mmol) was dissolved in 170 ml acetic acid. After the addition of  $POCl_3$  (42 ml, 460.2 mmol) the reaction mixture was refluxed for 2 h. At RT crystals were formed, which were collected by filtration, washed with several portions of dest.  $H_2O$  and  $Et_2O$  and finally dried under reduced pressure.

19.96 g (79 %) white/beige crystalline solid

$^1H$  NMR (DMSO, 250 MHz, 20 °C)  $\delta$  = 17.63 (s, 1H, OH), 7.95 (d,  $J$  = 7.7 Hz, 1H, PhH), 7.88 – 7.70 (m, 1H, PhH), 7.55 – 7.19 (m, 2H, PhH), 2.64 (s, 3H,  $CH_3$ )

$^{13}C$  NMR (DMSO, 250 MHz, 20 °C)  $\delta$  = 205.50 (s), 177.85 (s), 154.13 (s), 136.67 (s), 125.14 (s), 124.74 (s), 116.81 (s), 114.67 (s), 101.35 (s), 29.56 (s)

### 5.3.12 Synthesis of [1,2-Phenylbis(iminoethylidyne)]bis[2H-1-Benzopyran-2,4(3H)-Dione]

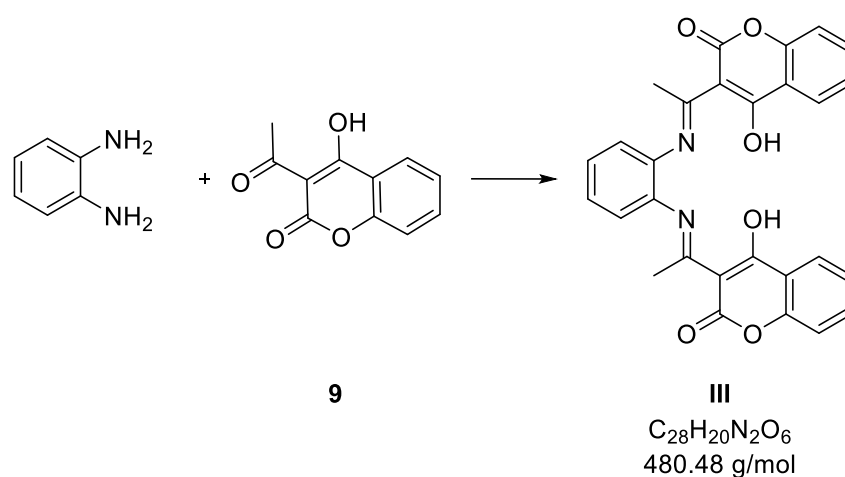


**Figure 71: Synthesis of [1,2-Phenylbis(iminoethylidyne)]bis[2H-1-benzopyran-2,4(3H)-dione]**

Synthesis according to: [86]

The synthesis was carried out according to I, using 1,2-phenylenediamine (1.50 g, 13.87 mmol) and **9** (6.80 g, 33.29 mmol).

3.00 g (45 %) light yellow crystalline solid

$^1\text{H}$  NMR (DMSO, 250 MHz, 20 °C)  $\delta$  = 15.33 (s, 2H, OH), 7.79 (d,  $J$  = 7.8 Hz, 2H, PhH), 7.74 – 7.53 (m, 6H, PhH), 7.33 – 7.06 (m, 4H, PhH), 2.58 (s, 6H,  $\text{CH}_3$ )

$^{13}\text{C}$  NMR (DMSO, 400 MHz, 20 °C)  $\delta$  = 176.57 (s), 166.98 (s), 153.17 (s), 143.78 (s), 134.72 (s), 132.22 (s), 129.35 (s), 128.00 (s), 125.68 (s), 123.91 (s), 116.41 (s), 97.84 (s), 91.00 (s), 20.69 (s)

IR (ATR,  $\text{cm}^{-1}$ ): 1605 ( $\nu_{\text{C}=\text{N}}$ ), 1574 ( $\nu_{\text{C}=\text{N}}$ ), 1420 ( $\nu_{\text{C}-\text{O}}$ )

UV/VIS (nm ( $\epsilon_{\lambda}[\text{m}^2/\text{mol}]$ ): 441 (2.08E+04)

### 5.3.13 Synthesis of (3E,3'E)-3,3'-[1,2-Ethanediybis (Iminoethylidyne)] Bis [2H-1-Benzopyran-2,4(3H)-Dione]

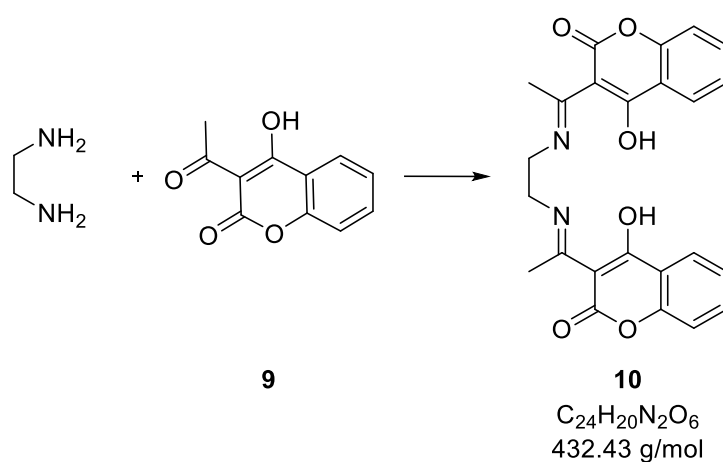


Figure 72: Synthesis of (3E,3'E)-3,3'-[1,2-Ethanediybis(iminoethylidyne)]bis[2H-1-benzopyran-2,4(3H)-dione]

Synthesis according to: [93]

The synthesis was carried out according to **8**, using 1,2-ethylenediamine (128.0 mg, 2.129 mmol) and **9** (1 g, 4.898 mmol).

766.1 mg (83 %) white solid

<sup>1</sup>H NMR (DMSO, 2504 MHz, 20 °C)  $\delta$  = 13.79 (s, 2H, OH), 7.93 (dd,  $J$  = 7.8, 1.5 Hz, 2H, PhH), 7.78 – 7.47 (m, 2H, PhH), 7.38 – 7.13 (m, 4H, PhH), 4.08 – 3.93 (m, 4H, CH<sub>2</sub>), 2.71 (s, 6H, CH<sub>3</sub>)

IR (ATR, cm<sup>-1</sup>): 1606 ( $\nu_{C=N}$ ), 1569 ( $\nu_{C=N}$ ), 1245 ( $\nu_{C-O}$ )

UV/VIS (nm ( $\epsilon_{\lambda}$ [m<sup>2</sup>/mol]): 337 (1.89E+06)

### 5.3.14 Synthesis of [1,2-Cyclohexylbis(Iminoethylidyne)]Bis[2H-1-Benzopyran-2,4(3H)-Dione]

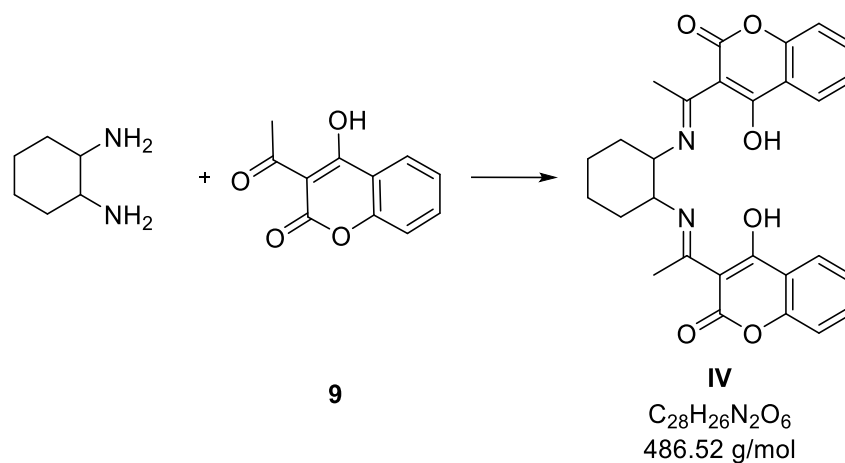


Figure 73: Synthesis of [1,2-Cyclohexylbis(iminoethylidyne)]bis[2H-1-benzopyran-2,4(3H)-dione]

Synthesis according to: [86]

The synthesis was carried out according to I, using 1,2-cyclohexanediamine (1.2 ml, 9.795 mmol) and **9** (4 g, 19.591 mmol).

4.39 g (90 %) white solid

$^1H$  NMR (DMSO, 400 MHz, 20 °C)  $\delta$  = 14.03 (d,  $J$  = 5.3 Hz, 2H, OH), 7.91 (dd,  $J$  = 7.9, 1.6 Hz, 2H, PhH), 7.61 (ddd,  $J$  = 8.4, 7.3, 1.7 Hz, 2H, PhH), 7.31 – 7.24 (m, 2H, PhH), 7.23 – 7.18 (m, 2H, PhH), 4.42 (t,  $J$  = 8.4 Hz, 2H, CH), 2.62 (s, 6H,  $CH_3$ ), 2.06 (d,  $J$  = 11.1 Hz, 2H,  $CH_2$ ), 1.75 (s, 4H,  $CH_2$ ), 1.52 (d,  $J$  = 10.1 Hz, 2H,  $CH_2$ )

$^{13}C$  NMR (DMSO, 400 MHz, 20 °C)  $\delta$  = 179.95 (s), 176.05 (s), 161.59 (s), 153.04 (s), 134.27 (s), 125.61 (s), 123.76 (s), 119.90 (s), 116.28 (s), 96.21 (s), 56.44 (s), 30.82 (s), 23.13 (s), 18.43 (s)

IR (ATR,  $cm^{-1}$ ): 1687 ( $\nu_{C=N}$ ), 1571 ( $\nu_{C=N}$ ), 1272 ( $\nu_{C-O}$ )

### 5.3.15 Synthesis of 2-Methyl-1,10-Phenanthroline

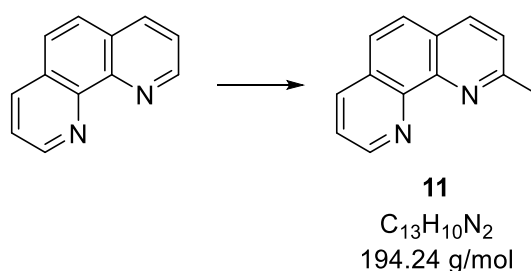


Figure 74: Synthesis of 2-Methyl-1,10-phenanthroline

Synthesis according to: [91]

Under an argon atmosphere MeLi (17.4 ml 1.6 M solution in  $Et_2O$ , 27.74 mmol) was dissolved in 75 ml abs. THF. The solution was then cooled to  $-10^\circ C$ . A suspension of 1,10-Phenanthroline (5.00 g, 27.74 mmol) in 50 ml abs. THF was prepared in a glovebox and added slowly to the prior prepared MeLi-solution. By doing so, the reaction mixture turned dark. It could then warm up to RT and was stirred for 20 h under an argon atmosphere.

To quench the reaction, it was cooled to  $0^\circ C$ . Afterwards, 15 ml of brine were added dropwise, by which it turned yellow. The received solution was then extracted with 20 ml of brine. The organic layer was then collected and the solvent was evaporated completely.

The so obtained oily residue was dissolved in 200 ml diethyl ether.  $MnO_2$  (31.2 g, 358.9 mmol) was added in small portions. The reaction mixture was stirred for 3 h at RT, then  $MgSO_4$  was added, after which it was stirred for 30 more min. The reaction mixture was then filtered through celith, by which a colourless filtrate could be obtained. The filter cake was washed with diethyl ether. The filtrate was evaporated completely, whereby a yellowish oily residue could be obtained. The residue was dissolved in the least amount of ethyl acetate and covered with n-hexane. After it was kept in the freezer overnight, a white solid was formed, which was collected by filtration. It was washed three times with small portions of n-hexane and dried.

3.36 g (62 %) white solid

$^1\text{H}$  NMR (DMSO, 400 MHz, 20 °C)  $\delta$  = 9.08 (dd,  $J$  = 4.3, 1.8 Hz, 1H, PhH), 8.44 (dd,  $J$  = 8.1, 1.8 Hz, 1H, PhH), 8.35 (d,  $J$  = 8.2 Hz, 1H, PhH), 7.91 (q,  $J$  = 8.8 Hz, 1H, PhH), 7.73 (dd,  $J$  = 8.1, 4.3 Hz, 1H, PhH), 7.63 (d,  $J$  = 8.2 Hz, 1H, PhH), 2.78 (s, 1H,  $\text{CH}_3$ )

$^{13}\text{C}$  NMR (DMSO, 400 MHz, 20 °C)  $\delta$  = 158.43 (s), 149.65 (s), 145.30 (s), 144.97 (s), 136.34 (s), 136.07 (s), 128.50 (s), 126.47 (s), 126.44 (s), 125.58 (s), 123.51 (s), 123.02 (s), 24.99 (s)

### 5.3.16 Synthesis of 1,10-Phenanthroline-2-Carbaldehyde

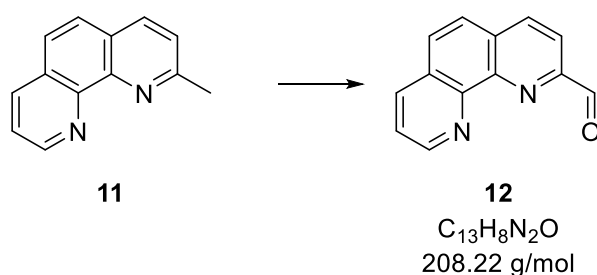


Figure 75: Synthesis of 1,10-Phenanthroline-2-carbaldehyde

Synthesis according to: [92]

In a first step **11** (500 mg, 2.574 mmol) and  $\text{SeO}_2$  (571.3 mg, 5.148 mmol) were dissolved in 10 ml 1,4-dioxane. The reaction mixture was refluxed for 25 min, after which it was finished according to TLC (EE:MeOH = 9:1 + 3 drops  $\text{NH}_3$ ). The reaction was stopped by a filtration trough celith. The filter cake was washed with EE and the solvent was evaporated completely.

517.9 mg (96 %) beige solid

$^1\text{H}$  NMR (DMSO, 400 MHz, 20 °C)  $\delta$  = 10.31 (d,  $J$  = 0.8 Hz, 1H, CH), 9.19 (dd,  $J$  = 4.3, 1.8 Hz, 1H, PhH), 8.71 (dd,  $J$  = 8.3, 0.6 Hz, 1H, PhH), 8.56 (dd,  $J$  = 8.1, 1.8 Hz, 1H, PhH), 8.23 (d,  $J$  = 8.2 Hz, 1H, PhH), 8.13 (dd,  $J$  = 26.6, 8.9 Hz, 2H, PhH), 7.85 (dd,  $J$  = 8.1, 4.3 Hz, 1H, PhH)

$^{13}\text{C}$  NMR (DMSO, 400 MHz, 20 °C)  $\delta$  = 193.95 (s), 151.80 (s), 150.56 (s), 145.37 (d,  $J$  = 9.3 Hz), 137.99 (s), 136.52 (s), 130.93 (s), 129.65 (s), 128.92 (s), 126.35 (s), 123.97 (s), 119.42 (s)

### 5.3.17 Synthesis of N,N'-(Ethane-1,2-Diyl)-Bis(1,10-Phenanthroline-2-yl)Methanimin

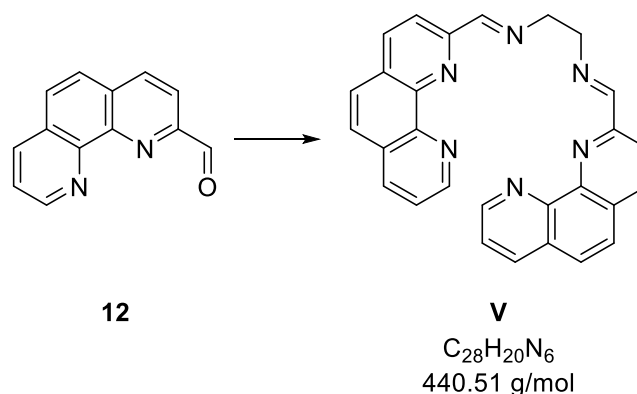


Figure 76: Synthesis of N,N'-(Ethane-1,2-diyl)-bis(1,10-phenanthroline-2-yl)methanimin

Synthesis according to: [93]

The synthesis was carried out according to **8**, using 1,2-ethylenediamine (36.6 mg, 0.6091 mmol) and **12** (279.0 mg, 1.3400 mmol).

188.0 mg (70 %) light brown solid

$^1H$  NMR ( $CDCl_3$ , 400 MHz, 20 °C)  $\delta$  = 9.20 (dd,  $J$  = 4.3, 1.5 Hz, 2H, PhH), 8.98 (s, 2H, CH), 8.41 (d,  $J$  = 8.4 Hz, 2H, PhH), 8.22 (dd,  $J$  = 12.1, 4.9 Hz, 4H, PhH), 7.77 (s, 4H, PhH), 7.61 (dd,  $J$  = 8.0, 4.4 Hz, 2H, PhH), 4.20 (s, 4H,  $CH_2$ )

$^{13}C$  NMR ( $CDCl_3$ , 400 MHz, 20 °C)  $\delta$  = 164.68 (s), 154.76 (s), 150.66 (s), 146.20 (s), 145.73 (s), 136.73 (s), 136.25 (s), 129.52 (s), 128.95 (s), 127.43 (s), 126.55 (s), 123.17 (s), 120.60 (s), 61.67 (s)

## 5.4 Synthesis of coordination Compounds

All coordination compounds were synthesized under inert conditions. To facilitate the ligand's deprotonation, a base, such as  $Et_3N$ ,  $tBuOK$  or  $MeLi$ , was added to the ligand's solution. This base was added before the coordination reaction was carried out, in order to facilitate the coordination to the respective metal.

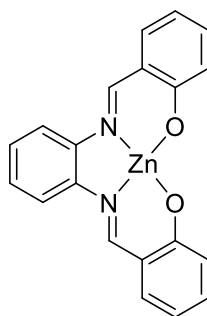


### 5.4.1 Coordination Compounds of Zn

A general procedure for the synthesis of the coordination compounds of Zn is given here:

$\text{Zn}(\text{NO}_3)_2 \cdot 6\text{H}_2\text{O}$  (1 eq.) was dissolved in 5 ml of abs. THF (colourless solution). The respective ligand (1.2 eq.) was dissolved in 5 ml abs. THF (yellow solution) and deprotonated with a base (2.4-3 eq.). The solutions were combined. By doing so, a slight colour change could be observed already into a much darker yellow/orange. It was only in the case of **10a** that all solutions were colourless at every time. The reaction mixture was stirred for 24 hours at RT. After that time, the product precipitated, was filtered off, washed three times with small amounts of abs. DCM and dried under reduced pressure.

#### 5.4.1.1 Synthesis of **8a**



**8a**

$\text{C}_{20}\text{H}_{14}\text{N}_2\text{O}_2\text{Zn}$   
379.72 g/mol

Figure 77: Synthesis of **8a**

**8a** was synthesized, using  $\text{Zn}(\text{NO}_3)_2 \cdot 6\text{H}_2\text{O}$  (117.5 mg, 0.4741 mmol) as metal precursor, **8** (150 mg, 0.4741 mmol) as ligand and  $\text{Et}_3\text{N}$  (0.13 ml, 0.9483 mmol) as deprotonating agent.

107.3 mg (72 %) yellow powder

$^1\text{H}$  NMR (DMSO, 400 MHz, 20 °C)  $\delta$  = 9.02 (s, 2H, CH), 7.95 – 7.86 (m, 2H, PhH), 7.42 (dd,  $J$  = 7.9, 1.8 Hz, 2H, PhH), 7.39 (dd,  $J$  = 6.1, 3.4 Hz, 2H, PhH), 7.25 (ddd,  $J$  = 8.7, 6.8, 1.9 Hz, 2H, PhH), 6.71 (dd,  $J$  = 8.5, 0.8 Hz, 2H, PhH), 6.52 (ddd,  $J$  = 7.9, 6.9, 1.1 Hz, 2H, PhH)

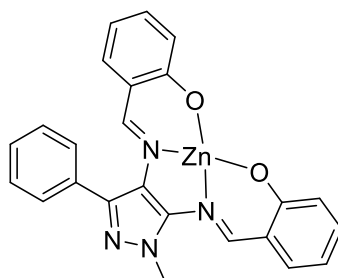
$^{13}\text{C}$  NMR (DMSO, 400 MHz, 20 °C)  $\delta$  = 172.27 (s), 162.83 (s), 139.37 (s), 136.24 (s), 134.33 (s), 127.26 (s), 123.09 (s), 119.44 (s), 116.48 (s), 112.97 (s)

EA (found (calculated), %): C: 63.02 (63.26), H: 4.64 (3.72), N: 7.11 (7.38)

IR (ATR,  $\text{cm}^{-1}$ ): 1528 ( $\nu_{\text{C=N}}$ ), 1244 ( $\nu_{\text{C-O}}$ ), 532 ( $\nu_{\text{Zn-O}}$ ), 490 ( $\nu_{\text{Zn-N}}$ )

UV/VIS (nm ( $\epsilon_{\lambda}[\text{m}^2/\text{mol}]$ ): 402 (2.25E+06), 297 (2.51E+06), 260 (1.93E+06)

#### 5.4.1.2 Synthesis of **1a**



**1a**

$\text{C}_{24}\text{H}_{18}\text{N}_4\text{O}_2\text{Zn}$   
458.07 g/mol

**Figure 78: Synthesis of **1a****

**1a** was synthesized, using  $\text{Zn}(\text{NO}_3)_2 \cdot 6\text{H}_2\text{O}$  (93.8 mg, 0.3153 mmol) as metal precursor, **1** (150 mg, 0.3784 mmol) as ligand and  $\text{Et}_3\text{N}$  (0.10 ml, 0.7567 mmol) as deprotonating agent.

80.5 mg (56 %) orange powder

$^1\text{H}$  NMR (DMSO, 400 MHz, 20 °C)  $\delta$  = 8.92 (s, 1H, CH), 8.49 (s, 1H, CH), 7.63 – 7.58 (m, 2H, PhH), 7.57 – 7.46 (m, 3H, PhH), 7.43 (dd,  $J$  = 8.0, 1.8 Hz, 1H, PhH), 7.27 (ddd,  $J$  = 8.7, 6.8, 1.9 Hz, 1H, PhH), 7.16 (ddd,  $J$  = 8.7, 6.9, 1.9 Hz, 1H, PhH), 6.72 (dd,  $J$  = 8.6, 0.8 Hz, 1H, PhH), 6.71 – 6.65 (m, 2H, PhH), 6.54 (ddd,  $J$  = 7.9, 6.9, 1.1 Hz, 1H, PhH), 6.42 – 6.36 (m, 1H), 4.20 (s, 3H,  $\text{CH}_3$ )

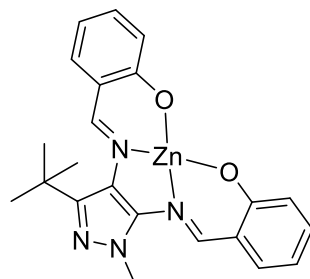
$^{13}\text{C}$  NMR (DMSO, 400 MHz, 20 °C)  $\delta$  = 172.35 (s), 171.36 (s), 161.87 (s), 158.77 (s), 139.12 (s), 138.87 (s), 136.31 (s), 134.63 (s), 134.49 (s), 133.36 (s), 132.93 (s), 128.89 (s), 128.58 (s), 128.15 (s), 123.48 (s), 122.98 (s), 120.27 (s), 119.56 (s), 118.98 (s), 113.22 (s), 112.97 (s)

EA (found (calculated), %): C: 62.54 (62.69), H: 4.61 (3.95), N: 11.94 (12.18)

IR (ATR,  $\text{cm}^{-1}$ ): 1602 ( $\nu_{\text{C=N}}$ ), 1526 ( $\nu_{\text{C=N}}$ ), 1395 ( $\nu_{\text{C-O}}$ ), 556 ( $\nu_{\text{Zn-O}}$ ), 490 ( $\nu_{\text{Zn-N}}$ )

UV/VIS (nm ( $\epsilon_{\lambda}$ [m<sup>2</sup>/mol]): 261 (2.54E+06), 299 (2.47E+06), 326 (2.25E+06), 343 (2.32E+06), 400 (2.80E+06), 451 (1.69E+06)

#### 5.4.1.3 Synthesis of IIa



**IIa**

C<sub>22</sub>H<sub>22</sub>N<sub>4</sub>O<sub>2</sub>Zn  
439.82 g/mol

**Figure 79: Synthesis of IIa**

**IIa** was synthesized, using Zn(NO<sub>3</sub>)<sub>2</sub> · 6H<sub>2</sub>O (98.8 mg, 0.3320 mmol) as metal precursor, **II** (150 mg, 0.3984 mmol) as ligand and Et<sub>3</sub>N (0.11 ml, 0.7969 mmol) as deprotonating agent.

85.6 mg (59 %) orange powder

<sup>1</sup>H NMR (DMSO, 400 MHz, 20 °C)  $\delta$  = 8.83 (s, 1H, CH), 8.64 (s, 1H, CH), 7.38 (dd, J = 7.9, 1.9 Hz, 1H, PhH), 7.29 – 7.16 (m, 3H, PhH), 6.69 (d, J = 8.6 Hz, 2H, PhH), 6.50 (tdd, J = 7.9, 2.3, 1.1 Hz, 2H, PhH), 4.08 (s, 3H, CH<sub>3</sub>), 1.42 (s, 9H, CCH<sub>3</sub>)

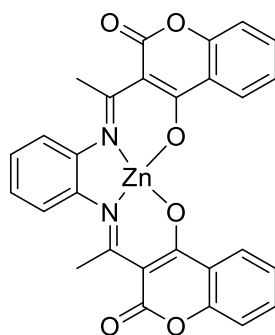
<sup>13</sup>C NMR (DMSO, 400 MHz, 20 °C)  $\delta$  = 172.39 (s), 170.64 (s), 161.96 (s), 161.49 (s), 147.36 (s), 139.48 (s), 136.22 (s), 134.89 (s), 134.60 (s), 133.18 (s), 123.34 (s), 122.79 (s), 120.65 (s), 119.43 (s), 119.33 (s), 113.05 (s), 112.99 (s), 45.76 (s), 32.39 (s), 29.24 (s)

EA (found (calculated), %): C: 60.01 (60.08), H: 5.27 (5.04), N: 12.56 (12.74)

IR (ATR, cm<sup>-1</sup>): 1602 ( $\nu_{C=N}$ ), 1548 ( $\nu_{C=N}$ ), 1365 ( $\nu_{C-O}$ ), 550 ( $\nu_{Zn-O}$ ), 478 ( $\nu_{Zn-N}$ )

UV/VIS (nm ( $\epsilon_{\lambda}$ [m<sup>2</sup>/mol]): 260 (1.25E+06), 295 (1.24E+06), 342 (2.23E+06), 393 (1.38E+06), 451 (9.10E+05)

#### 5.4.1.4 Synthesis of IIIa



**IIIa**

$C_{28}H_{18}N_2O_6Zn$

543.84 g/mol

**Figure 80: Synthesis of IIIa**

**IIIa** was synthesized, using  $Zn(NO_3)_2 \cdot 6H_2O$  (51.6 mg, 0.1734 mmol) as metal precursor, **III** (100 mg, 0.2081 mmol) as ligand and  $Et_3N$  (0.07 ml, 0.5202 mmol) as deprotonating agent.

45.0 mg (48 %) dark yellow powder

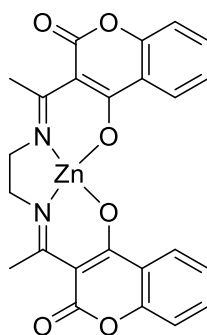
$^1H$  NMR (DMSO, 400 MHz, 20 °C)  $\delta$  = 8.61 (d,  $J$  = 7.2 Hz, 2H, PhH), 8.01 (t,  $J$  = 7.2 Hz, 2H, PhH), 7.70 (t,  $J$  = 7.0 Hz, 6H, PhH), 7.62 (d,  $J$  = 8.2 Hz, 2H, PhH), 3.12 (s, 6H,  $CH_3$ )

$^{13}C$  NMR (DMSO, 400 MHz, 20 °C)  $\delta$  = 153.94 (s), 140.18 (s), 133.07 (s), 131.61 – 130.52 (m), 126.86 (s), 125.75 (s), 124.91 (s), 123.73 (s), 123.42 (s), 116.04 (s), 105.47 (s), 102.04 (s), 46.78 (s)

IR (ATR,  $cm^{-1}$ ): 1604 ( $\nu_{C=N}$ ), 1561 ( $\nu_{C=N}$ ), 1389 ( $\nu_{C-O}$ ), 532 ( $\nu_{Zn-O}$ ), 496 ( $\nu_{Zn-N}$ )

UV/VIS (nm ( $\epsilon_{\lambda}[m^2/mol]$ ): 337 (2.45E+06)

#### 5.4.1.5 Synthesis of 10a



**10a**

$C_{24}H_{18}N_2O_6Zn$   
495.80 g/mol

**Figure 81: Synthesis of 10a**

**10a** was synthesized, using  $Zn(NO_3)_2 \cdot 6H_2O$  (119.3 mg, 0.3854 mmol) as metal precursor, **10** (200 mg, 0.4625 mmol) as ligand and tBuOK (129.7 mg, 1.1563 mmol) as deprotonating agent.

85.6 mg (45 %) white powder

$^1H$  NMR (DMSO, 250 MHz, 20 °C)  $\delta$  = 8.07 (d,  $J$  = 7.9 Hz, 1H, PhH), 7.89 (d,  $J$  = 8.2 Hz, 1H, PhH), 7.64 – 7.49 (m, 2H, PhH), 7.35 – 7.15 (m, 4H, PhH), 3.84 (s, 2H,  $CH_2$ ), 3.71 (s, 2H,  $CH_2$ ), 2.35 (s, 6H,  $CH_3$ )

EA (found (calculated), %): C: 57.59 (58.14), H: 4.45 (3.66), N: 5.71 (5.65)

IR (ATR,  $cm^{-1}$ ): 1594 ( $\nu_{C=N}$ ), 1561 ( $\nu_{C=N}$ ), 1232 ( $\nu_{C-O}$ ), 570 ( $\nu_{Zn-O}$ ), 496 ( $\nu_{Zn-N}$ )

UV/VIS (nm ( $\epsilon_{\lambda}[m^2/mol]$ ): 325 (6.56E+05)

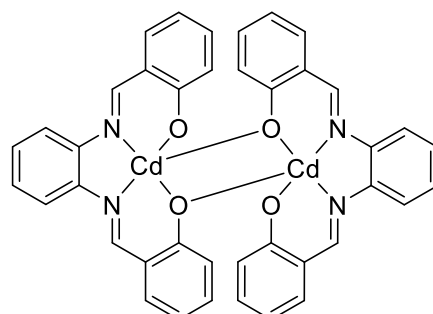
#### 5.4.2 Coordination Compounds of Cd

A general procedure for the synthesis of the coordination compounds of Cd is given here:

$Cd(NO_3)_2 \cdot 4H_2O$  (1 eq.) was dissolved in 5 ml of abs. THF (colourless solution). The respective ligand (1.2 eq.) was dissolved in 5 ml abs. THF (yellow solution) and deprotonated with a base (2.4-3 eq.). The solutions were combined. By doing so, a slight colour change could be observed already into a much darker yellow/orange. It was just in the case of **10b** that all solutions were colourless at every time. The reaction mixture was stirred for 24 hours at RT.

After that time, the product precipitated, was filtered off, washed three times with little amounts of abs. DCM and dried under reduced pressure.

#### 5.4.2.1 Synthesis of **8b**



**8b**

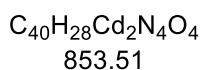


Figure 82: Synthesis of **8b**

**8b** was synthesized, using  $\text{Cd}(\text{NO}_3)_2 \cdot 4\text{H}_2\text{O}$  (121.9 mg, 0.4741 mmol) as metal precursor, **8** (150 mg, 0.4741 mmol) as ligand and  $\text{Et}_3\text{N}$  (0.13 ml, 0.9483 mmol) as deprotonating agent.

135.3 mg (80 %) yellow powder

$^1\text{H}$  NMR (DMSO, 400 MHz, 20 °C)  $\delta$  = 8.69 – 8.60 (m, 4H, CH), 7.62 – 7.56 (m, 4H, PhH), 7.33 (ddd,  $J$  = 9.8, 7.7, 2.8 Hz, 8H, PhH), 7.15 (ddd,  $J$  = 8.6, 6.8, 1.9 Hz, 4H, PhH), 6.60 (dd,  $J$  = 8.5, 1.0 Hz, 4H, PhH), 6.41 (ddd,  $J$  = 7.9, 6.9, 1.1 Hz, 4H, PhH)

$^{13}\text{C}$  NMR (DMSO, 400 MHz, 20 °C)  $\delta$  = 173.33 (s), 164.75 (s), 141.07 (s), 137.20 (s), 133.32 (s), 126.80 (s), 124.01 (s), 120.68 (s), 117.65 (s), 111.96 (s)

EA (found (calculated), %): C: 55.93 (56.29), H: 3.48 (3.31), N: 6.41 (6.56)

IR (ATR,  $\text{cm}^{-1}$ ): 1538 ( $\nu_{\text{C}=\text{N}}$ ), 1249 ( $\nu_{\text{C}-\text{O}}$ ), 525 ( $\nu_{\text{Cd}-\text{O}}$ ), 476 ( $\nu_{\text{Cd}-\text{N}}$ )

UV/VIS (nm ( $\epsilon_{\lambda}[\text{m}^2/\text{mol}]$ ): 260 (2.89E+06), 294 (2.74E+06), 400 (2.50E+06)

#### 5.4.2.2 Synthesis of Ib

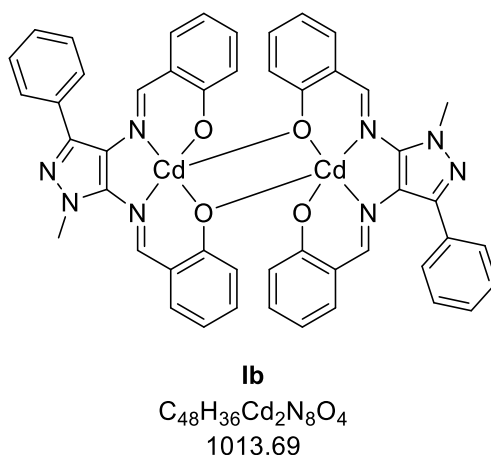


Figure 83: Synthesis of Ib

**Ib** was synthesized, using  $Cd(NO_3)_2 \cdot 4H_2O$  (97.6 mg, 0.3153 mmol) as metal precursor, **I** (150 mg, 0.3784 mmol) as ligand and tBuOK (106.1 mg, 0.9459 mmol) as deprotonating agent.

78.6 mg (49 %) dark orange powder

$^1H$  NMR (DMSO, 400 MHz, 20 °C)  $\delta$  = 8.75 – 8.65 (m, 2H, CH), 8.30 – 8.20 (m, 2H, CH), 7.56 (d,  $J$  = 7.0 Hz, 4H, PhH), 7.49 (t,  $J$  = 7.3 Hz, 4H, PhH), 7.44 (d,  $J$  = 7.1 Hz, 2H, PhH), 7.31 (d,  $J$  = 6.8 Hz, 2H, PhH), 7.21 – 7.14 (m, 2H, PhH), 7.05 (t,  $J$  = 6.9 Hz, 2H, PhH), 6.59 (d,  $J$  = 8.6 Hz, 2H, PhH), 6.53 (t,  $J$  = 8.0 Hz, 4H, PhH), 6.42 (t,  $J$  = 7.2 Hz, 2H, PhH), 6.25 (t,  $J$  = 7.1 Hz, 2H, PhH), 4.08 (s, 6H,  $CH_3$ )

$^{13}C$  NMR (DMSO, 400 MHz, 20 °C)  $\delta$  = 173.82 (s), 172.74 (s), 164.50 (s), 161.59 (s), 139.40 (s), 139.11 (s), 137.13 (s), 135.98 (s), 135.38 (s), 133.83 (s), 133.44 (s), 132.54 (s), 131.41 (s), 130.48 (s), 128.76 (s), 128.14 (s), 127.75 (s), 124.40 (s), 123.91 (s), 112.10 (s), 111.82 (s)

EA (found (calculated), %): C: 56.42 (56.87), H: 4.31 (3.58), N: 11.18 (11.05)

IR (ATR,  $cm^{-1}$ ): 1595 ( $\nu_{C=N}$ ), 1532 ( $\nu_{C=N}$ ), 1397 ( $\nu_{C-O}$ ), 554 ( $\nu_{Cd-O}$ ), 490 ( $\nu_{Cd-N}$ )

UV/VIS (nm ( $\epsilon_{\lambda}[m^2/mol]$ ): 262 (2.67E+06), 298 (1.96E+06), 344 (1.63E+06), 400 (2.31E+06), 450 (1.28E+06)

### 5.4.2.3 Synthesis of IIb

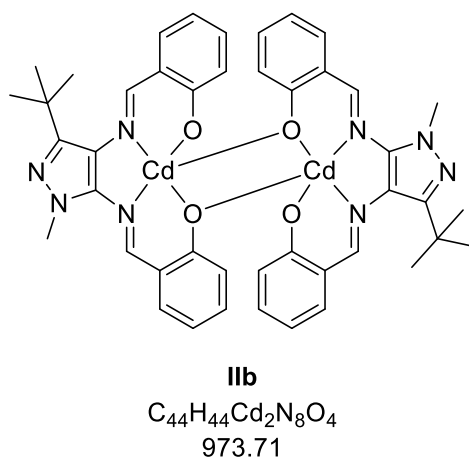


**Figure 84: Synthesis of IIb**

**IIb** was synthesized, using  $Cd(NO_3)_2 \cdot 4H_2O$  (137.0 mg, 0.4427 mmol) as metal precursor, **II** (200 mg, 0.5313 mmol) as ligand and MeLi (0.72 ml, 1.6 M solution in  $Et_2O$ , 1.1511 mmol) as deprotonating agent.

111.6 mg (52 %) orange powder

$^1H$  NMR (DMSO, 250 MHz, 20 °C)  $\delta$  = 8.67 (s, 2H, CH), 8.56 (s, 2H, CH), 7.32 (d,  $J$  = 6.3 Hz, 2H, PhH), 7.18 (dd,  $J$  = 7.8, 2.0 Hz, 2H, PhH), 7.13 – 6.87 (m, 4H, PhH), 6.55 (d,  $J$  = 6.5 Hz, 2H, PhH), 6.46 (d,  $J$  = 5.2 Hz, 2H, PhH), 6.32 (d,  $J$  = 8.5 Hz, 4H, PhH), 3.77 (s, 6H,  $CH_3$ ), 1.35 (s, 16H,  $CCH_3$ )

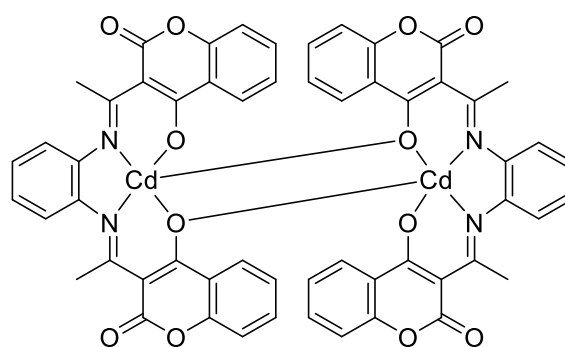
EA (found (calculated), %): C: 54.17 (54.28), H: 4.95 (4.55), N: 11.24 (11.51)

IR (ATR,  $cm^{-1}$ ): 1601 ( $\nu_{C=N}$ ), 1538 ( $\nu_{C=N}$ ), 1362 ( $\nu_{C-O}$ ), 554 ( $\nu_{Cd-O}$ ), 465 ( $\nu_{Cd-N}$ )

UV/VIS (nm ( $\epsilon_{\lambda}[m^2/mol]$ ): 261 (2.41E+06), 346 (1.01E+06), 386 (1.15E+06)



#### 5.4.2.4 Synthesis of IIIb



**IIIb**

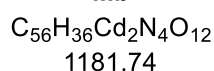


**Figure 85: Synthesis of IIIb**

**IIIb** was synthesized, using  $\text{Cd}(\text{NO}_3)_2 \cdot 4\text{H}_2\text{O}$  (53.7 mg, 0.1734 mmol) as metal precursor, **III** (100 mg, 0.2081 mmol) as ligand and  $\text{Et}_3\text{N}$  (0.07 ml, 0.5202 mmol) as deprotonating agent.

43.0 mg (42 %) dark yellow powder

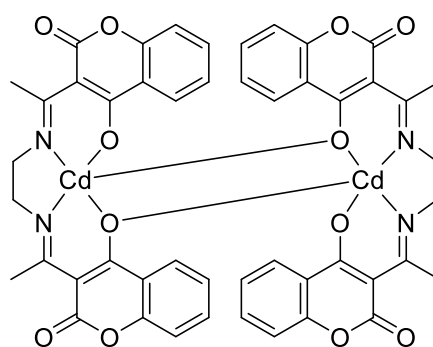
$^1\text{H}$  NMR (acetone  $\text{d}_6$ , 400 MHz, 20 °C)  $\delta$  = 8.08 (d,  $J$  = 8.1 Hz, 2H, PhH), 7.89 (d,  $J$  = 5.8 Hz, 2H, PhH), 7.75 – 7.62 (m, 2H, PhH), 7.54 – 7.39 (m, 6H, PhH), 7.26 (d,  $J$  = 7.4 Hz, 2H, PhH), 7.21 – 7.03 (m, 10H, PhH), 2.46 (s, 12H,  $\text{CH}_3$ )

EA (found (calculated), %): C: 56.87 (56.92), H: 3.15 (3.07), N: 4.92 (4.74)

IR (ATR,  $\text{cm}^{-1}$ ): 1601 ( $\nu_{\text{C}=\text{N}}$ ), 1568 ( $\nu_{\text{C}=\text{N}}$ ), 1387 ( $\nu_{\text{C}-\text{O}}$ ), 530 ( $\nu_{\text{Cd}-\text{O}}$ ), 497 ( $\nu_{\text{Cd}-\text{N}}$ )

UV/VIS (nm ( $\epsilon_{\lambda}[\text{m}^2/\text{mol}]$ ): 340 (1.20E+06)

### 5.4.2.5 Synthesis of 10b



**10b**

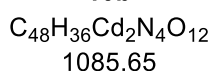


**Figure 86: Synthesis of 10b**

**10b** was synthesized, using  $\text{Cd}(\text{NO}_3)_2 \cdot 4\text{H}_2\text{O}$  (119.3 mg, 0.3854 mmol) as metal precursor, **10** (200 mg, 0.4625 mmol) as ligand and  $\text{tBuOK}$  (129.7 mg, 1.1563 mmol) as deprotonating agent.

98.3 mg (47 %) white powder

$^1\text{H}$  NMR ( $\text{CDCl}_3$ , 400 MHz, 20 °C)  $\delta$  = 8.01 (d,  $J$  = 47.4 Hz, 4H, PhH), 7.37 (d,  $J$  = 8.2 Hz, 4H, PhH), 7.21 – 6.90 (m, 8H, PhH), 3.68 (d,  $J$  = 41.1 Hz, 8H,  $\text{CH}_2$ ), 2.83 (s, 12H,  $\text{CH}_3$ )

EA (found (calculated), %): C: 53.21 (53.10), H: 3.79 (3.34), N: 5.10 (5.16)

IR (ATR,  $\text{cm}^{-1}$ ): 1597 ( $\nu_{\text{C}=\text{N}}$ ), 1563 ( $\nu_{\text{C}=\text{N}}$ ), 1231 ( $\nu_{\text{C}-\text{O}}$ ), 568 ( $\nu_{\text{Cd}-\text{O}}$ ), 495 ( $\nu_{\text{Cd}-\text{N}}$ )

UV/VIS (nm ( $\epsilon_\lambda[\text{m}^2/\text{mol}]$ ): 322 (2.02E+06)

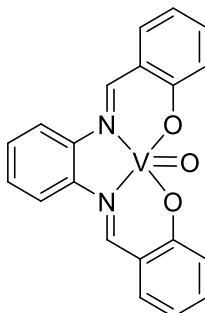
### 5.4.3 Coordination Compounds of V

A general procedure for the synthesis of the coordination compounds of V is given here:

$\text{VO}(\text{acac})_2$  (1 eq.) was dissolved in 5 ml of abs. MeOH (colourless solution). The respective ligand (1.1-1.2 eq.) was dissolved in 5 ml abs. THF (yellow solution) and deprotonated with a base (2.2-3 eq.). The solutions were combined. By doing so, a slight colour change could be observed already into a green. It was just in the case of **IVc** that all solutions were colourless at every time. The reaction mixture was stirred for 24 hours at RT. After that time, the product

precipitated, was filtered off, washed three times with little amounts of abs. DCM and dried under reduced pressure.

#### 5.4.3.1 Synthesis of **8c**



**8c**

$\text{C}_{20}\text{H}_{14}\text{N}_2\text{O}_3\text{V}$   
381.28 g/mol

Figure 87: Synthesis of **8c**

**8c** was synthesized, using  $\text{VO}(\text{acac})_2$  (228.6 mg, 0.08621 mmol) as metal precursor, **8** (300 mg, 0.09483 mmol) as ligand and tBuOK (212.8 mg, 1.8966 mmol) as deprotonating agent.

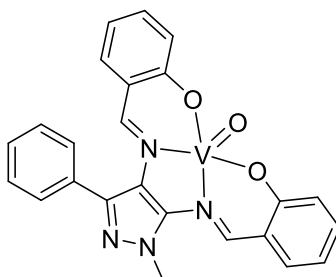
181.4 mg (55 %) green powder

EA (found (calculated), %): C: 62.43 (63.00), H: 4.03 (3.70), N: 7.17 (7.35)

IR (ATR,  $\text{cm}^{-1}$ ): 1534 ( $\nu_{\text{C}=\text{N}}$ ), 1257 ( $\nu_{\text{C}-\text{O}}$ ), 983 ( $\nu_{\text{V}=\text{O}}$ ), 540 ( $\nu_{\text{V}-\text{O}}$ ), 484 ( $\nu_{\text{V}-\text{N}}$ )

UV/VIS (nm ( $\epsilon_{\lambda}[\text{m}^2/\text{mol}]$ ): 261 (2.36E+06), 312 (2.09E+06), 406 (1.73E+06)

### 5.4.3.2 Synthesis of **Ic**



**Ic**  
 $C_{24}H_{18}N_4O_3V$   
 461.37 g/mol

**Figure 88: Synthesis of **Ic****

**Ic** was synthesized, using  $VO(acac)_2$  (100 mg, 0.3771 mmol) as metal precursor, **I** (164.5 mg, 0.4148 mmol) as ligand and no base as deprotonating agent.

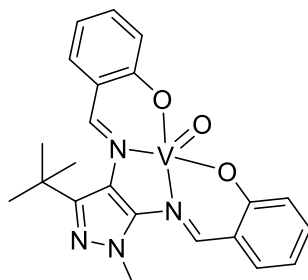
61.6 mg (36 %) green powder

EA (found (calculated), %): C: 62.07 (62.48), H: 4.35 (3.93), N: 11.87 (12.14)

IR (ATR,  $cm^{-1}$ ): 1598 ( $\nu_{C=N}$ ), 1533 ( $\nu_{C=N}$ ), 1390 ( $\nu_{C-O}$ ), 982 ( $\nu_{V=O}$ ), 567 ( $\nu_{V-O}$ ), 501 ( $\nu_{V-N}$ )

UV/VIS (nm ( $\epsilon_{\lambda}[m^2/mol]$ ): 260 (3.39E+05), 329 (2.48E+05), 348 (2.51E+05), 406 (2.41E+05)

### 5.4.3.3 Synthesis of **IIc**



**IIc**  
 $C_{22}H_{22}N_4O_3V$   
 441.38 g/mol

**Figure 89: Synthesis of **IIc****

**IIc** was synthesized, using VO(acac)<sub>2</sub> (64.0 mg, 0.2415 mmol) as metal precursor, **II** (100 mg, 0.2656 mmol) as ligand and Et<sub>3</sub>N (0.07 ml, 0.5313 mmol) as deprotonating agent.

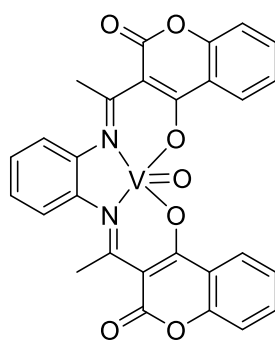
38.4 mg (36 %) dark green powder

EA (found (calculated), %): C: 59.59 (59.87), H: 5.46 (5.02), N: 12.69 (12.69)

IR (ATR, cm<sup>-1</sup>): 1603 (ν<sub>C=N</sub>), 1560 (ν<sub>C=N</sub>), 1361 (ν<sub>C-O</sub>), 995 (ν<sub>V=O</sub>), 561 (ν<sub>V-O</sub>), 484 (ν<sub>V-N</sub>)

UV/VIS (nm (ε<sub>λ</sub>[m<sup>2</sup>/mol]]): 266 (7.87E+05), 306 (2.98E+05)

#### 5.4.3.4 Synthesis of **IIIc**



**IIIc**  
C<sub>28</sub>H<sub>18</sub>N<sub>2</sub>O<sub>7</sub>V  
545.40

**Figure 90: Synthesis of **IIIc****

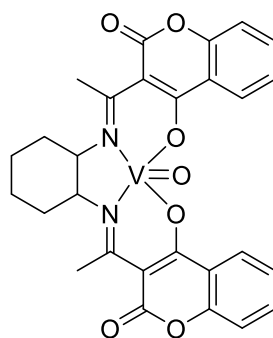
**IIIc** was synthesized, using VO(acac)<sub>2</sub> (46.0 mg, 0.1734 mmol) as metal precursor, **III** (100 mg, 0.2081 mmol) as ligand and Et<sub>3</sub>N (0.07 ml, 0.5202 mmol) as deprotonating agent.

29.3 mg (31 %) olive green powder

EA (found (calculated), %): C: 61.49 (61.66), H: 3.68 (3.33), N: 5.23 (5.11)

IR (ATR, cm<sup>-1</sup>): 1602 (ν<sub>C=N</sub>), 1563 (ν<sub>C=N</sub>), 1388 (ν<sub>C-O</sub>), 932 (ν<sub>V=O</sub>), 534 (ν<sub>V-O</sub>), 498 (ν<sub>V-N</sub>)

#### 5.4.3.5 Synthesis of IVc



**IVc**

$C_{28}H_{24}N_2O_7V$   
551.45 g/mol

**Figure 91: Synthesis of IVc**

**IVc** was synthesized, using  $VO(acac)_2$  (99.1 mg, 0.3737 mmol) as metal precursor, **IV** (200 mg, 0.4111 mmol) as ligand and  $Et_3N$  (0.11 ml, 0.8221 mmol) as deprotonating agent.

80.6 mg (39 %) light green powder

EA (found (calculated), %): C: 60.50 (60.99), H: 4.52 (4.39), N: 5.11 (5.08)

IR (ATR,  $cm^{-1}$ ): 1696 ( $\nu_{C=N}$ ), 1567 ( $\nu_{C=N}$ ), 1268 ( $\nu_{C-O}$ ), 931 ( $\nu_{V=O}$ ), 549 ( $\nu_{V-O}$ ), 486 ( $\nu_{V-N}$ )

## 6 Conclusion and Outlook

Over the course of this research, the researchers synthesized new tetradentate Schiff base ligands, which carry rigid building blocks, such as pyrazoline-derivatives, in their structure. Due to large aromatic building blocks and a higher rigidity of the ligand system, high fluorescence intensities were achieved in the final coordination compounds, due to the fact that non-radiative relaxation can be reduced, when motion within the molecules is inhibited. Since the used ligands carry hydroxyl-groups in their structures, which are involved in the formation of coordination compounds, the deprotonation thereof is a necessary step in the synthesis approach. The absence of these protons could even be observed in the  $^1\text{H}$  NMR spectra of the coordination compounds. As a result, different bases were tested with regard to their deprotonation-abilities, and  $\text{Et}_3\text{N}$  was found to provide the best results for the coordination of most metals. Since zinc compounds of the tetradentate Schiff bases were found to show the ability to form dynamic interactions to N-heterocycles, the possibility of an applicability of this system to be used as recognition sites for more functional molecules, which are important in biological systems (such as purines or imidazoles), is of great interest. This feature, in combination with an efficient luminescent behaviour of the coordination compounds themselves, enables its usage as specific sensor material.

Through the introduction of coumarin-building blocks into these tetradentate Schiff-bases, special photochemical properties were achieved in the coordination compounds of zinc and cadmium, leading to their easy applicability as laser dyes, fluorescent colours, and sensitizers in phototherapy. Coumarins as ligands, especially for rare earth metals like europium, exhibited very characteristic luminescence spectra with a line-like shape.

Finally, a new hexadentate pyridine-type ligand was synthesized, carrying phenanthroline-moieties in its structure. A higher rigidity of this structural part has a positive influence on the fluorescence behaviour of its lanthanide coordination compounds. Moreover, the  $\pi$ -aromatic system is expanded in the new ligand, which leads to higher fluorescence quantum yields through a better uptake of the energy of the absorbed light. Further research of coordination compounds of this ligand with rare earth metals is already in progress.

## 7 Appendix

### 7.1 UV/VIS spectra - detailed results

Table 12: Summarized data of the UV/VIS spectra of I

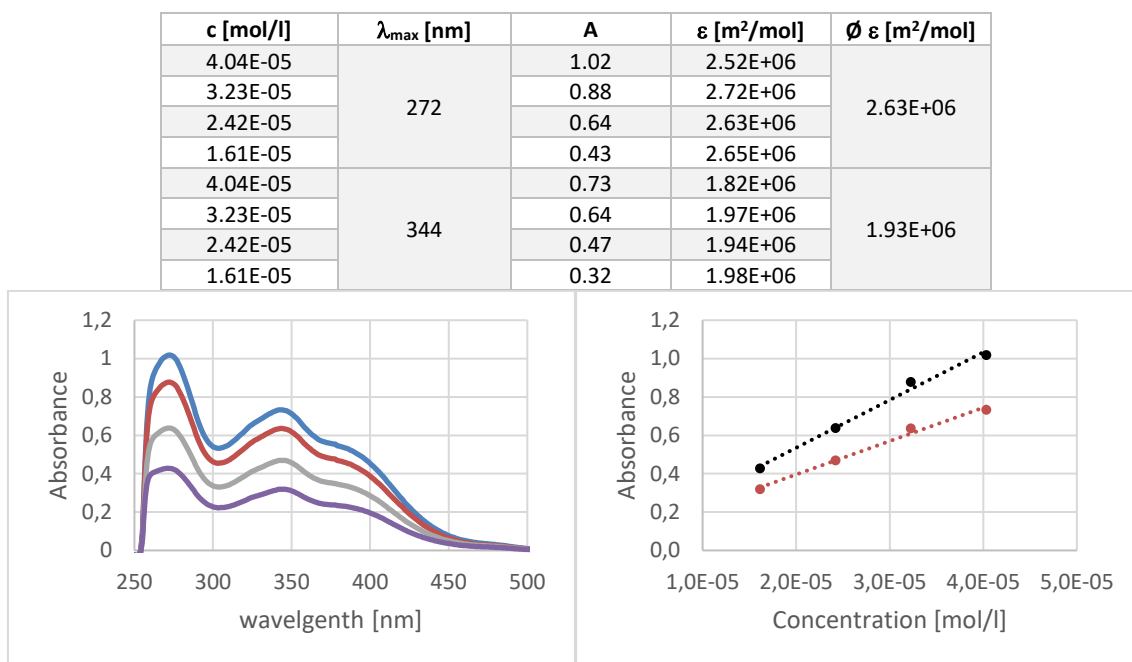


Figure 92: LEFT: UV/VIS-spectra of I, recorded with different concentrations (4.04E-05 / blue, 3.23E-05 / red, 2.42E-05 / grey, 1.61E-05 / violet); RIGHT: linear regression of the maxima at 272 nm (black) and 344 nm (red)

Table 13: Summarized data of the UV/VIS spectra of Ia

c [mol/l]	$\lambda$ [nm]	A	$\epsilon$ [m <sup>2</sup> /mol]	$\phi \epsilon$ [m <sup>2</sup> /mol]
2.62E-05	261	0.65	2.48E+06	2.54E+06
1.31E-05		0.35	2.63E+06	
3.27E-05		0.79	2.41E+06	
1.96E-05		0.51	2.61E+06	
2.62E-05	299	0.64	2.45E+06	2.47E+06
1.31E-05		0.33	2.50E+06	
3.27E-05		0.79	2.41E+06	
1.96E-05		0.50	2.53E+06	
2.62E-05	326	0.59	2.26E+06	2.25E+06
1.31E-05		0.30	2.28E+06	
3.27E-05		0.71	2.16E+06	
1.96E-05		0.45	2.30E+06	
2.62E-05	343	0.61	2.33E+06	2.32E+06
1.31E-05		0.31	2.37E+06	
3.27E-05		0.72	2.19E+06	
1.96E-05		0.47	2.37E+06	



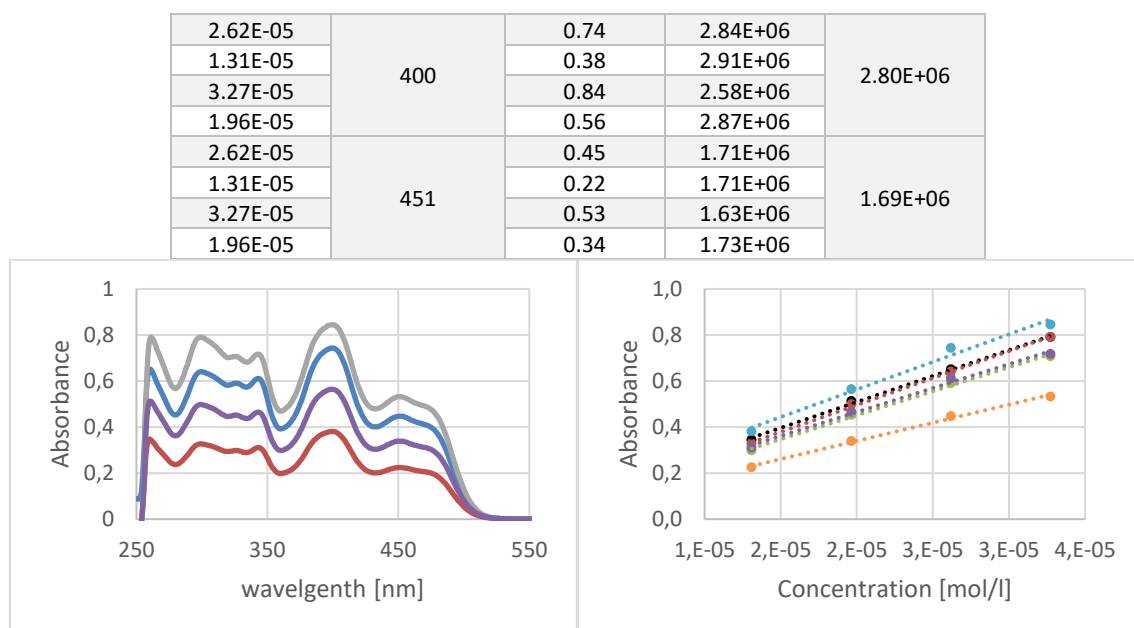


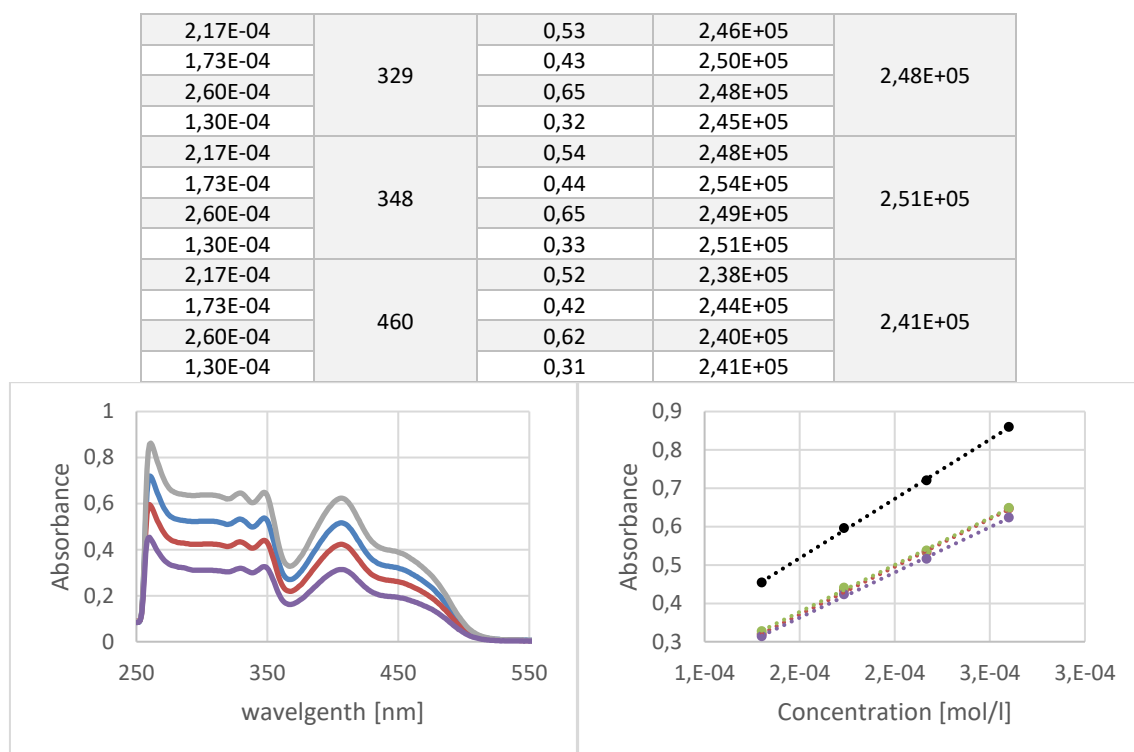
Figure 93: LEFT: UV/VIS-spectra of Ia, recorded with different concentrations (3.27E-05 / grey, 2.62E-05 / blue, 1.96E-05 / violet, 1.31E-05 / red); RIGHT: linear regression of the maxima at 261 nm (black), 299 nm (red), 326 nm (green), 343 nm (violet), 400 nm (light blue) and 451 nm (orange)

Table 14: Summarized data of the UV/VIS spectra of Ib

c [mol/l]	$\lambda$ [nm]	A	$\epsilon$ [m <sup>2</sup> /mol]	$\phi \epsilon$ [m <sup>2</sup> /mol]
2,96E-05	262	0,78	2,64E+06	2,67E+06
1,48E-05		0,42	2,83E+06	
2,22E-05		0,58	2,61E+06	
3,70E-05		0,97	2,62E+06	
2,96E-05	298	0,58	1,96E+06	1,96E+06
1,48E-05		0,30	2,04E+06	
2,22E-05		0,42	1,90E+06	
3,70E-05		0,72	1,94E+06	
2,96E-05	344	0,46	1,54E+06	1,63E+06
1,48E-05		0,26	1,77E+06	
2,22E-05		0,36	1,63E+06	
3,70E-05		0,58	1,57E+06	
2,96E-05	400	0,67	2,26E+06	2,31E+06
1,48E-05		0,36	2,45E+06	
2,22E-05		0,50	2,27E+06	
3,70E-05		0,83	2,25E+06	
2,96E-05	450	0,38	1,30E+06	1,28E+06
1,48E-05		0,19	1,31E+06	
2,22E-05		0,27	1,22E+06	
3,70E-05		0,48	1,29E+06	

Table 15: Summarized data of the UV/VIS spectra of Ic

c [mol/l]	$\lambda$ [nm]	A	$\epsilon$ [m <sup>2</sup> /mol]	$\phi \epsilon$ [m <sup>2</sup> /mol]
2,17E-04	260	0,72	3,32E+05	3,39E+05
1,73E-04		0,60	3,44E+05	
2,60E-04		0,86	3,30E+05	
1,30E-04		0,45	3,49E+05	



**Figure 94: LEFT: UV/VIS-spectra of Ic, recorded with different concentrations (2.60E-05 / grey, 2.17E-05 / blue, 1.73E-05 / red, 1.30E-05 / violet); RIGHT: linear regression of the maxima at 260 nm (black), 329 nm (red), 348 nm (green) and 406 nm (violet)**

**Table 16: Summarized data of the UV/VIS spectra of II**

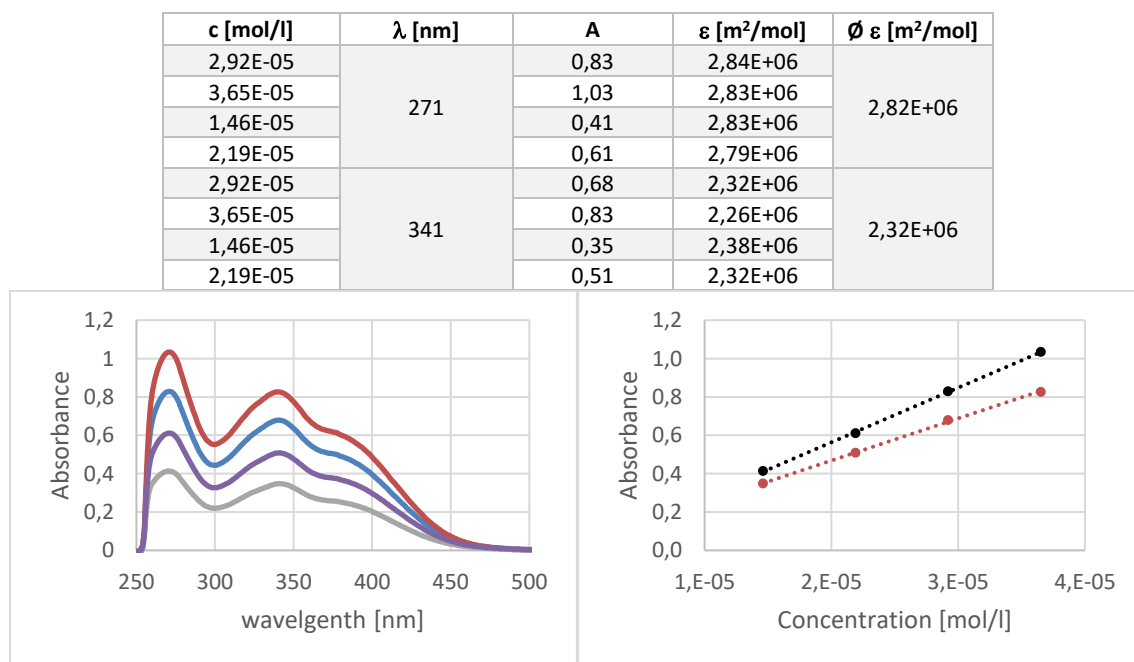


**Figure 95: LEFT: UV/VIS-spectra of II, recorded with different concentrations (3.65E-05 / red, 2.92E-05 / blue, 2.19E-05 / violet, 1.46E-05 / grey); RIGHT: linear regression of the maxima at 271 nm (black) and 341 nm (red)**

Table 17: Summarized data of the UV/VIS spectra of IIa

c [mol/l]	$\lambda$ [nm]	A	$\epsilon$ [m <sup>2</sup> /mol]	$\emptyset \epsilon$ [m <sup>2</sup> /mol]
4,32E-05	260	0,55	1,27E+06	1,25E+06
1,73E-05		0,22	1,26E+06	
6,91E-05		0,82	1,19E+06	
2,59E-05		0,33	1,27E+06	
4,32E-05	295	0,55	1,27E+06	1,24E+06
1,73E-05		0,21	1,22E+06	
6,91E-05		0,85	1,23E+06	
2,59E-05		0,32	1,24E+06	
4,32E-05	342	0,54	1,25E+06	1,23E+06
1,73E-05		0,21	1,24E+06	
6,91E-05		0,81	1,17E+06	
2,59E-05		0,33	1,26E+06	
4,32E-05	393	0,60	1,39E+06	1,38E+06
1,73E-05		0,25	1,43E+06	
6,91E-05		0,89	1,29E+06	
2,59E-05		0,37	1,42E+06	
4,32E-05	451	0,40	9,16E+05	9,10E+05
1,73E-05		0,16	9,31E+05	
6,91E-05		0,61	8,76E+05	
2,59E-05		0,24	9,16E+05	

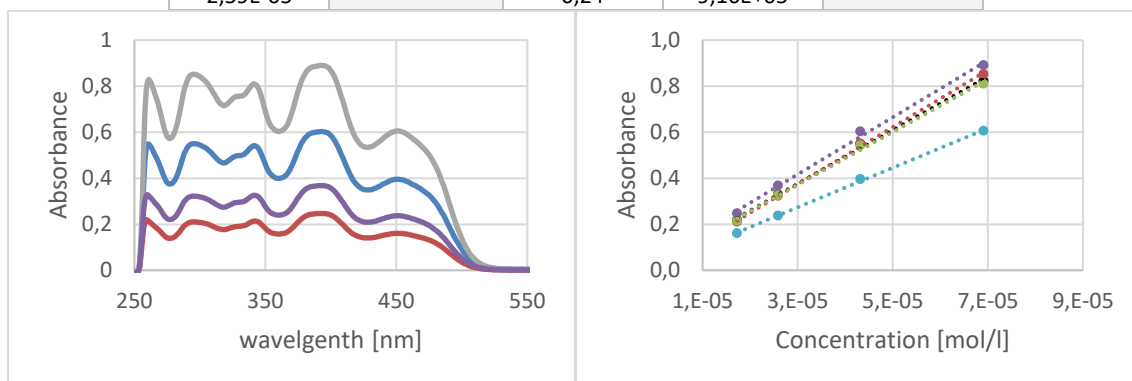
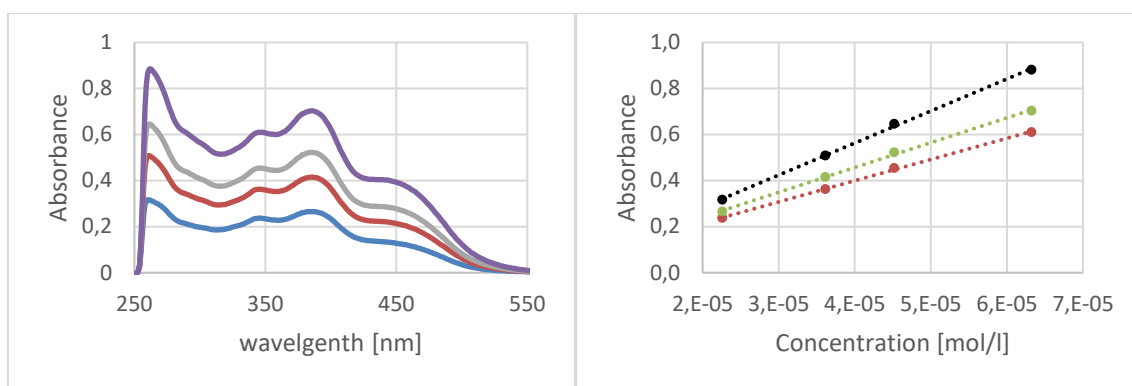


Figure 96: LEFT: UV/VIS-spectra of IIa, recorded with different concentrations (6.91E-05 / grey, 4.32E-05 / blue, 2.59E-05 / violet, 1.73E-05 / red); RIGHT: linear regression of the maxima at 260 nm (black), 295 nm (red), 342 nm (green), 393 nm (violet) and 451 nm (turquoise)

Table 18: Summarized data of the UV/VIS spectra of IIb

c [mol/l]	$\lambda$ [nm]	A	$\epsilon$ [m <sup>2</sup> /mol]	$\emptyset \epsilon$ [m <sup>2</sup> /mol]
2,26E-05	261	0,32	1,40E+06	1,41E+06
3,62E-05		0,51	1,41E+06	
4,52E-05		0,65	1,43E+06	
6,33E-05		0,88	1,39E+06	
2,26E-05	346	0,24	1,05E+06	1,01E+06
3,62E-05		0,36	1,00E+06	
4,52E-05		0,45	1,01E+06	
6,33E-05		0,61	9,65E+05	
2,26E-05	386	0,27	1,18E+06	1,15E+06
3,62E-05		0,41	1,15E+06	
4,52E-05		0,52	1,16E+06	
6,33E-05		0,70	1,11E+06	



**Figure 97: LEFT: UV/VIS-spectra of IIb, recorded with different concentrations (6.33E-05 / violet, 4.52E-05 / grey, 3.62E-05 / red, 2.26E-05 / blue); RIGHT: linear regression of the maxima at 261 nm (black), 346 nm (red) and 386 nm (green)**

**Table 19: Summarized data of the UV/VIS spectra of IIc**

c [mol/l]	$\lambda$ [nm]	A	$\epsilon$ [m <sup>2</sup> /mol]	$\emptyset \epsilon$ [m <sup>2</sup> /mol]
3,62E-05	266	0,28	7,70E+05	7,87E+05
5,44E-05		0,43	7,90E+05	
7,25E-05		0,58	7,95E+05	
9,06E-05		0,72	7,91E+05	
3,62E-05	306	0,28	7,85E+05	7,98E+05
5,44E-05		0,44	8,03E+05	
7,25E-05		0,59	8,12E+05	
9,06E-05		0,72	7,92E+05	

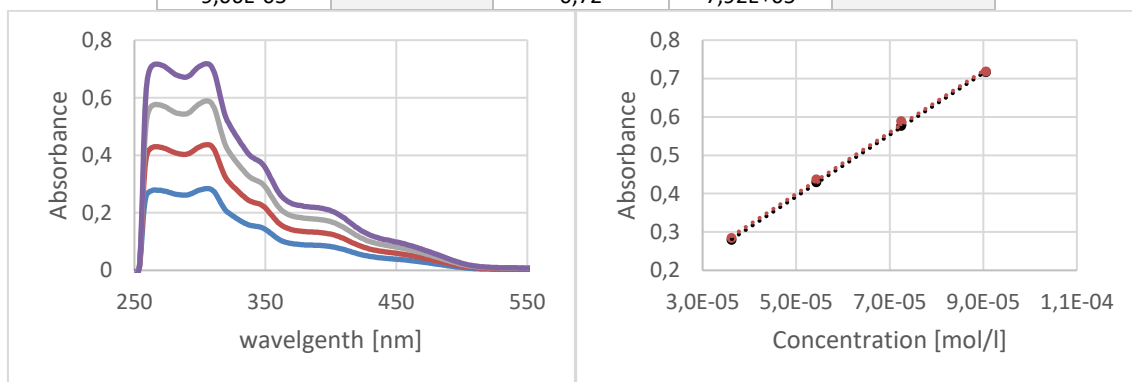


**Figure 98: LEFT: UV/VIS-spectra of IIc, recorded with different concentrations (9.06E-05 / violet, 7.25E-05 / grey, 5.44E-05 / red, 3.62E-05 / blue); RIGHT: linear regression of the maxima at 266 nm (black) and 306 nm (red)**

**Table 20: Summarized data of the UV/VIS spectra of 8**

c [mol/l]	$\lambda$ [nm]	A	$\epsilon$ [m <sup>2</sup> /mol]	$\emptyset \epsilon$ [m <sup>2</sup> /mol]
2,21E-05	334	0,35	1,59E+06	1,52E+06
3,32E-05		0,55	1,65E+06	
6,64E-05		0,74	1,12E+06	
1,11E-05		0,19	1,73E+06	

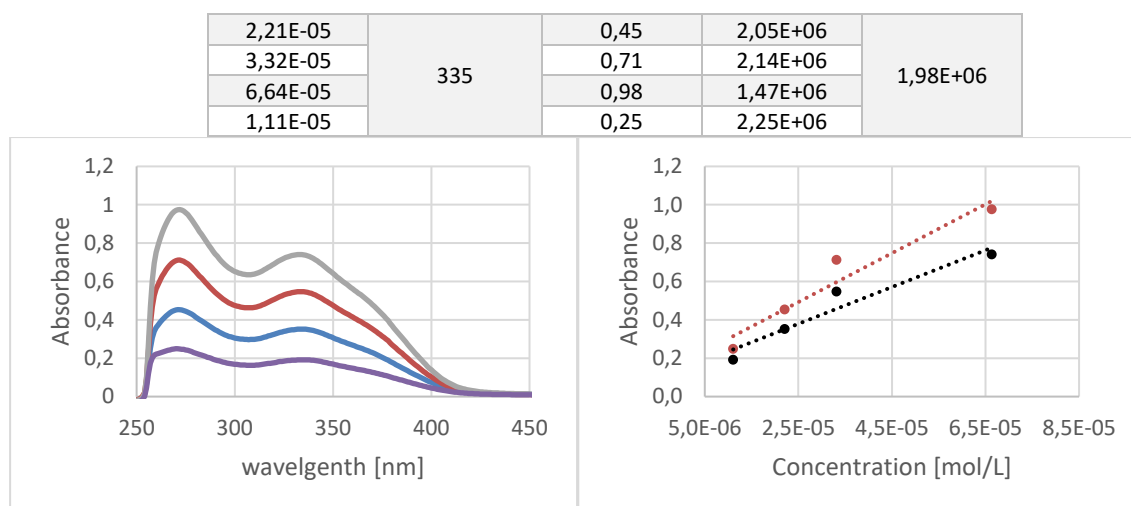


Figure 99: LEFT: UV/VIS-spectra of 8, recorded with different concentrations (6.64E-05 / grey, 3.32E-05 / red, 2.21E-05 / blue, 1.11E-05 / violet); RIGHT: linear regression of the maxima at 334 nm (black) and 272 nm (red)

Table 21: Summarized data of the UV/VIS spectra of 8a

c [mol/l]	$\lambda$ [nm]	A	$\epsilon$ [m <sup>2</sup> /mol]	$\emptyset \epsilon$ [m <sup>2</sup> /mol]
1,21E-05	260	0,26	2,14E+06	1,93E+06
2,42E-05		0,48	1,98E+06	
3,63E-05		0,65	1,79E+06	
4,85E-05		0,88	1,81E+06	
1,21E-05	402	0,29	2,40E+06	2,25E+06
2,42E-05		0,56	2,32E+06	
3,63E-05		0,77	2,12E+06	
4,85E-05		1,04	2,14E+06	
1,21E-05	403	0,32	2,66E+06	2,51E+06
2,42E-05		0,62	2,54E+06	
3,63E-05		0,85	2,34E+06	
4,85E-05		1,21	2,49E+06	

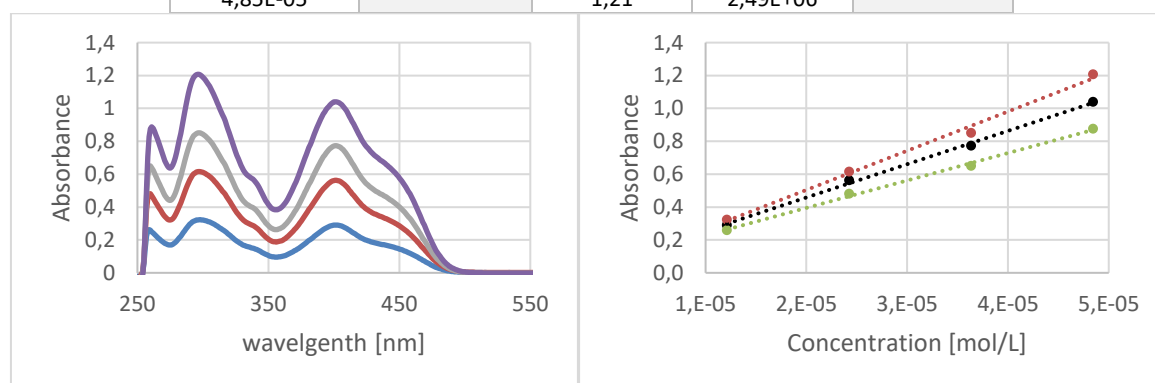


Figure 100: LEFT: UV/VIS-spectra of 8a, recorded with different concentrations (4.85E-05 / violet, 3.63E-05 / grey, 2.42E-05 / red, 1.21E-05 / blue); RIGHT: linear regression of the maxima at 260 nm (green, 402 nm (black) and 297 nm (red)

Table 22: Summarized data of the UV/VIS spectra of 8b

c [mol/l]	$\lambda$ [nm]	A	$\epsilon$ [m <sup>2</sup> /mol]	$\emptyset \epsilon$ [m <sup>2</sup> /mol]
2,46E-05	260	0,74	2,99E+06	2,89E+06
4,92E-05		1,31	2,65E+06	
1,23E-05		0,36	2,96E+06	
3,69E-05		1,09	2,96E+06	
2,46E-05	400	0,60	2,45E+06	2,50E+06
4,92E-05		1,12	2,27E+06	
1,23E-05		0,34	2,78E+06	
3,69E-05		0,92	2,51E+06	
2,46E-05	401	0,61	2,47E+06	2,74E+06
4,92E-05		1,27	2,58E+06	
1,23E-05		0,39	3,16E+06	
3,69E-05		1,01	2,74E+06	

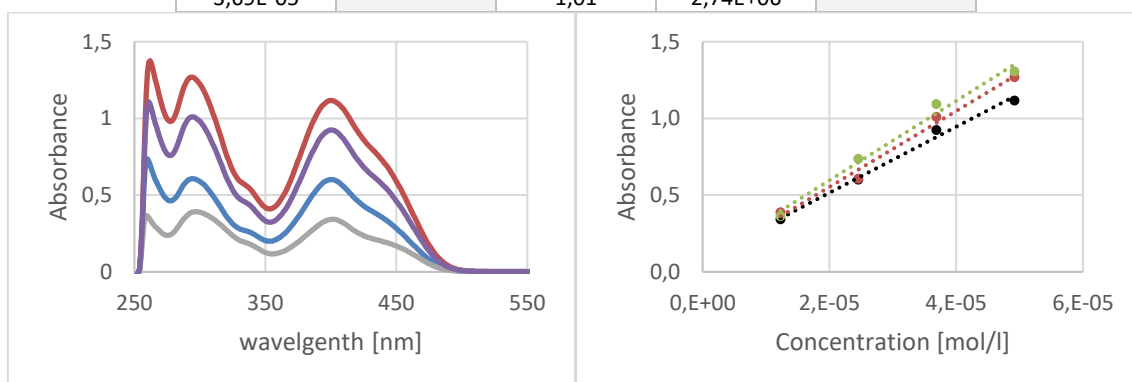


Figure 101: LEFT: UV/VIS-spectra of 8b, recorded with different concentrations (4.92E-05 / red, 3.69E-05 / violet, 2.46E-05 / blue, 1.23E-05 / grey); RIGHT: linear regression of the maxima at 260 nm (green), 400 nm (black) and 294 nm (red)

Table 23: Summarized data of the UV/VIS spectra of 8c

c [mol/l]	$\lambda$ [nm]	A	$\epsilon$ [m <sup>2</sup> /mol]	$\emptyset \epsilon$ [m <sup>2</sup> /mol]
1,36E-05	261	0,34	2,48E+06	2,36E+06
2,73E-05		0,64	2,33E+06	
4,09E-05		0,93	2,27E+06	
3,41E-05		0,80	2,34E+06	
1,36E-05	406	0,24	1,77E+06	1,73E+06
2,73E-05		0,46	1,68E+06	
4,09E-05		0,70	1,70E+06	
3,41E-05		0,60	1,75E+06	
1,36E-05	407	0,29	2,09E+06	2,09E+06
2,73E-05		0,56	2,06E+06	
4,09E-05		0,85	2,07E+06	
3,41E-05		0,72	2,12E+06	

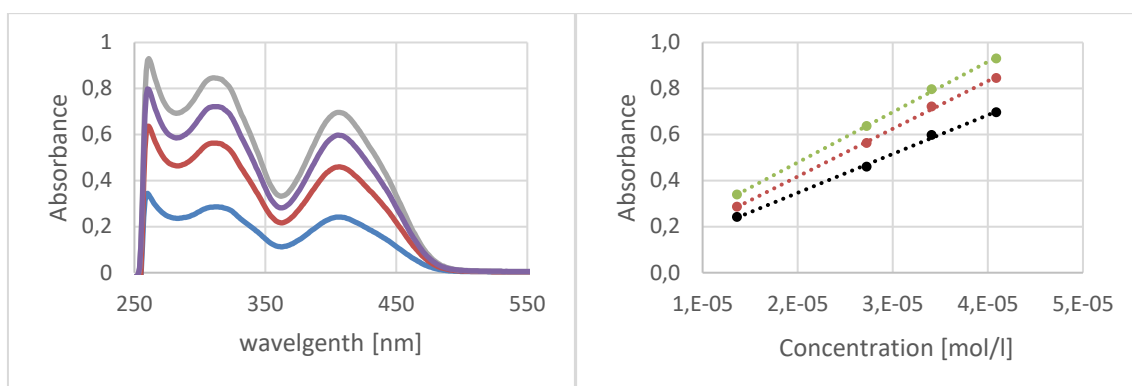


Figure 102: LEFT: UV/VIS-spectra of 8c, recorded with different concentrations (4.09E-05 / grey, 3.41E-05 / violet, 2.73E-05 / red, 1.36E-05 / blue); RIGHT: linear regression of the maxima at 261 nm (green), 406 nm (black) and 312 nm (red)

## 7.2 X-ray – detailed results

### 7.2.1 Ia pyridine

Table 24: Crystal data and structure refinement for Ia pyridine

Ia pyridine	
Empirical formula	C <sub>32</sub> H <sub>20</sub> N <sub>5</sub> O <sub>2</sub> Zn
Formula weight	571.90
Temperature	101(2) K
Wavelength	0.71073 Å
Crystal system	Triclinic
Space group	P-1
Unit cell dimensions	a = 9.6033(16) Å, α = 98.938(5)°. b = 12.542(2) Å, β = 93.618(5)°. c = 23.588(4) Å, γ = 106.777(5)°.
Volume	2669.6(8) Å <sup>3</sup>
Z	4
Density (calculated)	1.423 Mg/m <sup>3</sup>
Absorption coefficient	0.959 mm <sup>-1</sup>
F(000)	1172
Crystal size	0.550 x 0.490 x 0.200 mm <sup>3</sup>
Theta range for data collection	0.880 to 30.614°.
Index ranges	-13 ≤ h ≤ 13, -17 ≤ k ≤ 17, -33 ≤ l ≤ 33
Reflections collected	87009
Independent reflections	16401 [R(int) = 0.0635]
Completeness to theta = 25.242°	100.0 %
Refinement method	Full-matrix least-squares on F <sup>2</sup>
Data / restraints / parameters	16401 / 0 / 750
Goodness-of-fit on F <sup>2</sup>	0.866
Final R indices [I > 2σ(I)]	R1 = 0.0515, wR2 = 0.1278
R indices (all data)	R1 = 0.0858, wR2 = 0.1559
Absolute structure parpmmeter	
Extinction coefficient	n/a
Largest diff. peak and hole	1.024 and -1.712 e.Å <sup>-3</sup>

Atomic coordinates ( $\times 10^4$ ) and equivalent isotropic displacement parameters ( $\text{\AA}^2 \times 10^3$ ) for **1a** pyridine.  $U(\text{eq})$  is defined as one third of the trace of the orthogonalized  $U^{\text{ij}}$  tensor:

	x	y	z	$U(\text{eq})$
Zn(01)	13746(1)	9060(1)	9154(1)	15(1)
Zn(02)	3478(1)	3213(1)	5295(1)	30(1)
O(1)	1400(3)	3147(3)	5230(1)	66(1)
O(003)	14740(2)	8147(2)	9539(1)	18(1)
O(004)	15131(2)	9361(2)	8578(1)	23(1)
O(005)	3556(2)	2878(2)	4453(1)	35(1)
N(1)	11636(2)	10792(2)	10342(1)	16(1)
N(00A)	5728(2)	4188(2)	5372(1)	20(1)
N(00B)	11256(2)	11652(2)	10154(1)	18(1)
N(00C)	3706(2)	4122(2)	6143(1)	22(1)
N(00D)	7470(2)	5450(2)	6204(1)	26(1)
N(00E)	7376(3)	5803(2)	6774(1)	27(1)
N(2)	12848(2)	9384(2)	9941(1)	15(1)
N(007)	13141(2)	10516(2)	9030(1)	16(1)
N(009)	11937(2)	7783(2)	8669(1)	18(1)
C(00F)	12263(2)	10260(2)	9935(1)	15(1)
C(00G)	12603(3)	8690(2)	10307(1)	16(1)
C(00I)	13235(3)	7793(2)	10315(1)	16(1)
C(00J)	14303(3)	7590(2)	9946(1)	15(1)
C(00K)	13618(3)	11146(2)	8657(1)	19(1)
C(00L)	12327(2)	10816(2)	9466(1)	15(1)
C(00M)	5168(3)	4692(2)	6337(1)	19(1)
C(00N)	11657(3)	11674(2)	9621(1)	17(1)
C(00O)	15363(3)	10124(2)	8247(1)	18(1)
C(00P)	11333(3)	12518(2)	9306(1)	21(1)
C(00Q)	12822(3)	7114(2)	10740(1)	21(1)
C(00R)	14928(3)	6735(2)	10056(1)	18(1)
C(00S)	6157(3)	3459(2)	4410(1)	22(1)
C(00T)	6167(3)	4768(2)	5932(1)	21(1)
C(00U)	14628(3)	10961(2)	8255(1)	20(1)
C(00V)	10677(3)	7405(2)	8891(1)	22(1)
C(00W)	5898(3)	6576(2)	7789(1)	24(1)
C(00X)	16437(3)	10144(2)	7857(1)	23(1)
C(00Y)	11549(3)	10680(2)	10944(1)	20(1)
C(00Z)	14505(3)	6103(2)	10476(1)	22(1)
C(01A)	4687(3)	2870(2)	4178(1)	25(1)
C(01B)	12009(3)	7362(2)	8115(1)	27(1)
C(01C)	7301(3)	3398(3)	4070(1)	32(1)
C(01D)	8877(3)	5854(3)	5988(1)	32(1)
C(01E)	5986(3)	5333(2)	6863(1)	21(1)
C(01F)	11493(3)	13610(2)	9603(1)	29(1)
C(01G)	9516(3)	6212(3)	8000(1)	33(1)
C(01H)	7055(3)	2772(3)	3524(1)	31(1)
C(01I)	4174(3)	4716(2)	8186(1)	27(1)
C(01J)	14975(4)	11740(3)	7877(1)	32(1)
C(01K)	1124(3)	3722(3)	6232(1)	36(1)
C(01L)	135(3)	3775(3)	6646(2)	39(1)
C(01M)	10821(4)	6576(3)	7772(1)	37(1)
C(01N)	3778(4)	1445(3)	6000(1)	38(1)
C(01O)	5619(4)	2204(3)	3293(1)	37(1)
C(01P)	16007(4)	11732(3)	7502(1)	37(1)
C(01Q)	10492(4)	13045(3)	8438(2)	39(1)



C(01R)	11171(4)	14410(3)	9315(2)	40(1)
C(01T)	-1354(4)	3319(4)	6506(2)	49(1)
C(01U)	589(4)	3216(4)	5648(2)	54(1)
C(01V)	10680(4)	14127(3)	8733(2)	45(1)
C(01W)	3726(5)	419(3)	6136(2)	50(1)
C(01X)	4479(4)	2250(4)	3606(1)	47(1)
C(01Z)	-1882(4)	2834(5)	5943(2)	65(1)
C(3)	4225(9)	-357(6)	5771(3)	46(2)
C(4)	4390(12)	-115(6)	5237(4)	65(3)
C(7)	4164(10)	860(6)	5108(3)	48(2)
C(2)	2658(9)	-461(6)	5728(3)	48(2)
N(4)	3206(6)	1731(4)	5508(2)	22(1)
C(5)	1971(11)	-253(6)	5247(4)	69(3)
C(6)	2279(9)	839(6)	5147(4)	53(2)
C(8)	9431(4)	9093(4)	6460(2)	56(1)
C(9)	10632(8)	9684(6)	7397(3)	105(3)
C(10)	11012(6)	10702(5)	7363(5)	119(4)
C(010)	5398(3)	6712(2)	8327(1)	25(1)
C(11)	10664(11)	11013(6)	6907(6)	143(5)
C(011)	9444(3)	6623(2)	8572(1)	28(1)
C(12)	9795(8)	10205(9)	6398(3)	118(3)
C(012)	4521(3)	5788(2)	8521(1)	24(1)
C(13)	6592(3)	4117(2)	4979(1)	27(1)
C(013)	13421(3)	6272(2)	10822(1)	24(1)
C(014)	5522(3)	5505(2)	7442(1)	21(1)
C(015)	2649(3)	4240(3)	6436(1)	26(1)
C(017)	4670(3)	4575(2)	7649(1)	24(1)
C(018)	10823(3)	12242(2)	8721(1)	25(1)
C(019)	16746(3)	10922(3)	7496(1)	29(1)
C(020)	-963(4)	2797(5)	5522(2)	75(2)
C(021)	9833(6)	8842(4)	6963(2)	68(1)
N(5)	3800(5)	1602(4)	5493(2)	19(1)

## 7.2.2 Ia DMSO

Table 25: Crystal data and structure refinement for Ia DMSO

Ia DMSO	
Empirical formula	C <sub>24</sub> H <sub>18</sub> N <sub>4</sub> O <sub>2</sub> S <sub>0.25</sub> Zn
Formula weight	467.81
Temperature	100(2) K
Wavelength	0.71073 Å
Crystal system	Monoclinic
Space group	C2
Unit cell dimensions	a = 29.771(6) Å, α = 90°. b = 6.7978(14) Å, β = 115.210(4)°. c = 13.175(3) Å, γ = 90°.
Volume	2412.5(9) Å <sup>3</sup>
Z	4
Density (calculated)	1.288 Mg/m <sup>3</sup>
Absorption coefficient	1.065 mm <sup>-1</sup>
F(000)	960
Crystal size	0.570 x 0.500 x 0.220 mm <sup>3</sup>
Theta range for data collection	1.512 to 36.422°.
Index ranges	-48 ≤ h ≤ 49, -11 ≤ k ≤ 11, -22 ≤ l ≤ 22
Reflections collected	24626

Independent reflections	11728 [R(int) = 0.0527]
Completeness to theta = 25.242°	99.9 %
Refinement method	Full-matrix least-squares on F <sup>2</sup>
Data / restraints / parameters	11728 / 1 / 319
Goodness-of-fit on F <sup>2</sup>	1.028
Final R indices [I>2sigma(I)]	R1 = 0.0424, wR2 = 0.1068
R indices (all data)	R1 = 0.0482, wR2 = 0.1100
Absolute structure parameter	0.275(5)
Extinction coefficient	n/a
Largest diff. peak and hole	0.852 and -0.800 e.Å <sup>-3</sup>

Atomic coordinates (x 10<sup>4</sup>) and equivalent isotropic displacement parameters (Å<sup>2</sup> x 10<sup>3</sup>) for **1a**  
DMSO. U(eq) is defined as one third of the trace of the orthogonalized U<sup>ij</sup> tensor:

	x	y	z	U(eq)
Zn(1)	6477(1)	3756(1)	6506(1)	14(1)
S(1)	6238(1)	8524(1)	6381(1)	27(1)
O(1)	5787(1)	3233(3)	6255(1)	18(1)
C(1)	6669(1)	3397(3)	4481(2)	15(1)
O(2)	6350(1)	3588(4)	4917(1)	20(1)
N(2)	7224(1)	2968(3)	6978(2)	14(1)
C(2)	6507(1)	3752(4)	3318(2)	18(1)
N(3)	6690(1)	2847(3)	8219(2)	15(1)
O(3)	6571(1)	6739(3)	6801(2)	23(1)
C(3)	6818(1)	3505(3)	2796(2)	20(1)
N(4)	7522(1)	2651(3)	9853(2)	16(1)
C(4)	7312(1)	2898(4)	3397(2)	20(1)
C(5)	7484(1)	2589(3)	4532(2)	17(1)
N(5)	8000(1)	2650(3)	9992(2)	16(1)
C(6)	7178(1)	2839(3)	5098(2)	14(1)
C(7)	7422(1)	2605(3)	6297(2)	14(1)
C(8)	5589(1)	2856(3)	6947(2)	15(1)
C(9)	5064(1)	2895(4)	6535(2)	20(1)
C(00Y)	6024(2)	8499(8)	4884(4)	72(2)
C(00Z)	5674(2)	7949(6)	6467(6)	71(2)
C(10)	4830(1)	2450(4)	7216(2)	24(1)
C(11)	5102(1)	1916(5)	8340(2)	27(1)
C(12)	5611(1)	1864(5)	8769(2)	24(1)
C(13)	5866(1)	2354(3)	8110(2)	17(1)
C(14)	6398(1)	2291(3)	8664(2)	17(1)
C(15)	7202(1)	2755(3)	8754(2)	14(1)
C(16)	7485(1)	2806(3)	8141(2)	14(1)
C(17)	7988(1)	2729(3)	8964(2)	15(1)
C(18)	8467(1)	2732(3)	8880(2)	16(1)
C(19)	8545(1)	3907(4)	8103(2)	19(1)
C(20)	9001(1)	3889(5)	8048(2)	25(1)
C(21)	9384(1)	2681(5)	8763(3)	30(1)
C(22)	9308(1)	1517(4)	9540(3)	27(1)
C(23)	8855(1)	1560(4)	9613(2)	21(1)
C(24)	7426(1)	2759(4)	10844(2)	18(1)

## 7.2.3 IIa DMSO

**Table 26: Crystal data and structure refinement for IIa DMSO**

IIa DMSO	
Empirical formula	C <sub>24</sub> H <sub>28</sub> N <sub>4</sub> O <sub>3</sub> S Zn
Formula weight	489.71
Temperature	100(2) K
Wavelength	0.71073 Å
Crystal system	Monoclinic
Space group	P2 <sub>1</sub> /c
Unit cell dimensions	a = 7.245 Å, α = 90°. b = 24.848 Å, β = 97.75°. c = 13.384 Å, γ = 90°.
Volume	2387.2 Å <sup>3</sup>
Z	4
Density (calculated)	1.363 Mg/m <sup>3</sup>
Absorption coefficient	1.147 mm <sup>-1</sup>
F(000)	968
Crystal size	0.430 x 0.450 x 0.190 mm <sup>3</sup>
Theta range for data collection	2.246 to 33.647°.
Index ranges	-9 ≤ h ≤ 11, -38 ≤ k ≤ 38, -20 ≤ l ≤ 20
Reflections collected	31915
Independent reflections	9387 [R(int) = 0.0825]
Completeness to theta = 25.242°	100.0 %
Refinement method	Full-matrix least-squares on F <sup>2</sup>
Data / restraints / parameters	9387 / 0 / 304
Goodness-of-fit on F <sup>2</sup>	0.768
Final R indices [I > 2σ(I)]	R1 = 0.0493, wR2 = 0.1225
R indices (all data)	R1 = 0.0979, wR2 = 0.1611
Extinction coefficient	n/a
Largest diff. peak and hole	0.728 and -0.761 e.Å <sup>-3</sup>

Atomic coordinates (x 10<sup>4</sup>) and equivalent isotropic displacement parameters (Å<sup>2</sup> × 10<sup>3</sup>) for IIa DMSO. U(eq) is defined as one third of the trace of the orthogonalized U<sup>ij</sup> tensor:

	x	y	z	U(eq)
Zn(1)	7260(1)	6198(1)	4553(1)	13(1)
C(1)	5862(3)	5371(1)	3122(2)	12(1)
S(1)	4150(1)	6942(1)	5195(1)	19(1)
O(1)	9009(3)	5940(1)	5710(1)	15(1)
N(1)	6738(3)	5387(1)	4113(2)	13(1)
O(2)	8144(3)	6952(1)	4655(1)	17(1)
C(2)	5716(3)	5834(1)	2519(2)	12(1)
N(2)	6505(3)	6304(1)	2970(2)	13(1)
N(3)	5030(3)	4962(1)	2549(2)	14(1)
O(3)	4800(3)	6357(1)	5142(2)	18(1)
C(3)	4710(4)	5666(1)	1573(2)	14(1)
N(4)	4326(3)	5142(1)	1612(2)	15(1)
C(4)	4000(4)	5970(1)	606(2)	18(1)
C(9)	7219(3)	4968(1)	4671(2)	14(1)
C(8)	4819(4)	4394(1)	2768(2)	16(1)
C(7)	2597(5)	5616(1)	-69(2)	26(1)

C(6)	2986(4)	6493(1)	843(2)	24(1)
C(5)	5622(5)	6093(1)	8(2)	25(1)
C(10)	8227(3)	4989(1)	5673(2)	12(1)
C(11)	8444(4)	4493(1)	6201(2)	16(1)
C(12)	9409(4)	4454(1)	7163(2)	18(1)
C(13)	10226(4)	4922(1)	7626(2)	18(1)
C(14)	10081(4)	5406(1)	7129(2)	15(1)
C(15)	9077(3)	5466(1)	6135(2)	13(1)
C(16)	6945(4)	6722(1)	2468(2)	15(1)
C(17)	7682(4)	7223(1)	2900(2)	15(1)
C(18)	7883(4)	7646(1)	2201(2)	18(1)
C(19)	8455(4)	8157(1)	2517(2)	21(1)
C(20)	8835(4)	8258(1)	3560(2)	20(1)
C(21)	8693(4)	7852(1)	4258(2)	16(1)
C(22)	8152(3)	7321(1)	3961(2)	14(1)
C(23)	2345(4)	6909(1)	5983(2)	25(1)
C(24)	2761(5)	7060(2)	4002(3)	33(1)

## 7.2.4 8b DMSO

**Table 27: Crystal data and structure refinement for 8b DMSO**

<b>8b DMSO</b>	
Empirical formula	C <sub>44</sub> H <sub>40</sub> Cd <sub>2</sub> N <sub>4</sub> O <sub>6</sub> S <sub>2</sub>
Formula weight	1009.72
Temperature	100(2) K
Wavelength	0.71073 Å
Crystal system	Triclinic
Space group	P-1
Unit cell dimensions	a = 9.0108(13) Å, α = 71.395(5)° b = 10.2831(15) Å, β = 90°. c = 11.5105(16) Å, γ = 90°.
Volume	1010.8(3) Å <sup>3</sup>
Z	1
Density (calculated)	1.659 Mg/m <sup>3</sup>
Absorption coefficient	1.210 mm <sup>-1</sup>
F(000)	508
Crystal size	0.390 x 0.320 x 0.150 mm <sup>3</sup>
Theta range for data collection	1.867 to 41.028°.
Index ranges	-16 ≤ h ≤ 16, -15 ≤ k ≤ 18, -20 ≤ l ≤ 21
Reflections collected	26047
Independent reflections	11017 [R(int) = 0.1110]
Completeness to theta = 25.242°	63.4 %
Refinement method	Full-matrix least-squares on F <sup>2</sup>
Data / restraints / parameters	11017 / 0 / 264
Goodness-of-fit on F <sup>2</sup>	0.595
Final R indices [I > 2σ(I)]	R1 = 0.0510, wR2 = 0.1055
R indices (all data)	R1 = 0.1482, wR2 = 0.1576
Extinction coefficient	n/a
Largest diff. peak and hole	1.373 and -1.517 e.Å <sup>-3</sup>

## 7.2.5 Ic

Table 28: Crystal data and structure refinement for Ic

Ic	
Empirical formula	C <sub>24</sub> H <sub>18</sub> N <sub>4</sub> O <sub>3</sub> V
Formula weight	461.36
Temperature	100 K
Wavelength	0.71073 Å
Crystal system	Monoclinic
Space group	P2 <sub>1</sub> /c
Unit cell dimensions	a = 12.233(4) Å, a = 90°. b = 17.377(6) Å, b = 105.560(9)°. c = 9.676(3) Å, g = 90°.
Volume	1981.5(11) Å <sup>3</sup>
Z	4
Density (calculated)	1.547 Mg/m <sup>3</sup>
Absorption coefficient	0.538 mm <sup>-1</sup>
F(000)	948
Crystal size	0.12 x 0.08 x 0.05 mm <sup>3</sup>
Theta range for data collection	2.088 to 27.908°.
Index ranges	-16<=h<=16, -22<=k<=22, -12<=l<=12
Reflections collected	30537
Independent reflections	4715 [R(int) = 0.2385]
Completeness to theta = 25.242°	99.9 %
Absorption correction	Semi-empirical from equivalents
Refinement method	Full-matrix least-squares on F <sup>2</sup>
Data / restraints / parameters	4715 / 0 / 290
Goodness-of-fit on F <sup>2</sup>	1.005
Final R indices [I>2sigma(I)]	R1 = 0.0819, wR2 = 0.1247
R indices (all data)	R1 = 0.1916, wR2 = 0.1547
Extinction coefficient	n/a
Largest diff. peak and hole	0.441 and -0.592 e.Å <sup>-3</sup>

Atomic coordinates (x 10<sup>4</sup>) and equivalent isotropic displacement parameters (Å<sup>2</sup>x 10<sup>3</sup>) for Ic.

U(eq) is defined as one third of the trace of the orthogonalized U<sup>ij</sup> tensor:

	x	y	z	U(eq)
V(1)	4454(1)	5682(1)	6712(1)	15(1)
O(1)	6039(3)	5927(2)	7354(3)	20(1)
O(2)	4421(3)	6210(2)	4967(3)	22(1)
O(3)	3813(3)	6187(2)	7622(3)	19(1)
N(1)	3195(3)	4965(2)	5479(4)	12(1)
N(2)	4849(3)	4657(2)	7895(4)	14(1)
N(3)	2766(3)	3131(2)	7048(4)	16(1)
N(4)	3753(3)	3419(2)	7902(4)	15(1)
C(1)	3545(4)	6315(3)	3818(5)	17(1)
C(2)	2611(4)	5804(2)	3411(4)	13(1)
C(3)	1752(4)	5938(3)	2129(5)	16(1)
C(4)	1798(4)	6564(3)	1287(5)	16(1)
C(5)	2708(4)	7070(3)	1688(5)	19(1)
C(6)	3563(4)	6951(3)	2926(5)	18(1)
C(7)	2545(4)	5119(3)	4213(5)	15(1)
C(8)	6792(4)	5740(3)	8569(4)	15(1)

C(9)	6660(4)	5089(3)	9412(5)	14(1)
C(10)	7534(4)	4913(3)	10638(5)	20(1)
C(11)	8488(4)	5349(3)	11071(5)	21(1)
C(12)	8596(4)	5988(3)	10258(5)	22(1)
C(13)	7772(4)	6184(3)	9035(5)	21(1)
C(14)	5732(4)	4562(3)	8995(5)	15(1)
C(15)	3981(4)	4120(2)	7419(5)	12(1)
C(16)	3116(4)	4276(3)	6207(4)	12(1)
C(17)	2372(4)	3643(2)	6016(5)	15(1)
C(18)	4359(4)	2964(3)	9136(5)	21(1)
C(19)	1280(4)	3513(3)	4905(4)	12(1)
C(20)	322(4)	3934(3)	4922(5)	23(1)
C(21)	-693(4)	3819(3)	3895(5)	24(1)
C(22)	-761(4)	3283(3)	2812(5)	20(1)
C(23)	195(4)	2859(3)	2790(5)	23(1)
C(24)	1206(4)	2970(3)	3841(5)	20(1)

## 7.2.6 I

**Table 29: Crystal data and structure refinement for I**

I	
Empirical formula	C <sub>20</sub> H <sub>20</sub> N <sub>4</sub> O <sub>2</sub> Zn
Formula weight	413.77
Temperature	100(2) K
Wavelength	0.71073 Å
Crystal system	Triclinic
Space group	P-1
Unit cell dimensions	a = 7.2149(14) Å, a = 88.47(3)°. b = 11.313(2) Å, b = 74.69(3)°. c = 13.111(3) Å, g = 72.77(3)°.
Volume	984.3(4) Å <sup>3</sup>
Z	2
Density (calculated)	1.396 Mg/m <sup>3</sup>
Absorption coefficient	1.269 mm <sup>-1</sup>
F(000)	428
Crystal size	0.540 x 0.520 x 0.200 mm <sup>3</sup>
Theta range for data collection	2.413 to 35.056°.
Index ranges	-11 ≤ h ≤ 11, -15 ≤ k ≤ 17, -21 ≤ l ≤ 21
Reflections collected	11447
Independent reflections	7066 [R(int) = 0.0277]
Completeness to theta = 25.242°	87.9 %
Refinement method	Full-matrix least-squares on F <sup>2</sup>
Data / restraints / parameters	7066 / 0 / 280
Goodness-of-fit on F <sup>2</sup>	1.003
Final R indices [I > 2σ(I)]	R1 = 0.0486, wR2 = 0.1389
R indices (all data)	R1 = 0.0722, wR2 = 0.1574
Extinction coefficient	n/a
Largest diff. peak and hole	0.429 and -0.276 e.Å <sup>-3</sup>

Atomic coordinates ( $\times 10^4$ ) and equivalent isotropic displacement parameters ( $\text{\AA}^2 \times 10^3$ ) for I.

$U(\text{eq})$  is defined as one third of the trace of the orthogonalized  $U^{ij}$  tensor:

	x	y	z	$U(\text{eq})$
O(001)	7170(1)	573(1)	2906(1)	25(1)
O(002)	5719(1)	677(1)	8243(1)	24(1)
N(003)	3556(1)	3879(1)	4787(1)	15(1)
N(004)	5746(1)	1864(1)	4726(1)	14(1)
N(005)	4699(1)	2718(1)	7180(1)	14(1)
N(006)	2359(1)	4874(1)	5433(1)	15(1)
C(007)	5871(1)	2681(1)	8747(1)	14(1)
C(008)	7856(1)	-236(1)	4542(1)	13(1)
C(009)	3992(1)	3394(1)	6370(1)	13(1)
C(00A)	6173(2)	1402(1)	8887(1)	17(1)
C(00B)	1286(1)	5476(1)	7303(1)	14(1)
C(00C)	5099(1)	3302(1)	7891(1)	14(1)
C(00D)	4546(1)	2949(1)	5309(1)	13(1)
C(00E)	6706(2)	912(1)	5155(1)	14(1)
C(00F)	338(2)	5051(1)	8259(1)	17(1)
C(00G)	2607(1)	4591(1)	6406(1)	14(1)
C(00H)	8057(2)	-375(1)	3441(1)	16(1)
C(00I)	9882(2)	-2389(1)	4499(1)	18(1)
C(00J)	8787(2)	-1270(1)	5052(1)	16(1)
C(00K)	806(2)	6751(1)	7169(1)	16(1)
C(00L)	9185(2)	-1502(1)	2881(1)	18(1)
C(00M)	10075(2)	-2501(1)	3411(1)	18(1)
C(00N)	6961(2)	860(1)	9715(1)	21(1)
C(00O)	3523(2)	3840(1)	3681(1)	19(1)
C(00P)	6396(2)	3381(1)	9439(1)	19(1)
C(00Q)	-1088(2)	5898(1)	9044(1)	20(1)
C(00R)	7445(2)	1570(1)	10392(1)	24(1)
C(00S)	-621(2)	7594(1)	7955(1)	20(1)
C(00T)	-1591(2)	7163(1)	8892(1)	22(1)
C(00U)	7181(2)	2832(1)	10256(1)	24(1)

## 7.2.7 II

**Table 30: Crystal data and structure refinement for II**

II	
Empirical formula	$\text{C}_{22} \text{H}_{24} \text{N}_4 \text{O}_2$
Formula weight	376.45
Temperature	180(2) K
Wavelength	0.71073 $\text{\AA}$
Crystal system	Orthorhombic
Space group	$P2_12_12_1$
Unit cell dimensions	$a = 11.2965(4) \text{\AA}$ , $a = 90^\circ$ . $b = 11.9886(4) \text{\AA}$ , $b = 90^\circ$ . $c = 15.4365(5) \text{\AA}$ , $c = 90^\circ$ .
Volume	$2090.55(12) \text{\AA}^3$
Z	4
Density (calculated)	$1.196 \text{ Mg/m}^3$
Absorption coefficient	$0.079 \text{ mm}^{-1}$
$F(000)$	800

Crystal size	0.2 x 0.12 x 0.08 mm <sup>3</sup>
Theta range for data collection	2.81 to 26.37°
Index ranges	-14<= <i>h</i> <=14, -14<= <i>k</i> <=14, -18<= <i>l</i> <=19
Reflections collected	40717
Independent reflections	4264 [R(int) = 0.0267]
Completeness to theta = 26.37°	99.8 %
Absorption correction	Semi-empirical from equivalents
Max. and min. transmission	0.957 and 0.898
Refinement method	Full-matrix least-squares on F <sup>2</sup>
Data / restraints / parameters	4264 / 0 / 259
Goodness-of-fit on F <sup>2</sup>	1.068
Final R indices [I>2sigma(I)]	R1 = 0.0298, wR2 = 0.0781
R indices (all data)	R1 = 0.032, wR2 = 0.0798
Largest diff. peak and hole	0.149 and -0.176 e.Å <sup>-3</sup>

Atomic coordinates (x 10<sup>4</sup>) and equivalent isotropic displacement parameters (Å<sup>2</sup> x 10<sup>3</sup>) for II.

U(eq) is defined as one third of the trace of the orthogonalized U<sup>ij</sup> tensor:

	x	y	z	U(eq)
N(2)	542(1)	2871(1)	8982(1)	24(1)
N(1)	2851(1)	4086(1)	8537(1)	24(1)
O(1)	-1454(1)	3429(1)	9683(1)	37(1)
O(2)	2829(1)	5851(1)	9561(1)	43(1)
N(4)	2554(1)	2996(1)	7207(1)	25(1)
N(3)	1772(1)	2246(1)	6880(1)	26(1)
C(1)	-868(2)	3981(1)	11950(1)	42(1)
C(2)	320(2)	3720(1)	12018(1)	42(1)
C(3)	936(1)	3400(1)	11283(1)	34(1)
C(4)	369(1)	3312(1)	10483(1)	26(1)
C(5)	1047(1)	3010(1)	9717(1)	25(1)
C(6)	1223(1)	2747(1)	8228(1)	23(1)
C(7)	2261(1)	3307(1)	8026(1)	23(1)
C(8)	3986(1)	4074(1)	8611(1)	24(1)
C(9)	4613(1)	4889(1)	9133(1)	25(1)
C(10)	4020(1)	5749(1)	9576(1)	29(1)
C(11)	4667(1)	6528(1)	10045(1)	37(1)
C(12)	5886(1)	6459(1)	10072(1)	38(1)
C(13)	-852(1)	3543(1)	10430(1)	30(1)
C(14)	-1453(1)	3905(1)	11168(1)	38(1)
C(15)	6486(1)	5610(1)	9651(1)	37(1)
C(16)	5851(1)	4831(1)	9188(1)	30(1)
C(17)	963(1)	2088(1)	7496(1)	24(1)
C(18)	-36(1)	1262(1)	7372(1)	32(1)
C(19)	66(1)	688(1)	6493(1)	38(1)
C(20)	19(2)	384(2)	8092(1)	65(1)
C(21)	3471(1)	3432(1)	6638(1)	34(1)
C(22)	-1220(1)	1891(2)	7409(1)	53(1)



## 7.2.8 III

Table 31: Crystal data and structure refinement for III

III	
Empirical formula	C <sub>28</sub> H <sub>18</sub> N <sub>2</sub> O <sub>6</sub>
Formula weight	478.44
Temperature	100(2) K
Wavelength	0.71073 Å
Crystal system	Monoclinic
Space group	P2 <sub>1</sub> /c
Unit cell dimensions	a = 11.98(2) Å, a = 90°. b = 14.01(3) Å, b = 107.13(4)°. c = 13.54(3) Å, c = 90°.
Volume	2171(8) Å <sup>3</sup>
Z	4
Density (calculated)	1.464 Mg/m <sup>3</sup>
Absorption coefficient	0.105 mm <sup>-1</sup>
F(000)	992
Crystal size	0.450 x 0.470 x 0.220 mm <sup>3</sup>
Theta range for data collection	1.779 to 28.837°.
Index ranges	-16 ≤ h ≤ 16, -18 ≤ k ≤ 18, -18 ≤ l ≤ 18
Reflections collected	31831
Independent reflections	5630 [R(int) = 0.0649]
Completeness to theta = 25.242°	99.7 %
Refinement method	Full-matrix least-squares on F <sup>2</sup>
Data / restraints / parameters	5630 / 0 / 335
Goodness-of-fit on F <sup>2</sup>	0.874
Final R indices [I > 2σ(I)]	R1 = 0.0769, wR2 = 0.2266
R indices (all data)	R1 = 0.1097, wR2 = 0.2505
Extinction coefficient	n/a
Largest diff. peak and hole	0.595 and -0.392 e.Å <sup>-3</sup>

Atomic coordinates (x 10<sup>4</sup>) and equivalent isotropic displacement parameters (Å<sup>2</sup> × 10<sup>3</sup>) for III.

U(eq) is defined as one third of the trace of the orthogonalized U<sup>ij</sup> tensor:

	x	y	z	U(eq)
O(1)	8889(2)	6078(2)	7192(2)	23(1)
C(1)	8128(3)	3434(2)	7229(2)	18(1)
N(1)	8423(2)	4370(2)	7622(2)	18(1)
O(2)	6261(2)	5853(2)	6251(2)	20(1)
C(2)	7270(3)	3325(2)	6282(2)	17(1)
N(2)	6730(2)	4172(2)	5784(2)	19(1)
O(4)	5722(3)	5192(2)	2727(2)	33(1)
C(4)	7490(3)	1621(2)	6451(3)	22(1)
O(3)	8787(3)	5430(2)	10582(2)	32(1)
C(3)	6932(3)	2405(2)	5908(3)	21(1)
C(9)	8640(3)	5645(2)	8801(2)	19(1)
C(8)	7920(4)	4008(3)	9189(3)	29(1)
C(7)	8363(3)	4680(2)	8530(2)	20(1)
O(6)	5778(2)	6667(2)	3260(2)	24(1)
C(6)	8706(3)	2640(3)	7753(3)	23(1)
O(5)	8921(2)	6895(2)	10088(2)	25(1)
C(5)	8387(3)	1732(2)	7361(3)	22(1)

---

C(10)	8803(3)	6309(2)	8053(2)	18(1)
C(11)	8849(3)	7330(2)	8350(2)	19(1)
C(12)	8811(3)	8059(2)	7633(3)	21(1)
C(13)	8876(3)	8998(3)	7942(3)	24(1)
C(14)	8968(3)	9236(3)	8958(3)	26(1)
C(15)	8976(3)	8520(3)	9679(3)	26(1)
C(16)	8909(3)	7573(2)	9349(2)	18(1)
C(17)	8764(3)	5940(3)	9859(3)	23(1)
C(18)	6565(3)	4449(2)	4813(2)	18(1)
C(19)	6834(3)	3757(3)	4070(3)	26(1)
C(20)	6209(3)	5398(2)	4547(2)	18(1)
C(21)	6174(3)	6077(2)	5342(2)	17(1)
C(22)	6043(3)	7089(2)	5039(2)	18(1)
C(23)	6093(3)	7807(2)	5767(3)	21(1)
C(24)	5962(3)	8756(3)	5463(3)	24(1)
C(25)	5780(3)	8986(3)	4425(3)	k25(1)
C(26)	5751(3)	8286(2)	3697(3)	23(1)
C(27)	5873(3)	7341(2)	4012(2)	20(1)
C(28)	5904(3)	5694(2)	3472(3)	22(1)

---

## 8 Abbreviations

A	absorbance
abs	absolute
aliph	aliphatic
arom	aromatic
bp	boiling point
c	concentration [mol/l]
conc	concentrated
DCM	dichloromethane
dest	destillated
DMSO	dimethyl sulfoxide
E	energy
EE	ethyl acetate
eq	equivalents
Et <sub>2</sub> O	diethyl ether
Et <sub>3</sub> N	triethylamine
EtOH	ethanol
h	hour
h	Planck constant ( $h = 6.626 \times 10^{-34}$ Js) [109]
hal	halide
I	intensity of the incident light [W/m <sup>2</sup> ]
I <sub>0</sub>	intensity of the transmitted light [W/m <sup>2</sup> ]
IC	internal conversion
iPrOH	isopropanol
IR	infrared
ISC	intersystem crossing
J	joule
K	kelvin
L	litre
Ln	lanthanide

---

M	molar mass [g/mol]
MeLi	methyllithium
MeOH	methanol
ml	millilitre
MOF	metal-organic framework
PCP	porous coordination polymer
PE	petrol ether
pH	Lat.: “pondus hydrogenii”
ppm	parts per million
R <sub>f</sub> -value	retardation factor
RT	room temperature
s	seconds
sat	saturated
tBuOK	potassium <i>tert</i> -butoxide
TLC	thin layer chromatography
TMS	trimethyl silane
UV	ultraviolet
VO(acac) <sub>2</sub>	vanadyl acetylacetonate
$\varepsilon$	molar attenuation coefficient [m <sup>2</sup> /mol]
$\lambda$	wavelength [nm]

## 9 List of Figures

Figure 1: Synthesis of the Schiff-base Ligands I and II .....	3
Figure 2: Synthesis of the simple Schiff-base Ligand 8 .....	3
Figure 3: Synthesis of the Schiff-base Ligands III, IV and 10 .....	4
Figure 4: Hexadentate N-containing Ligand.....	4
Figure 5: Coordination Compounds of Zn .....	4
Figure 6: Coordination Compounds of Cd .....	5
Figure 7: Coordination Compounds of V.....	5
Figure 8: Coordination Compound of Eu.....	6
Figure 9: Under UV-light the 20 euro note exhibits luminescence of Eu-oxides [10] .....	7
Figure 10: The Austrian passport exhibits luminescence of Ln-compounds under UV-light [10] .....	8
Figure 11: the electromagnetic spectrum [14] .....	8
Figure 12: Perrin-Jablonski diagram [18] .....	10
Figure 13: periodic table of the elements [25] .....	13
Figure 14: Ionic radii of the lanthanides [30] .....	15
Figure 15: Synthesis of Bis(salicylaldehyde)ethylenediamine (sal <sub>2</sub> en) .....	17
Figure 16: LEFT: Rhodopsin [40], RIGHT: Retinal in its cis- and trans-conformation.....	18
Figure 17: Fluorescence behaviour of the azacryptand system with different metal ions - selectivity [47] .....	19
Figure 18: pyrazoline-derivative [48] .....	19
Figure 19: Logic gate system based on salen-ligand .....	20
Figure 20: Selectivity of the salen-system in the presence of Zn <sup>2+</sup> -ions (LEFT) and Zn <sup>2+</sup> - and Al <sup>3+</sup> - ions (RIGHT) [8] .....	21
Figure 21: Pyridine-type ligands [52] .....	22
Figure 22: Energy-transfer in coordination compounds of pyridyl-like ligands [53] .....	23

Figure 23: Transitions of luminescent lanthanide complexes in the energy diagram [53] .....	23
Figure 24: Structure of Ln-complexes with a hexadentate ligand (LEFT) and crystal structure of Eu-coordination compound (RIGHT) [68] .....	24
Figure 25: Molecular structure of a polymeric lanthanide-coordination compound [69] .....	24
Figure 26: Coumarin building block .....	25
Figure 27: Synthetic pathway of 9 and its Eu-complex 9d .....	26
Figure 28: Approach of the synthesis of tetradentate Schiff bases, based on 9 .....	27
Figure 29: Approach of the synthesis of a tetradentate Schiff bases I (R = Ph) and II (R = tBu) .....	28
Figure 30: Coordination compounds of tetradentate Schiff base I as an example .....	30
Figure 31: Approach of the synthesis of the hexadentate ligand V .....	31
Figure 32: Comparison of the $^1\text{H}$ NMR-spectra of I in $\text{CDCl}_3$ (red) and after addition of $\text{D}_2\text{O}$ (turquoise) .....	32
Figure 33: Comparison of the $^1\text{H}$ NMR-spectra of I (red) and Ia (blue) in DMSO .....	33
Figure 34: Comparison of the $^1\text{H}$ NMR spectra of Ia (red) and Ib (blue) in DMSO .....	34
Figure 35: LEFT: UV/VIS-spectra of Ib, recorded with different concentrations ( $3.70\text{E-}05$ / violet, $2.96\text{E-}05$ / blue, $2.22\text{E-}05$ / grey, $1.48\text{E-}05$ / red); RIGHT: linear regression of the maxima at 262 nm (black), 298 nm (red), 344 nm (green), 400 nm (violet) and 450 nm (turquoise) ..	36
Figure 36: Plotted UV/VIS spectra of the Zn-complex Ia (black) and its ligand I (red), measured of DMSO-solutions with same concentrations ( $3\text{E-}5$ mol/l) .....	38
Figure 37: Plotted UV/VIS spectra of Ia (black) and Ib (blue) measured of DMSO-solutions with same concentrations ( $3\text{E-}5$ mol/l) .....	39
Figure 38: Plotted UV/VIS spectra of Ia (black) and IIa (green) measured of DMSO-solutions with same concentrations ( $3\text{E-}5$ mol/l) .....	40
Figure 39: Plotted UV/VIS spectra of Ia (black) and 8a (violet) measured of DMSO-solutions with same concentrations ( $3\text{E-}5$ mol/l) .....	41
Figure 40: Plotted UV/VIS spectra of III (red), IIIa (grey) and IIIb (blue) measured of acetone-solutions with the concentrations $3.1\text{E-}05$ , $2.5\text{E-}05$ and $3.9\text{E-}05$ mol/l, respectively .....	42

Figure 41: Emission ( $\lambda = 528$ nm) and excitation ( $\lambda = 475$ nm) spectra for the solid sample Ia. (Quantum yield = 4.95 %)	43
Figure 42: Emission spectra for $10^{-5}$ M DMSO-solutions of IIa (black) and IIb (red)	44
Figure 43: Emission spectra for $10^{-5}$ M DMSO-solutions of 10a (black) and 10b (red)	45
Figure 44: Emission spectra for $10^{-5}$ M DMSO-solutions of IIIb (black) and IIIa (red)	45
Figure 45: Emission spectra for $10^{-5}$ M DMSO-solutions of Ib (black) and Ia (red)	45
Figure 46: Emission spectra for $10^{-5}$ M DMSO-solutions of 8a (black) and 8b (red)	46
Figure 47: LEFT: Emission ( $\lambda = 550$ nm) and excitation ( $\lambda = 490$ nm) spectra for a MeOH solution of Ia; RIGHT: Emission ( $\lambda = 563$ nm) and excitation ( $\lambda = 496$ nm) spectra for a THF solution of Ia.	46
Figure 48: LEFT: Emission ( $\lambda = 550$ nm) and excitation ( $\lambda = 490$ nm) spectra for a MeOH solution of IIa; RIGHT: Emission ( $\lambda = 560$ nm) and excitation ( $\lambda = 500$ nm) spectra for a THF solution of IIa.	47
Figure 49: LEFT: Emission ( $\lambda = 396$ nm) and excitation ( $\lambda = 350$ nm) spectra for a MeOH solution of IIIa; RIGHT: Emission ( $\lambda = 413$ and $440$ nm) and excitation ( $\lambda = 365$ nm) spectra for a THF solution of IIIa.	47
Figure 50: Emission ( $\lambda = 614$ nm) and excitation ( $\lambda = 371$ nm) spectra for complex 9d.	48
Figure 51: LEFT: Molecular structure of Ia Pyridine (H-atoms are omitted for clarity). Selected bond-lengths (in Å) and bond angles (in deg): Zn01-O003 1.973, Zn01-N2 2.126, Zn01-N007 2.124, Zn01-O004 1.963, Zn01-N009 2.114, O003-Zn01-O004 95.11, O004-Zn01-N007 89.28, N007-Zn01-N2 80.29, N2-Zn01-O003 87.15; RIGHT: Molecular structure of Ia DMSO (H-atoms are omitted for clarity). Selected bond-lengths (in Å) and bond angles (in deg): Zn1-O1 1.968, Zn1-N3 2.159, Zn1-N2 2.108, Zn1-O2 1.965, Zn1-O3 2.061, O1-Zn1-N3 86.86, N3-Z1-N2 79.38, N2-Zn1-O2 90.00, O2-Zn1-O1 95.59	49
Figure 52: Molecular structure of IIa DMSO (H-atoms are omitted for clarity). Selected bond-lengths (in Å) and bond angles (in deg): Zn1-O1 1.970, Zn1-N1 2.118, Zn1-N2 2.132, Zn1-O2 1.979, Zn1-O3 2.082, O1-Zn1-N1 88.98, N1-Zn1-N2 80.14, N2-Zn1-O2 89.34, O2-Zn1-O1 94.90	49

Figure 53: Molecular structure of 8b DMSO (H-atoms are omitted for clarity). Selected bond-lengths (in Å) and bond angles (in deg): Cd01-O003 2.278, Cd01-N1 2.310, Cd01-N008 2.272, Cd01-O004 2.171, Cd01-O006 2.391, O003-Cd01-N1 78.78, N1-Cd01-N008 72.64, N008-Cd01-O004 86.17, O004-Cd01-O003 122.71 .....	51
Figure 54: Molecular structure of Ic (H-atoms are omitted for clarity). Selected bond-lengths (in Å) and bond angles (in deg): V1-O1 1.919, V1-N2 2.103, V1-N2 2.088, V1-O2 1.912, V1-O3 1.590, O1-V1-N2 86.94, N2-V1-N1 80.33, N1-V1-O2 86.83, O2-V1-O1 87.67 .....	52
Figure 55: Molecular structure of I. Selected bond-lengths (in Å) and bond angles (in deg): O001-N004 2.623, N004-N005 3.211, N005-O002 2.680, O001-C00H 1.357, O002-C00A 1.356, N005-C00C 1.294, N005-C009 1.408, N004-C00E 1.299, N004-C00D 1.383, C00E-N004-C00D 122.14, C00C-N005-C009 118.64 .....	52
Figure 56: Molecular structure of II. Selected bond-lengths (in Å) and bond angles (in deg): O1-C13 1.345, O2-C10 1.350, N1-C8 1.287, N1-C7 1.393, N2-C5 1.280, N2-C6 1.404, O1-N2 2.589, N1-N2 3.066, N1-O2 2.642, C7-N2-C8 121.30, C5-N2-C6 120.32 .....	53
Figure 57: Molecular structure of III. Selected bond-lengths (in Å) and bond angles (in deg): O1-C10 1.243, O2-C21 1.244, N1-C1 1.420, N1-C7 1.326, N2-C2 1.423, N2-C18 1.329, O1-N1 2.562, N1-N2 2.722, N2-O2 2.544, C1-N1-C7 125.07, C2-N2-C18 128.83 .....	54
Figure 58: LEFT: HOMO of Ia, RIGHT: LUMO of Ia .....	55
Figure 59: Spin density plot of Ic, iso-surface value 0.02 .....	56
Figure 60: Synthesis of benzoyl acetonitrile .....	61
Figure 61: Synthesis of 1-methyl-3-phenyl-1H-pyrazol-5-amine .....	62
Figure 62: Synthesis of 1-methyl-3-phenyl-1H-pyrazole-4,5-diamine .....	63
Figure 63: Synthesis of 4.5-[di(phenylimino)methyl]-1-methyl-3-phenyl-1H-pyrazole .....	64
Figure 64: Synthesis of methyl pivalate .....	65
Figure 65: Synthesis of 4,4-dimethyl-3-oxo-pentanenitrile .....	65
Figure 66: Synthesis of 3-(1,1-dimethylethyl)-1-methyl-1H-pyrazol-5-amine .....	66
Figure 67: Synthesis of 3-(1,1-dimethylethyl)-1-methyl-1H-pyrazole-4,5-diamine .....	67



Figure 68: Synthesis of 3-(1,1-dimethylethyl)-4,5-[di(phenylimino)methyl]-1-methyl-1H-Pyrazole .....	68
Figure 69: Synthesis of 1,2-Bis[[(2-hydroxyphenyl)methylene]amino]benzene .....	69
Figure 70: Synthesis of 3-acetyl-4-hydroxychromen-2-one:.....	70
Figure 71: Synthesis of [1,2-Phenylbis(iminoethylidene)]bis[2H-1-benzopyran-2,4(3H)-dione] .....	71
Figure 72: Synthesis of (3E,3'E)-3,3'-[1,2-Ethanediy]bis(iminoethylidene)]bis[2H-1-benzopyran-2,4(3H)-dione] .....	72
Figure 73: Synthesis of [1,2-Cyclohexylbis(iminoethylidene)]bis[2H-1-benzopyran-2,4(3H)-dione] .....	73
Figure 74: Synthesis of 2-Methyl-1,10-phenanthroline .....	74
Figure 75: Synthesis of 1,10-Phenanthroline-2-carbaldehyde .....	75
Figure 76: Synthesis of N,N'-(Ethane-1,2-diyl)-bis(1,10-phenanthroline-2-yl)methanimine.....	76
Figure 77: Synthesis of 8a.....	77
Figure 78: Synthesis of Ia.....	78
Figure 79: Synthesis of IIa.....	79
Figure 80: Synthesis of IIIa.....	80
Figure 81: Synthesis of 10a .....	81
Figure 82: Synthesis of 8b .....	82
Figure 83: Synthesis of Ib .....	83
Figure 84: Synthesis of IIb .....	84
Figure 85: Synthesis of IIIb .....	85
Figure 86: Synthesis of 10b .....	86
Figure 87: Synthesis of 8c.....	87
Figure 88: Synthesis of Ic.....	88
Figure 89: Synthesis of IIc.....	88

Figure 90: Synthesis of IIIc.....	89
Figure 91: Synthesis of IVc .....	90
Figure 92: LEFT: UV/VIS-spectra of I, recorded with different concentrations (4.04E-05 / blue, 3.23E-05 / red, 2.42E-05 / grey, 1.61E-05 / violet); RIGHT: linear regression of the maxima at 272 nm (black) and 344 nm (red).....	92
Figure 93: LEFT: UV/VIS-spectra of Ia, recorded with different concentrations (3.27E-05 / grey, 2.62E-05 / blue, 1.96E-05 / violet, 1.31E-05 / red); RIGHT: linear regression of the maxima at 261 nm (black), 299 nm (red), 326 nm (green), 343 nm (violet), 400 nm (light blue) and 451 nm (orange).....	93
Figure 94: LEFT: UV/VIS-spectra of Ic, recorded with different concentrations (2.60E-05 / grey, 2.17E-05 / blue, 1.73E-05 / red, 1.30E-05 / violet); RIGHT: linear regression of the maxima at 260 nm (black), 329 nm (red), 348 nm (green) and 406 nm (violet) .....	94
Figure 95: LEFT: UV/VIS-spectra of II, recorded with different concentrations (3.65E-05 / red, 2.92E-05 / blue, 2.19E-05 / violet, 1.46E-05 / grey); RIGHT: linear regression of the maxima at 271 nm (black) and 341 nm (red).....	94
Figure 96: LEFT: UV/VIS-spectra of IIa, recorded with different concentrations (6.91E-05 / grey, 4.32E-05 / blue, 2.59E-05 / violet, 1.73E-05 / red); RIGHT: linear regression of the maxima at 260 nm (black), 295 nm (red), 342 nm (green), 393 nm (violet) and 451 nm (turquois) .....	95
Figure 97: LEFT: UV/VIS-spectra of IIb, recorded with different concentrations (6.33E-05 / violet, 4.52E-05 / grey, 3.62E-05 / red, 2.26E-05 / blue); RIGHT: linear regression of the maxima at 261 nm (black), 346 nm (red) and 386 nm (green).....	96
Figure 98: LEFT: UV/VIS-spectra of IIc, recorded with different concentrations (9.06E-05 / violet, 7.25E-05 / grey, 5.44E-05 / red, 3.62E-05 / blue); RIGHT: linear regression of the maxima at 266 nm (black) and 306 nm (red).....	96
Figure 99: LEFT: UV/VIS-spectra of 8, recorded with different concentrations (6.64E-05 / grey, 3.32E-05 / red, 2.21E-05 / blue, 1.11E-05 / violet); RIGHT: linear regression of the maxima at 334 nm (black) and 272 nm (red).....	97
Figure 100: LEFT: UV/VIS-spectra of 8a, recorded with different concentrations (4.85E-05 / violet, 3.63E-05 / grey, 2.42E-05 / red, 1.21E-05 / blue); RIGHT: linear regression of the maxima at 260 nm (green, 402 nm (black) and 297 nm (red).....	97

Figure 101: LEFT: UV/VIS-spectra of 8b, recorded with different concentrations ( $4.92\text{E-}05$  / red,  $3.69\text{E-}05$  / violet,  $2.46\text{E-}05$  / blue,  $1.23\text{E-}05$  / grey); RIGHT: linear regression of the maxima at 260 (green), 400 nm (black) and 294 nm (red) ..... 98

Figure 102: LEFT: UV/VIS-spectra of 8c, recorded with different concentrations ( $4.09\text{E-}05$  / grey,  $3.41\text{E-}05$  / violet,  $2.73\text{E-}05$  / red,  $1.36\text{E-}05$  / blue); RIGHT: linear regression of the maxima at 261 nm (green), 406 nm (black) and 312 nm (red)..... 99

## 10 List of Formulas

Formula 1: Relation between energy and wavelength [16] .....	10
Formula 2: Lambert-Beer law [9] .....	36
Formula 3: Determination of the quantum yields .....	59
Formula 4: Lifetime-studies .....	59

## 11 List of Tables

Table 1: Tested conditions for the synthesis of 8a .....	29
Table 2: Comparison of the IR-bands of the C=N-, C-O-, M-O-, M-N- and V-O-bonds in cm <sup>-1</sup> .....	35
Table 3: Maxima of the UV/VIS spectra of ligand I and its coordination compounds of Zn (Ia), Cd (Ib) and V (Ic) .....	37
Table 4: Maxima of the UV/VIS spectra of ligand II and its coordination compounds of Zn (IIa), Cd (IIb) and V (IIc) .....	39
Table 5: Maxima of the UV/VIS spectra of ligand 8 and its coordination compounds of Zn (8a), Cd (8b) and V (8c) .....	40
Table 6: Maxima of the UV/VIS spectra of the ligands III and 10 and their coordination compounds of Zn and Cd .....	41
Table 7: Summarized data of the fluorescence measurements of all zinc and cadmium complexes in DMSO-solutions with a concentration of 10 <sup>-5</sup> mol/l at 298 K, upon ultraviolet and visible excitation .....	43
Table 8: Summarized bond lengths of the central metal of compounds Ia, IIa and 8b in Å ....	50
Table 9: Comparison of calculated and experimentally determined metrical parameters of complex Ia (closed shell (S = 0) .....	55
Table 10: Comparison of calculated and experimentally determined metrical parameters of complex Ic .....	56
Table 11: Comparison of calculated and experimentally determined metrical parameters of complex 8b (closed shell (S = 0) .....	57
Table 12: Summarized data of the UV/VIS spectra of I .....	92
Table 13: Summarized data of the UV/VIS spectra of Ia .....	92
Table 14: Summarized data of the UV/VIS spectra of Ib .....	93
Table 15: Summarized data of the UV/VIS spectra of Ic .....	93
Table 16: Summarized data of the UV/VIS spectra of II .....	94
Table 17: Summarized data of the UV/VIS spectra of IIa .....	95

Table 18: Summarized data of the UV/VIS spectra of IIb.....	95
Table 19: Summarized data of the UV/VIS spectra of IIc .....	96
Table 20: Summarized data of the UV/VIS spectra of 8.....	96
Table 21: Summarized data of the UV/VIS spectra of 8a.....	97
Table 22: Summarized data of the UV/VIS spectra of 8b.....	98
Table 23: Summarized data of the UV/VIS spectra of 8c .....	98
Table 24: Crystal data and structure refinement for Ia pyridine .....	99
Table 25: Crystal data and structure refinement for Ia DMSO .....	101
Table 26: Crystal data and structure refinement for IIa DMSO .....	103
Table 27: Crystal data and structure refinement for 8b DMSO .....	104
Table 28: Crystal data and structure refinement for Ic.....	105
Table 29: Crystal data and structure refinement for I .....	106
Table 30: Crystal data and structure refinement for II .....	107
Table 31: Crystal data and structure refinement for III .....	109

## 12 List of References

1. Silva, P.A.d., N.H.Q. Gunaratne, and C.P. McCoy, *A molecular photoionic AND gate based on fluorescent signalling*. Nature, 1993. **364**(6432): p. 42-44.
2. Silva, A.P., H.Q. Nimalá-Gunaratne, and E.M. Glenn, *'Off-on' fluorescent sensors for physiological levels of magnesium ions based on photoinduced electron transfer (PET), which also behave as photoionic OR logic gates*. Journal of the Chemical Society, Chemical Communications, 1994(10): p. 1213-1214.
3. Silva, P.A.d., H.Q.N. Gunaratne, and C.P. McCoy, *Molecular photoionic AND logic gates with bright fluorescence and "off-on" digital action*. Journal of the American Chemical Society, 1997. **119**(33): p. 7891-7892.
4. Lavigne, J.J. and E.V. Anslyn, *Sensing a paradigm shift in the field of molecular recognition: from selective to differential receptors*. Angewandte Chemie International Edition, 2001. **40**(17): p. 3118-3130.
5. Silva, A.P.D., et al., *Combining luminescence, coordination and electron transfer for signalling purposes*. Coordination Chemistry Reviews, 2000. **205**(1): p. 41-57.
6. Greenwood, N.N. and A. Earnshaw, *Chemistry of the Elements*. 1984: Pergamo Press Ltd. .
7. Bryce-Smith, D., *Zn deficiency - the neglected factor*. Chemistry in Britain, 1989. **25**: p. 783.
8. Huerta-Aguilar, C.A., et al., *Three novel input logic gates supported by fluorescence studies: Organic nanoparticles (ONPs) as chemo-sensor for detection of Zn 2+ and Al 3+ in aqueous medium*. Spectrochimica Acta Part A: Molecular and Biomolecular Spectroscopy, 2015. **146**: p. 142-150.
9. Wöhrle, D., M.W. Tausch, and W.D. Stohrer, *Photochemie: Konzepte, Methoden, Experimente*. 1998, Wiley-VCH Verlag GmbH, Weinheim.
10. Mathuber, M., *Synthesis of Compounds using Hard/Hard and Soft/Soft Lewis Acid - Base Interactions and Investigation of their Properties for Possible Industrial Applications*. 2016: Vienna UT.
11. Riehl, N., *Einführung in die Lminescenz*. 1970, K. Thiemig Verlag, München.
12. Moore, W.J. and D.O. Hummel, *Physikalische Chemie*. 1986, Walter de Gruyter Verlag, Berlin.
13. Falbe, J. and M. Regitz, *Römpf Chemielexikon*. 1995, G. Thieme Verlag, Stuttgart.
14. Theophanides, T., *Infrared Spectroscopy - Materials Science, Engineering and Technology*. 2012.
15. Campbell, A.K., M.B. Hallett, and I. Weeks, *Methods of Biochemical Analysis*. Vol. 31. 1985, John Wiley & Sons, Inc.
16. Gipert, J.R., *Coordination Chemistry*. 2008: Wiley-VCH Verlag GmbH & Co. KGaA, Weinheim.

17. Porterfield, W.F., *Inorganic Chemistry. A Unified Approach*. 1993, Academic Press, New York.
18. Valeur, B. and M.N. Berberan-Santos, *Molecular Fluorescence: Principles and Applications*. Vol. 2. 2012, Wiley-VCH Verlag GmbH & Co. KGaA.
19. Öttinger, H.C., *Beyond Equilibrium Thermodynamics*. 2005, John Wiley & Sons, Inc. .
20. Jortner, J., R.D. Levine, and S.A. Rice, *Advance in Chemical Physics*. Vol. 47. 1981, John Wiley & Sons, Inc. .
21. Liu, S., W. Liu, and H. Niu, *Supercontinuum Generation With Photonic Crystal Fibers and Its Application in Nano-imaging*, in *Photonic Crystals*, A. Bananej, Editor. 2015, InTech: Rijeka. p. Ch. 02.
22. Jr., W.A.N., G.S. Hammond, and J.N.P. Jr., *Advances in Photochemistry*. Vol. 2. 1964, John Wiley & Sons, Inc. .
23. Burns, R.G., *Mineralogical Applications of Crystal Field Theory*. 1970: Cambridge University Press, Cambridge.
24. Philips, C.S.G. and R.J.P. Williams, *Inorganic Chemistry*. Vol. 2. 1966, Oxford University Press, Oxford.
25. *online available at: <https://sciencenotes.org/printable-periodic-table/> (access date: 2017-10-03).*
26. Kaim, W., *Bioanorganische Chemie - Zur Funktion chemischer Elemente in Lebensprozessen*. 1995: B. G. Teubner Stuttgart.
27. Roat-Malone, R.M., *Bioinorganic Chemistry - A Short Course*. Vol. 2. 2008: Wiley-Interscience.
28. Silva, J.J.R.F.d. and R.J.P. Williams, *The Biological Chemistry of the Elements - The Inorganic Chemistry of Life*. 1993, Clarendon Press, Oxford.
29. Dobson, S., *Cadmium-Environmental Aspekts. World Health Organization: Geneva*. Molecular Nutrition & Food Research, 1994. **38**(4): p. 454-454.
30. Riedel, E. and C. Janiak, *Anorganische Chemie*. 2007, de Gruyter, Berlin.
31. Calligaris, M., G.T. Nardini, and L. Randaccio, *Structural aspects of metal complexes with some tetradentate schiff bases*. Coordination Chemistry Reviews, 1972. **7**(4): p. 385-403.
32. Casellato, U., P.A. Vigato, and M. Vidali, *Transition metal complexes with binucleating ligands*. Coordination Chemistry Reviews, 1977. **23**(1): p. 31-117.
33. Fenton, D.E. and S.E. Gayda, *Compartmental ligands. Part 3. Homo-and hetero-binuclear transition-metal complexes of acyclic Schiff bases derived from 1, 3, 5-triketones*. Journal of the Chemical Society, Dalton Transactions, 1977(21): p. 2109-2115.
34. Sacconi, L., *Four-, five-and six-coordinated complexes of 3D metals with substituted salicylaldimines*. Coordination Chemistry Reviews, 1966. **1**(1-2): p. 192-204.
35. Sinn, E. and C.M. Harris, *Schiff base metal complexes as ligands*. Coordination Chemistry Reviews, 1969. **4**(4): p. 391-422.



36. Yamada, S., *Recent aspects of the stereochemistry of Schiff-base-metal complexes*. Coordination Chemistry Reviews, 1966. **1**(4): p. 415-437.
37. Cotton, F.A. and G. Wilkinson, *Advanced Inorganic Chemistry*. Vol. 4. 1980: John Wiley & Sons, Inc.
38. Hobday, M.D. and T.D. Smith, *N, N'-ethylenebis (salicylideneiminato) transition metal ion chelates*. Coordination Chemistry Reviews, 1973. **9**(3): p. 311-337.
39. Fabbrizzi, L., M. Licchelli, and P. Pallavicini, *Transition metals as switches*. Accounts of chemical research, 1999. **32**(10): p. 846-853.
40. Palczewski, K., et al., *Crystal structure of rhodopsin: AG protein-coupled receptor*. science, 2000. **289**(5480): p. 739-745.
41. Balzani, V., M. Gómez-López, and J.F. Stoddart, *Molecular machines*. Accounts of Chemical Research, 1998. **31**(7): p. 405-414.
42. Sauvage, J.P., *Transition metal-containing rotaxanes and catenanes in motion: toward molecular machines and motors*. Accounts of chemical research, 1998. **31**(10): p. 611-619.
43. Clayden, J. and J.H. Pink, *Concerted rotation in a tertiary aromatic amide: towards a simple molecular gear*. Angewandte Chemie International Edition, 1998. **37**(13-14): p. 1937-1939.
44. Franceschi, F., et al., *Molecular batteries based on carbon-carbon bond formation and cleavage in titanium and vanadium Schiff base complexes*. Chemistry-a European Journal, 1999. **5**(2): p. 708-721.
45. Ishow, E., et al., *A Molecular-Level Plug/Socket System: Electronic Energy Transfer from a Binaphthyl Unit Incorporated into a Crown Ether to an Anthracenyl Unit Linked to an Ammonium Ion*. Chemistry-A European Journal, 1999. **5**(3): p. 984-989.
46. Bag, B. and P.K. Bharadwaj, *Attachment of an electron-withdrawing fluorophore to a cryptand for modulation of fluorescence signaling*. Inorganic chemistry, 2004. **43**(15): p. 4626-4630.
47. Peng, X., et al., *A selective fluorescent sensor for imaging Cd<sup>2+</sup> in living cells*. Journal of the American Chemical Society, 2007. **129**(6): p. 1500-1501.
48. Rurack, K. and U. Resch-Genger, *Rigidization, preorientation and electronic decoupling—the 'magic triangle' for the design of highly efficient fluorescent sensors and switches*. Chemical Society Reviews, 2002. **31**(2): p. 116-127.
49. Ivanova, B.B. and M. Spiteller, *Optical and nonlinear optical properties of new Schiff's bases: experimental versus theoretical study of inclusion interactions*. Journal of Inclusion Phenomena and Macrocyclic Chemistry, 2013. **75**(1-2): p. 211-221.
50. Amendola, V., et al., *Molecular machines based on metal ion translocation*. Accounts of chemical research, 2001. **34**(6): p. 488-493.
51. Kelly, N., et al., *New Heterodinuclear Zn/Ln (Ln= Gd, Tb, Er, Yb) Complexes of Hexadentate N, N'-Bis (3-alkoxy-2-hydroxybenzyl) cyclohexane-1, 2-diamines: Synthesis and Structure*. Australian Journal of Chemistry, 2017. **70**(5): p. 601-607.

52. Das, D.K. and K. Dutta, *pH dependent fluorescence switching in salicylideneaniline: 'off-on-off' operation controlled by surfactant micelles*. Journal of Luminescence, 2014. **145**: p. 454-458.
53. Huang, C.H., *Rare earth coordination chemistry: fundamentals and applications*. 2011: John Wiley & Sons.
54. Werts, M.H.V., *Making sense of lanthanide luminescence*. Science progress, 2005. **88**(2): p. 101-131.
55. Katkova, M.A. and M.N. Bochkarev, *New trends in design of electroluminescent rare earth metallo-complexes for OLEDs*. Dalton Transactions, 2010. **39**(29): p. 6599-6612.
56. Kido, J. and Y. Okamoto, *Organo lanthanide metal complexes for electroluminescent materials*. Chemical Reviews, 2002. **102**(6): p. 2357-2368.
57. Wang, J., et al., *First oxadiazole-functionalized terbium (III)  $\beta$ -diketonate for organic electroluminescence*. Journal of the American Chemical Society, 2001. **123**(25): p. 6179-6180.
58. Chen, Z., et al., *Synthesis and electroluminescent property of novel europium complexes with oxadiazole substituted 1, 10-phenanthroline and 2, 2'-bipyridine ligands*. New Journal of Chemistry, 2010. **34**(3): p. 487-494.
59. Yeh, S.J., et al., *New dopant and host materials for Blue-Light-Emitting phosphorescent organic electroluminescent devices*. Advanced Materials, 2005. **17**(3): p. 285-289.
60. Xin, H., et al., *Efficient electroluminescence from a new terbium complex*. Journal of the American Chemical Society, 2003. **125**(24): p. 7166-7167.
61. Katkova, M.A., et al., *Near-infrared electroluminescent lanthanide [Pr (III), Nd (III), Ho (III), Er (III), Tm (III), and Yb (III)] N, O-chelated complexes for organic light-emitting devices*. Journal of Materials Chemistry, 2011. **21**(41): p. 16611-16620.
62. Wuister, S.F., C.d.M. Donegá, and A. Meijerink, *Efficient energy transfer between nanocrystalline YAG: Ce and TRITC*. Physical Chemistry Chemical Physics, 2004. **6**(8): p. 1633-1636.
63. Ende, B.M.V.D., L. Aarts, and A. Meijerink, *Lanthanide ions as spectral converters for solar cells*. Physical Chemistry Chemical Physics, 2009. **11**(47): p. 11081-11095.
64. Pal, R., D. Parker, and L.C. Costello, *A europium luminescence assay of lactate and citrate in biological fluids*. Organic & biomolecular chemistry, 2009. **7**(8): p. 1525-1528.
65. Montgomery, C.P., et al., *Cell-penetrating metal complex optical probes: targeted and responsive systems based on lanthanide luminescence*. Accounts of chemical research, 2009. **42**(7): p. 925-937.
66. Shinoda, S., et al., *Ytterbium-substituted transferrin and lactoferrin for near-infrared luminescent pH indication*. New Journal of Chemistry, 2012. **36**(8): p. 1545-1547.
67. Miyake, H. and H. Tsukube, *Coordination chemistry strategies for dynamic helicates: time-programmable chirality switching with labile and inert metal helicates*. Chemical Society Reviews, 2012. **41**(21): p. 6977-6991.

68. Ariga, K., et al., *Molecular recognition: from solution science to nano/materials technology*. Chemical Society Reviews, 2012. **41**(17): p. 5800-5835.
69. Hasegawa, M., et al., *Luminescence behaviour in acetonitrile and in the solid state of a series of lanthanide complexes with a single helical ligand*. New Journal of Chemistry, 2014. **38**(3): p. 1225-1234.
70. Sato, S., et al., *Luminescence of fusion materials of polymeric chain-structured lanthanide complexes*. Polymer Journal, 2015. **47**(2): p. 195.
71. Masoomi, M.Y. and A. Morsali, *Applications of metal-organic coordination polymers as precursors for preparation of nano-materials*. Coordination Chemistry Reviews, 2012. **256**(23): p. 2921-2943.
72. Higuchi, M., *Electrochromic organic-metallic hybrid polymers: Fundamentals and device applications*. Polymer journal, 2009. **41**(7): p. 511.
73. Doherty, C.M., et al., *Using functional nano-and microparticles for the preparation of metal-organic framework composites with novel properties*. Accounts of chemical research, 2013. **47**(2): p. 396-405.
74. Bradshaw, D., A. Garai, and J. Huo, *Metal-organic framework growth at functional interfaces: thin films and composites for diverse applications*. Chemical Society Reviews, 2012. **41**(6): p. 2344-2381.
75. Bétard, A. and R.A. Fischer, *Metal-Organic Framework Thin Films: From Fundamentals to Applications*. Chemical reviews, 2011. **112**(2): p. 1055-1083.
76. Hosseini, M.W., *Molecular tectonics: from simple tectons to complex molecular networks*. Accounts of chemical research, 2005. **38**(4): p. 313-323.
77. Valeur, B. and M.N. Berberan-Santos, *Chemical sensing via fluorescence*. Molecular Fluorescence: Principles and Applications, Second Edition, 2012: p. 409-478.
78. He, P., et al., *Solid-state laser based on PMMA doped with Coumarin 540A*. Optics & Laser Technology, 2012. **44**(2): p. 341-343.
79. Anufrik, S.S. and V.V. Tarkovsky, *3-(2-Benzimidazolyl) coumarin derivatives—highly effective laser media*. Journal of Applied Spectroscopy, 2010. **77**(5): p. 640-647.
80. Creaven, B.S.A., et al., *Copper (II) complexes of coumarin-derived Schiff bases and their anti-Candida activity*. Journal of inorganic biochemistry, 2009. **103**(9): p. 1196-1203.
81. Sathisha, M.P., et al., *Synthesis and antitumor studies on novel Co (II), Ni (II) and Cu (II) metal complexes of bis (3-acetylcoumarin) thiocarbohydrazone*. European journal of medicinal chemistry, 2008. **43**(11): p. 2338-2346.
82. Gudasi, K.B., M.S. Patil, and R.S. Vadavi, *Synthesis, characterization of copper (II), cobalt (II), nickel (II), zinc (II) and cadmium (II) complexes of [7-hydroxy-4-methyl-8-coumarinyl] glycine and a comparative study of their microbial activities*. European journal of medicinal chemistry, 2008. **43**(11): p. 2436-2441.
83. Hanshaw, R.G., et al., *An indicator displacement system for fluorescent detection of phosphate oxyanions under physiological conditions*. Tetrahedron letters, 2004. **45**(47): p. 8721-8724.

84. Shcherbakov, K.V., Y.V. Burgart, and V.I. Saloutin, *Metal complexes based on functionalized 4-hydroxypolyfluorocoumarins*. Russian Journal of Organic Chemistry, 2014. **50**(6): p. 815-821.
85. V., G.M. and S.S. G., *Synthesis, characterization and Biological studies of Cu(II) and Ni(II) complexes with New Bidentate Schiff's base ligands as 4-hydroxy-3-(1-(arylimino)ethyl)chromen-2-one*. Research Journal of Recent Sciences, 2012. **1**: p. 110-116.
86. Siega, P., et al., *A Novel Series of CoIII (salen-type) Complexes Containing a Seven-Membered Metallacycle: Synthesis, Structural Characterization and Factors Affecting the Metallacyclization Rate*. Organometallics, 2014. **33**(4): p. 909-920.
87. Kertsus-Banchik, E., et al., *Hydride migration from silicon to an adjacent unsaturated imino carbon: Intramolecular hydrosilylation*. Organometallics, 2008. **27**(20): p. 5285-5294.
88. Badiger Sangamesch, B.D., Betschart Claudia, Chaudhari Vinod, Chebrolu Murali, Costesta Simona, Hintermann Samuel, Pandit Chetan, *Distributed heteroaryl-fused pyridines*. WO2011076744 (A1), 2011.
89. Bertrand, C. and W. Ann, *C3A Antagonists and pharmaceutical compositions thereof*. WO2007/034279A2, 2007.
90. Blass, B.E., et al., *A simple method for the preparation and selective functionalization of 4, 5-diaminopyrazoles*. Tetrahedron letters, 2003. **44**(14): p. 3009-3011.
91. Poole, R.A., et al., *Synthesis and characterisation of highly emissive and kinetically stable lanthanide complexes suitable for usage 'in cellulose'*. Organic & biomolecular chemistry, 2005. **3**(6): p. 1013-1024.
92. Zhang, M., et al., *2-Oxazoline/benzoxazole-1, 10-phenanthroline/metal (iron, cobalt or nickel) dichloride: Synthesis, characterization and their catalytic reactivity for the ethylene oligomerization*. Journal of Organometallic Chemistry, 2008. **693**(26): p. 3867-3877.
93. Bruice, P., *Organic Chemistry 7th Edition*. Pearson, 2014.
94. Pretsch, E., et al., *Spektroskopische Daten zur Strukturaufklärung organischer Verbindungen*. Vol. 5. 2010, Springer, Berlin.
95. Nuñez-Dallos, N., A.F. Posada, and J. Hurtado, *Coumarin salen-based zinc complex for solvent-free ring opening polymerization of  $\epsilon$ -caprolactone*. Tetrahedron Letters, 2017. **58**(10): p. 977-980.
96. Zhao, J., et al., *Bis-Zn II salphen complexes bearing pyridyl functionalized ligands for efficient organic light-emitting diodes (OLEDs)*. Dalton Transactions, 2017. **46**(18): p. 6098-6110.
97. Escudero-Adán, E.C., J. Benet-Buchholz, and A.W. Kleij, *Autocatalytic demetalation of a Zn (salphen) complex provoked by unprotected N-heterocycles*. Dalton Transactions, 2008(6): p. 734-737.
98. Fedorova, E.V., et al., *Synthesis and structure of oxovanadium(IV) complexes [VO(Acac)<sub>2</sub>] and [VO(Sal: L-alanine)(H<sub>2</sub>O)]*. Crystallography Reports, 2005. **50**(2): p. 224-229.

99. Constable, E.C., et al., *Hierarchical multicomponent assembly utilizing sequential metal–ligand and hydrogen-bonding interactions*. CrystEngComm, 2009. **11**(4): p. 657-662.
100. Kelly, N., et al., *Spacer-Controlled Supramolecular Assemblies of Cu (II) with Bis (2-Hydroxyphenylimine) Ligands. from Monoligand Complexes to Double-Stranded Helicates and Metallomacrocycles*. Crystals, 2016. **6**(9): p. 120.
101. Fulmer, G.R., et al., *NMR Chemical Shifts of Trace Impurities: Common Laboratory Solvents, Organics, and Gases in Deuterated Solvents Relevant to the Organometallic Chemist*. Organometallics, 2010. **29**(9): p. 2176-2179.
102. Gottlieb, H.E., V. Kotlyar, and A. Nudelman, *NMR Chemical Shifts of Common Laboratory Solvents as Trace Impurities*. Journal of Organometallic Chemistry, 1997. **62**: p. 7512-7515.
103. Crosby, G.A. and J.N. Demas, *Measurement of photoluminescence quantum yields. Review*. The Journal of Physical Chemistry, 1971. **75**(8): p. 991-1024.
104. APEX2, et al., *Bruker AXS Inc., Madison, WI, . 2012*.
105. Sheldrick, G., *A short history of SHELX*. Acta Crystallographica Section A, 2008. **64**(1): p. 112-122.
106. Palatinus, L. and G. Chapuis, *SUPERFLIP - a computer program for the solution of crystal structures by charge flipping in arbitrary dimensions*. Journal of Applied Crystallography, 2007. **40**(4): p. 786-790.
107. Mercury, C., P. Macrae, and P.M. Edgington, *E. Pidcock, GP Shields, R. Taylor, M. Towler and J. van de Streek*. J. Appl. Crystallogr, 2006. **39**: p. 453.
108. Frisch, M.J., G.W. Trucks, and H.B. Schlegel, *Gaussian 09, Gaussian. Inc., Wallingford, CT, 2009*.
109. Schlamminger, S., et al., *Determination of the Planck constant using a watt balance with a superconducting magnet system at the National Institute of Standards and Technology*. Metrologia, 2014. **51**: p. 15-24.

# ESTHER THERESA KNITTL

## PERSONAL DETAILS

---

- Esther Theresa Knittl  
Panikengasse 43/13  
A-1160 Wien
- Phone: +43 660 737 14 92
- E-Mail: esther@knittl.com
- Date and Place of Birth:  
October 11<sup>th</sup>, 1989 in Oberpullendorf
- Citizenship: Austria



## EDUCATION

---

- |             |  |
|-------------|--|
| Since 2014  | Studies in Technical Chemistry (PhD)<br>at the Vienna University of Technology<br><br>PhD thesis:<br>„Synthesis and Characterization of Coordination<br>Compounds Using Novel Tetradentate Schiff Bases<br>Aiming for Potential Fluorescence Applications “<br>(Research group: Univ. Prof. Wolfgang Linert) |
| 2008 - 2014 | Studies in Technical Chemistry<br>at the Vienna University of Technology<br><br>Master thesis:<br>„Synthesis and Applications of Oxo-Molybdenum<br>Compounds“<br>(Research group: Univ. Prof. Dr. Işıl Topaloğlu-Sözüer)<br>Izmir Yüksek Teknoloji Enstitüsü   |
| 2000 - 2008 | High School in Eisenstadt with concentration in languages<br><i>Graduation from high school with great honor</i>   |
| 1995 - 2008 | Studies in Music with concentration in piano<br>at the Conservatory “Joseph Haydn“ in Eisenstadt   |

## WORK EXPERIENCE

---

- |            |   |
|------------|---|
| Since 2014 | Vienna UT<br>1040 Vienna, Austria<br><i>University Assistant</i>  |
| July 2008  | SRB Consulting Team GmbH<br>1190 Vienna, Austria<br><i>Personal Assistant to the Chief of Marketing</i> |

## EXPERIENCE ABROAD

---

- |             |   |
|-------------|---|
| 2015        | Internship at the LCC-CNRS in Toulouse, France<br>(Research group: Univ. Prof. Dr. Azzedine Boussekoun) |
| 2012 - 2013 | ERASMUS-year at the IYTE in Izmir, Turkey<br>(Research group: Univ. Prof. Dr. Işıl Topaloğlu-Sözüer)    |

## LANGUAGES

---

- German: native language
- English: fluent in speech and writing
- Turkish: fluent in speech and writing
- Russian: semi-fluent
- Latin

## PERSONAL INTERESTS

---

- Travelling
- Playing the piano and accordion
- Cooking
- Ultimate Frisbee

## PUBLICATIONS

---

„Characterization of a novel dioxomolybdenum complex by cyclic voltammetry”.

Esther Theresa Knittl, D. A. Rusakov, E. I. Korotkova, E. V. Dorozhko, O. A. Voronova, E. V. Plotnikov, Isil Topaloglu-Sozuer & Wolfgang Linert, Analytical Letters, 2015. **48**(15): p. 2369-2379

„Syntheses, spectroscopic characterization and inhibitory activity on novel Mono and binuclear transition metal complexes of hydrazones Schiff base derived from coumarine derivatives and oxalyldihydrazine”,

Esther Theresa Knittl, Wolfgang Linert, A.A. Abou-Hussein, Monatshefte für Chemie, special Issue – Gamsjäger in the press (2017).

“Thermal Decomposition Studies on Iron(III) Complexes of 1,2-Bis(imino-4'-antipyrinyl)ethane with Varying Counter Ions”,

Nayathuparambil Thomas Madhu, Esther Theresa Knittl, Kibret Fekadu, Hagos Feleke, Endalkachew Asefaa, Kassa Abuyea and Wolfgang Linert, Journal of Chemistry and Applied Chemical Engineering , inaugural issue-invited contribution 1:1 (2017) 1-23.

“Room-temperature spin-transition iron compounds”,

Nayathuparambil Thomas Madhu, Alemu Gonfa Robi, Tegene Desalegn Zeleke, Esther Theresa Knittl and Wolfgang Linert, Journal of Chemistry and Applied Chemical Engineering, J Chem Appl Chem Eng, 1:2 (2017) 1-23 in the press.